이학박사학위논문

Loophole-Free Test of Quantum Nonlocality and Efficient Noiseless Amplification for Large Optical Fields

허점 없는 양자 비국소성 테스트와 큰 광학적 필드에 효율적인 소음없는 증폭

2015년 8월

서울대학교 대학원
물리·천문학부
박 진 우

Loophole-Free Test of Quantum Nonlocality and Efficient Noiseless Amplification for Large Optical Fields

허점 없는 양자 비국소성 테스트와 큰 광학적 필드에 효율적인 소음없는 증폭

지도교수 정 현 석

이 논문을 이학박사 학위논문으로 제출함

2015년 5월

서울대학교 대학원

물리·천문학부

박 진 우

박진우의 박사 학위논문을 인준함

2015년 6월

위 원 장	안 경 원	(인)
부위원장	정 현 석	(인)
위 원	제 원 호	(인)
위 원	신 용 일	(인)
위 원	손 원 민	(인)

Loophole-Free Test of Quantum Nonlocality and Efficient Noiseless Amplification for Large Optical Fields

Jinwoo Park

Supervised by

Professor Hyunseok Jeong

A Dissertation
Submitted to the Faculty of
Seoul National University
in Partial Fulfillment of
the Requirements for the Degree of
Doctor of Philosophy

June 2015

Department of Physics and Astronomy
Graduate School
Seoul National University

Abstract

Loophole-Free Test of Quantum Nonlocality and Efficient Noiseless Amplification for Large Optical Fields

Jinwoo Park
Department of Physics & Astronomy
The Graduate School
Seoul National University

The concept of quantum nonlocality was used first by Einstein, Podolsky, and Rosen with intention to indicate the paradox of quantum physics. However, quantum nonlocality turns out to be one of the most important resource for quantum information processing, which can be used for quantum teleportation and device-independent quantum key distribution not to mention of violation of local realism assumed by classical physics.

In the beginning of this dissertation, we investigate the hierarchy of quantum nonlocality with emphasis on relation between EPR-steerable states and quantum teleportable states. Efficient ways to demonstrate Bell nonlocality and EPR steering are followed.

Demonstration of Bell nonlocality can rule out local realism assumed by classical physics. The major two loopholes are required to be closed for the perfect demon-

stration, which are so called detection loophole and locality loophole. Locality loophole was solely closed by using photonic quantum system, while detection loophole could be closed alone by using atomic quantum system with high detection efficiency. Up to now, demonstration which closes both of loopholes does not exist. Taking advantage from both systems, we have proposed a scheme which uses a photon in cavity and a Rydberg atom is suggested and experimental conditions which can close locality loophole is analyzed. If we can inhibit spontaneous emission by using thin cryogenic superconducting cylindrical cavity and enhance photon storage time of the main cavity, the locality loophole can be avoided.

EPR steering is the ability to change the quantum phenomena of space-likely separated system from the measurement on the other system. Demonstration of EPR steering less suffers from detection loophole and locality loophole than Bell nonlocality. We investigate the EPR steering of entangled coherent states using homodyne detection, photon parity detection, and photon on/off detection. The maximum value of EPR steering inequality is achieved by low-efficiency homodyne detection with enough amplitude of entangled coherent state. If entangled coherent state can be successfully generated, the demonstration of EPR steering may be feasible considering the practical efficiency of photon on/off detection.

The remainder of this dissertation is about efficient noiseless linear amplification using photon addition and subtraction. Numerous studies have shown that various quantum information processing can be enhanced by the noiseless amplification of continuous variable quantum states. It has been verified that the photon-addition-then-subtraction operator is efficient noiseless amplifier for small coherent states. We show that the double-photon-addition operator is more effective amplifier for medium and large amplitude coherent states in terms of equivalent input noise, which consid-

ers the noise and the gain caused by the amplifier on equal footing. The extension to superpositions of coherent states is also made with analogous results followed, which can be inferred from the optimal phase uncertainty computed from quantum Fisher information.

Keywords : quantum nonlocality, noiseless amplification, Bell inequality, EPR steering, quantum teleportation, hierarchy

Student Number : 2008-20433

Table of Contents

List of Figures

List of Tables

Chapter 1

Introduction

What is quantum nonlocality? There are many studies about theoretical and experimental aspects of quantum nonlocality. To be precise, we only know several experimental evidence with loophole [2, 3, 4, 5, 6, 7], which suggests local-realism should be banned from our philosophy. However, we do not known whether localism or realism is wrong. For example, the phrase nonlocality is valid when the collapse process of quantum states actually occurs when the meausurement is performed [8]. When one accepts the many world interpretation, nonlocality actually vanishes as suggested in Ref. [8]. But, most physicists seem to want to believe realism more than localism to use the term 'nonlocality' to indicate the violation of local-realism. However, not only the rigorous definition but also the scope of usage is still vague. As mentioned, some physicists use the term to indicate Bell nonlocality, the others use it to indicate both Bell nonlocality and Einstein-Podolsky-Rosen (EPR) Steering [9]. Throughout this dissertation, we refer quantum nonlocality as the phenomena which cannot explained by stochastic sums of local quantum states, *i. e.* entanglement.

When higher hierarchical quantum nonlocalty is used, it can be used to prove the violation of local hidden variable model (Bell nonlocality) and the violation of local hidden state model (EPR steering). Although strict experimental demonstrations of above-mentioned quantum nonlocality without loophole has been realized only for EPR steering [10], the most physicists also seem to believe the existence of Bell nonlocality. In our opinion, it is indeed plausible to believe the existence of quantum

nonlocality rather than not to believe fair sampling assumption. However, the demonstration of such forms of quantum nonlocality without loophole is still fundamentally important. Besides, the demonstration can prove the use of such nonlocal states may be resources for device-independent quantum key distribution [11, 12]. We propose such schemes to demonstrate Bell nonlocality and EPR steering without loophole, and analyze experimental parameters required to close the loophole.

The following hierarchy between entanglement, EPR steering, and Bell nonlocality is proven by Ref. [9]:

$$\text{Bell nonlocality} \subset \text{EPR steering} \subset \text{Entanglement} \tag{1.1}$$

Quantum teleportation is another important information task, which also uses quantum nonlocality as resource [13]. In the process of quantum teleportation, the nonlocal information transfer is performed by Bell measurement [1]. However, the nonlocality form which quantum teleportation exploits are inequivalent to Bell nonlocality [14]. All the two dimensional bipartite quantum states which violate generalized (linear-type) Bell inequalities are useful for quantum teleportation [15]. Thus, the states useful for quantum teleportation (we will refer these as quantum teleportable states) seems to be in the mid-class hierarchical position between Bell nonlocality and entanglement, although rigorous proof for general argument is not available. As EPR steering is also in the mid-class hierarchical position between Bell nonlocality and entanglement, we examine the hierarchical relation between quantum teleportable states and EPR steering, and conclude there are no subset relation.

In the latter part of this dissertation, we propose a scheme for noiseless linear amplification of coherent states using the two-photon addition. Noiseless linear am-

plification can not only be used to enhance quantum nonlocality [16, 17] in a probabilistic way [18] but also many interesting quantum information tasks, such as entanglement distillation [19], continuous variable quantum key distribution [20, 21], loss suppression [22], quantum repeater [23], phase estimation [24], error correction [25], and high-accuracy homodyne detection with low-efficiency detector [26]. We compare it with the previous proposal using the photon addition-then-subtraction scheme that appropriately works well only for very weak light fields [27, 28]. We show that when the amplitude of a coherent state is larger than about 0.91, the two-photon addition serves as a more efficient amplifier compared to the photon addition-then-subtraction operation in terms of equivalent input noise. The two-photon addition also exhibits similar behaviors both for the amplification of superpositions of coherent states and squeezed states as their approximations. The enhancement of the maximum fidelity can be observed when a squeezed state is used to approximate a superposition of coherent states. Our work provides an efficient method to implement a noiseless amplifier for light fields with medium and large amplitudes.

The remainder of this dissertation is organized as follows. In chapter 2, we review the basic concepts of quantum nonlocality and the known hierarchy therein. Our results about hierarchical relation between EPR-steerable states and quantum teleportable states are also discussed. Chapter 3 is devoted into the demonstration of Bell nonlocality with entangled atom-photon system. Rydberg atom and microwave cavity photon are used to close loopholes and required experimental parameters are analyzed. In Chapter. 4, we examine EPR steering of entangled coherent states, which demands less experimental conditions than Bell nonlocality. Chapter 5 contains the results about efficient noiseless amplification for the large and the medium amplitude of coherent states. Concluding remarks are followed in Chapter 6.

Chapter 2

Basic Concepts and Hierarchy of Quantum Nonlocality

In this chaper, we review the definition of nonlocal correlations of quantum states in historical orders. We introduce how the concept of quantum nonlocality was first captured and used to claim the incompleteness of quantum theory by Einstein, Podolsky, and Rosen. The precise formulations of different classes of nonlocality of quantum states, Bell nonlocality, states useful for quantum teleportation, entanglement and EPR steering; will be briefly reviewed in historical orders. Then, the studies of hierarchy between the above-mentioned correlations are also reviewed with emphasis on two-level system. Finally, we show that there is no subset relation between EPR-steerable states and the states useful for quantum teleportation.

2.1 EPR paradox

"Quantum mechanics is certainly imposing. But an inner voice tells me that it is not yet the real thing. The theory says a lot, but does not really bring us any closer to the secret of the 'old one.' I, at any rate, am convinced that He does not throw dice." This is what Einstein wrote in a letter to Born [29]. Einstein seem to dislike the probabilistic nature of quantum theory, and he believed that the probabilistic nature should be amended by higher physical theory which explains the universe in a deterministic way. One of his most sharp and logical attack on the quantum theory was done by

Ref. [30] coauthored by Podolsky and Rosen. Actually there is a minor tautology in their argument [31]. Therefore, we review the modified version of Einstein, Podolsky, and Rosen's (EPR's) argument [31] for the simplicity of logical deduction.

EPR claimed the incompleteness of quantum mechanical description based on three premises [31]. The first premise is a necessary condition for completeness: Every element of the physical reality must have a counterpart in the physical theory. The second premise is a sufficient condition for reality: If without in any way disturbing a system, we can predict with certainty the value of a physical quantity, then there exists an element of physical reality corresponding to this physical quantity. Actually, there is a hidden premise in the second premise, which is a necessary condition for locality: No real change can take place in the second system in consequence of anything that may be done to the first system.

Based on these three premises, Einstein, Podolsky, and Rosen argued the following. First let us consider the following two statements:

(A) The quantum-mechanical description of reality given by the wave function is not complete.

(B) When the operators corresponding to two physical quantities do not commute, the two quantities cannot have simultaneous reality.

Then the following relation holds using the uncertainty principle [32]:

$$(A) \rightarrow (B). \tag{2.1}$$

Using the following spin singlet state, so called EPR-Bohm pair [33],

$$
\begin{aligned}
|\Psi_{EPR-Bohm}\rangle &= \frac{1}{\sqrt{2}}(|\uparrow_{\hat{z}}\rangle_A |\downarrow_{\hat{z}}\rangle_B - |\downarrow_{\hat{z}}\rangle_A |\uparrow_{\hat{z}}\rangle_B) \\
&= \frac{1}{\sqrt{2}}(|\uparrow_{\hat{n}}\rangle_A |\downarrow_{\hat{n}}\rangle_B - |\downarrow_{\hat{n}}\rangle_A |\uparrow_{\hat{n}}\rangle_B),
\end{aligned}
\tag{2.2}
$$

where $|\uparrow_{\hat{n}}\rangle$ and $|\downarrow_{\hat{n}}\rangle$ are the spin up and the spin down states in the direction $\hat{n}$. We can always predict the $\hat{n}$ directional spin-value of the system A by measuring the $\hat{n}$ directional spin of the system B without disturbing A, which is guranteed by the third premise. Thus by the second premise, namely x-spin and z-spin measurements which do not commute have simultaneous reality for EPR-Bohm state. Thus one can conclude that the statement ¬(B) is true. Therefore the converse of Eq. (2.1) leads the statement (1) is true. However, the premises which seems plausible require a careful consideration. The local-realism where the second and the third premises are combined can be tested by the inequality proposed by Bell, and is not compatible with quantum theory [34].

2.2 Schrödigner's Response to EPR

Schrödinger, the founder of quantum theory, immediately noticed the significance of the EPR paper and coined the term 'entanglement' [35] and 'steer' [36]:

"If two separated bodies, each by itself known maximally, enter a situation in which they influence each other, and separate again, then there occurs regularly that which I have just called **entanglement** of our knowledge of the two bodies." (The Ref. [35] is written in German, and the following is the quote from the translated version from Ref. [37])

"It is rather discomforting that the theory should allow a system to be **steer**ed or

piloted into one or the other type of state at the experimenter's mercy in spite of his having no access to it." [36]

Although, he grasped the term 'entanglement' and 'steer', he had no doubt in the second and the third premises which EPR assumed. Instead, he claimed that although global description quantum states may not be complete [38], the local description of quantum states are complete, which later triggers the rigorous definition of EPR steering [9]. On the other hand, the entanglement was also rigorously defined by Ref. [39].

2.3 Bell Nonlocality

Bell nonlocality is the first form of quantum nonlocality which have been rigorously defined by Bell [34]. For a bipartite quantum state $\hat{\rho}_{AB}$, the state is Bell nonlocal, if there exist no local hidden variable model. The quantum state has local hidden variable (local-realism) model in the following case:

For any measurments $\hat{A}$ on system A and $\hat{B}$ on system B with outcome result a and b, there exist probability distribution $p(\lambda)$, $p_A(a|\lambda,\hat{A})$, and $p_B(b|\lambda,\hat{B})$ satisfying the relation

$$p(a,b|\hat{A},\hat{B}) = \sum_{\lambda} p(\lambda) p_A(a|\lambda,\hat{A}) p_B(b|\lambda,\hat{B}). \tag{2.3}$$

Although the definition is quite straight forward, determining whether a quantum state is Bell nonlocal is generally hard problem. It is often determined by violation of Bell's inequalities [34, 40, 41], which is not a necessary but sufficient condition for a quantum state to be Bell nonlocal. One of the most frequently used Bell's inequalities is called Bell-CHSH inequality [40]. Assuming local hidden variable model, the magnitude of Bell-CHSH function (Fig. 1) is bounded above by 2, whereas quan-

Figure 1: Scheme of Bell-CHSH test. After Alice and Bob's sharing a bipartite entangled state, one of dichotomic measurements $\hat{A}_1$, $\hat{A}_2$ and $\hat{B}_1$, $\hat{B}_1$ are respectively performed by Alice and Bob. The expectation value of the operator $\hat{A}_1 \otimes \hat{B}_1 + \hat{A}_1 \otimes \hat{B}_2 + \hat{A}_2 \otimes \hat{B}_1 - \hat{A}_2 \otimes \hat{B}_2$, Bell-CHSH function, is measured.

tum theory allows its value to be bounded above by $2\sqrt{2}$. By observing violation of Bell's inequality, one can confirm the violation of local realism assumed by classical physics.

2.4 Entanglement

Although, the word 'entanglement' was first captured by Schrödinger, it took more than a half of century to be rigorously defined. Entanglement is one of the most important quantum correlation which may be useful for quantum information processing. Quantum states are called entangled if it cannot be represented as the following stochastic sum of local quantum states (local quantum state model):

$$\hat{\rho}_{AB} = \sum_{\lambda} p(\lambda) \hat{\rho}_{\lambda,A} \otimes \hat{\rho}_{\lambda,B}, \tag{2.4}$$

which is equivalent to the following [42]:

For any measurments $\hat{A}$ on system A and $\hat{B}$ on system B with outcome result a and b, there exist probability distributions $p(\lambda)$ and quantum probability distribution

$p_A^Q(a|\lambda,\hat{A})$, and $p_B^Q(b|\lambda,\hat{B})$ satisfying the relation

$$p(a,b|\hat{A},\hat{B}) = \sum_{\lambda} p(\lambda) p_A^Q(a|\lambda,\hat{A}) p_B^Q(b|\lambda,\hat{B}). \tag{2.5}$$

It is trivial to see the local quantum state model is subset of the local hidden variable model, thus Bell nonlocality is the subset of the entanglement, which makes Bell nonlocality more higher hierarchy. There are some successful results on the quantification of entanglement [43, 44].

2.5 Quantum Teleportation

As the fundamental no cloning theorem resticts, quantum state cannot be copied [45]. It can only be transfered from one place to another. The one obvious way to transfer quantum information is direct transmission of the physics states, and the other way is to use entangled channel to teleport a quantum state. There is a study which compares the efficiency of both methods under photon loss [46]. Besides, quantum teleportation is especially useful for continuous variable elementary gate operation and it can be used to transfer quantum information from one physical system to other physical system.

Quantum teleportation was first introduced by Bennett *et al.* in Ref. [13]. Using the teleportation scheme, one can transfer unknown quantum information from one place to another. This information transfer scheme differs from the direct transmission. Because, the actual physical system carrying the information actually goes with the information for the direct transmission, while initial physical system carrying the information stays at the same place, and it is the information only which transfers from one physical system to the other physical system. A brief sketch of the quantum

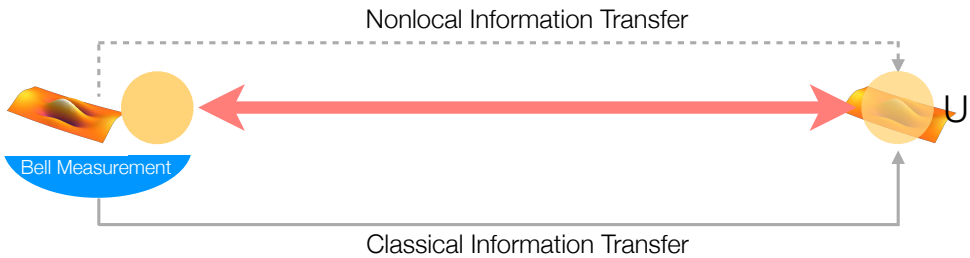

Figure 2: Scheme of quantum teleportation. First, distribution of entangled channel is required between two parties, namely Alice and Bob. Then, Bell measurements are performed on one side of entangled channel and the actual physical system which carries the quantum information that we want to teleport. When the Bell measurement is performed, the quantum system under measurement is collapsed to the quantum state which refers to the outcome of the Bell measurement, then the other side of the entangled channel is instantaneously transformed to the quantum states (nonlocal information is transferred to other side of the channel since quantum state was entangled [1]) which can be transformed to the desired quantum state after certain unitary operation depending on the outcome of the Bell measurement.

teleportation scheme is illustrated in Fig. 2

As nonlocal information transfer using entangled state was key concept for quantum teleportation. It is natural to ask what forms of quantum nonlocality is required for quantum teleportation. It has been verified in Ref. [15] that two dimensional bipartite quantum states which violates Bell-CHSH inequality may be used for quantum teleportation. The necessary and sufficient condition for a entangled channel to be useful for quantum teleportation can be calculated from singlet fraction [47].

2.6 EPR Steering

As mentioned earlier, although Schrödinger was the first one who come up with the term ‘steering’ [36] and the idea of local hidden state model [38], the rigorous mathematical definition of EPR steering was provided by Wiseman *et al.* [9]. The bipartite

quantum state $\hat{\rho}_{AB}$ is EPR-steerable, if it does not have a local hidden state model. The state has a local hidden state model when the following condition is true:
For any measurment $\hat{A}$ on system A and $\hat{B}$ on system B with outcome result a and b, there exist probability distribution $p(\lambda)$, $p_A(a|\lambda,\hat{A})$, and quantum probability distribution $p_B^Q(b|\lambda,\hat{B})$ satisfying the relation

$$p(a,b|\hat{A},\hat{B}) = \sum_{\lambda} p(\lambda) p_A(a|\lambda,\hat{A}) p_B^Q(b|\lambda,\hat{B}). \tag{2.6}$$

Demanding only one subsystem to have quantum probability distribution reflects the idea of Schrödinger who believed the local quantum mechanical description is complete [38]. By definitions of Bell nonlocality (Eq. 2.3), entanglement (Eq. 2.5), and EPR steering (Eq. 2.6) the following hierarchy is trivially derived [9]:

$$\text{Bell nonlocality} \subset \text{EPR steering} \subset \text{Entanglement} \tag{2.7}$$

2.7 EPR Steering and Quantum Teleportation

As both the EPR-steerable states and states useful for quantum teleportation are in the mid hierarchy between entanglement and Bell-CHSH nonlocality [15, 9]. It is intriguing to ask the hierarchical relation between EPR steering and the nonlocalty used for quantum teleportation.

Unfortunately, we show that these forms of nonlocality have no subset relation. The proof of this can be done by showing the existence of the following states:
(1) There exists a state which is EPR-steerable, but cannot be used for nonclassical teleportation.
(2) There is a state which can be used for nonclassical teleportation, but is not EPR-

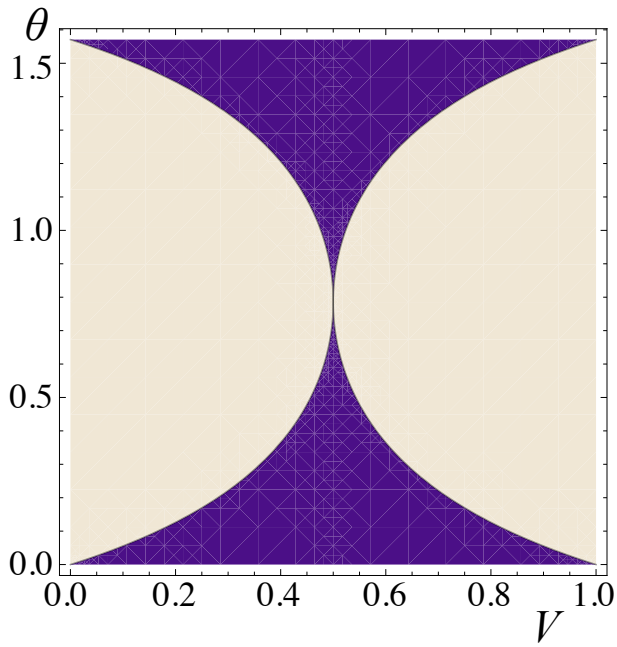

Figure 3: Region of spin-X state which is useful for nonclassical teleportation. Light colored region is useful for nonclassical teleportation, whereas dark colored region is not useful for teleportation.

steerable.

The statement (1) can be proven by the two dimensional Werner state [39],

$$W_2^{\eta} = \frac{(1-\eta)}{4} I + \eta P_+, \tag{2.8}$$

where $P_+ = |\psi_+\rangle\langle\psi_+|$, where $|\psi_+\rangle = \frac{1}{\sqrt{2}}(|1\rangle|1\rangle + |2\rangle|2\rangle)$. It has proven in Ref. [9] that for W_2^{η} is EPR-steerable if and only if $\eta > \frac{1}{2}$. However, this state is useful for nonclassical teleportation if and only if $\eta > \frac{1}{3}$ [47].

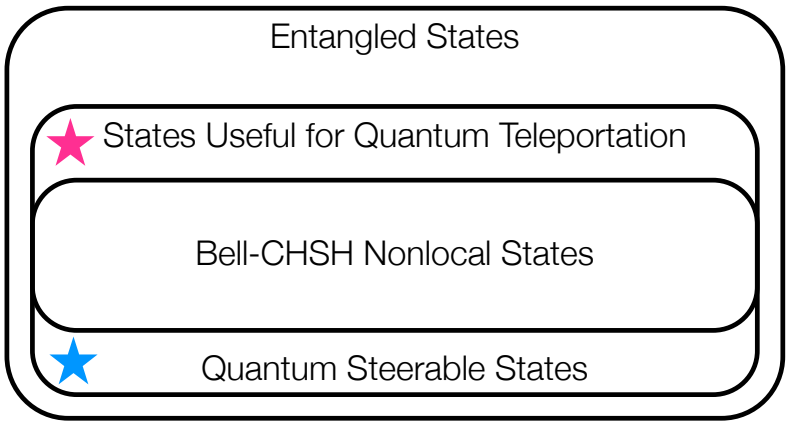

Figure 4: Hierarchy of quantum nonlocalty for bipartite two-dimensional states.

The statement (2) can be proven by the two dimensional spin-X state,

$$\rho_X = \begin{pmatrix} V\cos^2\theta & 0 & 0 & V\cos\theta\sin\theta \\ 0 & (1-V)\sin^2\theta & (1-V)\cos\theta\sin\theta & 0 \\ 0 & (1-V)\cos\theta\sin\theta & (1-V)\cos^2\theta & 0 \\ V\cos\theta\sin\theta & 0 & 0 & V\sin^2\theta \end{pmatrix}. \tag{2.9}$$

Ref. [48] prove that it is EPR-steerable if and only if $V \in [0,1/2) \cup (1/2,1]$ and $\theta \in (0,\frac{\pi}{2})$. However, we show that in Fig. 3 that there exists a region which is not useful for nonclassical teleportation, but EPR-steerable.

Therefore, there is no subset relation between EPR-steering and the states useful for quantum teleportation as Fig. 4

Chapter 3

Bell Inequality Test with Atom-Photon Entangled States

Notice: The content of this chapter has been published in: J. Park, M. Saunders, Y. Shin, K. An and H. Jeong, Phys. Rev. A 85, 022120 (2012).

We study Bell inequality tests with entanglement between a coherent-state field in a cavity and a two-level atom. In order to detect the cavity field for such a test, photon on/off measurements and photon number parity measurements, respectively, are investigated. When photon on/off measurements are used, at least 50% of detection efficiency is required to demonstrate violation of the Bell inequality. Photon number parity measurements for the cavity field can be effectively performed using ancillary atoms and an atomic detector, which leads to large degrees of Bell violations up to Cirel'son's bound. We also analyze decoherence effects in both field and atomic modes and discuss conditions required to perform a Bell inequality test free from the locality loophole.

3.1 Introduction

Einstein, Podolsky, and Rosen (EPR) presented an argument known as the EPR paradox [30], which triggered the debate on quantum mechanics versus local realism. Bell's theorem [34] enables one to perform experiments in which failure of local

realism is demonstrated by the violation of Bell's inequality. Various versions of Bell's inequality have been developed including Clauser, Horne, Shimony and Holt (CHSH)'s one [40], and substantial amount of experimental efforts have been devoted to the successful demonstration of violation of Bell's inequality. So far, many experiments have been performed to show violation of Bell-type inequalities, and most physicists now seem to believe that local realism can be violated.

On the other hand, all the experiments performed to date are subject to some loopholes, so that the experimental data can still be explained somehow based on a classical (often impellent) argument. Experiments using optical fields [2, 3, 4, 5] typically suffer from the "detection loophople" [49], and recent experiments using atomic states [6, 7] with the maximum separation of ~ 1 m [7], suffer from the "locality loophole" [50]. While most of Bell inequality tests have been performed using entangled optical fields [2, 3, 4, 5], it is an interesting possibility to explore Bell inequality tests using atom-field entanglement [51, 52, 53, 54, 55], particularly for a loophole-free test. In fact, there exist theoretical proposals for a loophole-free Bell inequality test using hybrid entanglement between atoms and photons [53, 54, 56, 57] and relevant experimental efforts [58, 54, 7] have been reported.

In this chapter, we study Bell inequality tests with an entangled state of a two-level atom and a coherent-state field. When the amplitude of the coherent state is large enough, such an entangled state is often called a "Schrödinger cat state" (e.g. in Ref. [59]) as an analogy of Schrödinger's paradox where entanglement between a microscopic atom and a classical object is illustrated [35]. Entanglement between atoms and coherent states has been experimentally demonstrated using cavities [60, 61, 62].

In our study, photon on/off measurements and photon number parity measure-

ments, respectively, are employed in order to detect the cavity field. We find that when photon on/off measurements are used, at least 50% of detection efficiency is required to demonstrate violation of the Bell-CHSH inequality. One may effectively perform photon number parity measurements for the cavity field using ancillary probe atoms and an atomic detector so that nearly the maximum violation of the Bell-CHSH inequality can be achieved.

The remainder of this chapter is organized as follows. In Sec. 3.2, we briefly discuss the atom-field entanglement under consideration and review basic elements of Bell inequality tests in our framework. We then investigate the Bell-CHSH inequality with photon on/off measurements and parity measurements, respectively, in Sec. 3.3. Sec. 3.4 is devoted to the investigation of the Bell-CHSH inequality test using indirect measurements within a 'circular Rydberg atom'-'microwave cavity' system. In Sec. 3.5, we analyze decoherence effects in both field and atomic modes. This analysis enables us to provide quantitative information on the requirements to perform a loophole-free Bell test. We conclude with final remarks in Sec. 3.8.

3.2 Basic Elements for Bell Inequality Tests

We are interested in testing the Bell-CHSH inequality with an atom-field entangled state:

$$|\Psi\rangle_{AC} = \frac{1}{\sqrt{2}} \left(|e\rangle_A |\alpha\rangle_C + |g\rangle_A |-\alpha\rangle_C \right), \tag{3.1}$$

where $|e\rangle_A$ ($|g\rangle_A$) is the excited (ground) state for the atomic mode A, and $|\pm\alpha\rangle_C$ are coherent states of amplitudes $\pm\alpha$ for the field mode C. States (3.1) for reasonably large values of α are considered entanglement between a microscopic system and a classical system [59, 63, 64, 65]. There have been studies on Bell inequality tests with

this type of entangled state [59], and similar states such as entanglement between an atom and a single photon [51, 52, 53, 54] and entanglement between coherent states [66, 67, 68, 69, 70, 63, 71, 72, 73]. Experimental demonstration of state (3.1) has been performed using a system composed of a circular Rydberg atom and a microwave cavity field [60, 61, 62].

In order to test a Bell type inequality, a bipartite entangled state should be shared by two separate parties. After sharing the entangled state, each of the two parties may locally perform appropriate unitary operations and dichotomic measurements. Violation of the Bell-CHSH inequality can be obtained by choosing certain values for the parameters of the unitary operations. The correlation function is defined as the expectation value of the joint measurement

$$E(\zeta,\beta) = \langle \hat{E}_A(\zeta) \otimes \hat{E}_C(\beta) \rangle, \tag{3.2}$$

where $\hat{E}_A(\zeta) = \hat{U}_A(\zeta)\hat{\Gamma}_A\hat{U}_A^{\dagger}(\zeta)$ is a dichotomic measurement $\hat{\Gamma}_A$ combined with unitary operation $\hat{U}_A(\zeta)$ parameterized by ζ, and $\hat{E}_C(\beta)$ can be defined accordingly. The Bell function $\mathcal{B}$ is then defined as

$$\mathcal{B} = \left| E(\zeta,\beta) + E(\zeta',\beta) + E(\zeta,\beta') - E(\zeta',\beta') \right|, \tag{3.3}$$

which should obey the inequality forced by local realism, *i.e.*, $\mathcal{B} \leq 2$. The maximum bound for the absolute value of the Bell function is $2\sqrt{2}$, known as Cirel'son's bound [74].

An atomic dichotomic measurement can be represented by a 2 by 2 matrix

$$\hat{\Gamma} = \begin{pmatrix} 1 & 0 \\ 0 & -1 \end{pmatrix} \tag{3.4}$$

where we choose the basis as $\{|e\rangle, |g\rangle\}$. We define the displaced dichotomic measurement $\hat{\Gamma}(\zeta)$ with the atomic displacement operator $\hat{D}(\zeta)$ as

$$\hat{\Gamma}(\zeta) = \hat{D}(\zeta)\hat{\Gamma}\hat{D}^{\dagger}(\zeta) \tag{3.5}$$

with

$$\begin{aligned} \hat{D}(\zeta) &= \exp\left[\zeta\hat{\sigma}_{+} - \zeta^{*}\hat{\sigma}_{-}\right] = \begin{pmatrix} \cos|\zeta| & \frac{\zeta}{|\zeta|}\sin|\zeta| \\ -\frac{\zeta^{*}}{|\zeta|}\sin|\zeta| & \cos|\zeta|, \end{pmatrix}, \\ \zeta(\theta,\,\phi) &= -\frac{\theta}{2}e^{-i\phi}, \end{aligned} \tag{3.6}$$

and $0 \leq \theta \leq \pi$ and $0 \leq \phi \leq 2\pi$, where $\hat{\sigma}_{\pm}$ are the standard ladder operators in the 2-dimensional Hilbert space. We note that $\hat{D}(\zeta)$ corresponds to a single qubit rotation for an atomic qubit and it can be achieved by applying a Ramsey pulse to the atom [75]. We consider measurement $\hat{\Gamma}(\zeta)$ for the atomic mode A throughout this chapter, while some different measurement schemes are considered for the field mode C.

3.3 Bell-CHSH Inequality Tests with Atom-Field Entanglement

3.3.1 On/Off Measurement for Field Mode

We first investigate the Bell-CHSH inequality with photon on/off measurements and the displacement operator for the cavity field mode. The displaced on/off measurement for the field C is

$$\hat{O}_C(\beta) = \hat{\mathcal{D}}_C(\beta)\Big(\sum_{n=1}^{\infty}|n\rangle\langle n| - |0\rangle\langle 0|\Big)\hat{\mathcal{D}}_C^{\dagger}(\beta), \tag{3.7}$$

where $\hat{\mathcal{D}}_C(\beta) = \exp[\beta\hat{a}_C^{\dagger} - \beta^*\hat{a}_C]$ is the displacement operator with the field annihilation (creation) operator $\hat{a}_C$ ($\hat{a}_C^{\dagger}$) and β as the displacement parameter for field C.

We model a photodetector with efficiency η by a perfect photodetector together with a beam splitter of transmissivity $\sqrt{\eta}$ in front of it [76]. The signal field C is mixed with the vacuum state $|0\rangle_v$ at a beam splitter. The beam splitter operator between modes C and v is $\hat{B}_{Cv} = \exp[(\cos^{-1}\sqrt{\eta})(\hat{a}_C^{\dagger}\hat{a}_v - \hat{a}_C\hat{a}_v^{\dagger})/2]$ [77], where $\hat{a}_v$ ($\hat{a}_v^{\dagger}$) is the field annihilation (creation) operator for the ancilla mode v. After passing through the beam splitter, the atom-field entangled state $|\Psi\rangle_{AC}$ is changed to a mixed state as

$$\begin{aligned}\rho_{AC}^{\eta} =& \mathrm{Tr}_v\left[\hat{B}_{Cv}\Big(|\Psi\rangle\langle\Psi|\Big)_{AC}\otimes\Big(|0\rangle\langle 0|\Big)_v\hat{B}_{Cv}^{\dagger}\right]\\ =&\frac{1}{2}\Big\{|e\rangle\langle e|\otimes|\sqrt{\eta}\alpha\rangle\langle\sqrt{\eta}\alpha| + |g\rangle\langle g|\otimes|-\sqrt{\eta}\alpha\rangle\langle-\sqrt{\eta}\alpha|\\ &+ e^{-2(1-\eta)|\alpha|^2}|e\rangle\langle g|\otimes|\sqrt{\eta}\alpha\rangle\langle-\sqrt{\eta}\alpha|\\ &+ e^{-2(1-\eta)|\alpha|^2}|g\rangle\langle e|\otimes|-\sqrt{\eta}\alpha\rangle\langle\sqrt{\eta}\alpha|\Big\}_{AC}.\end{aligned} \tag{3.8}$$

The correlation function with the photon detection efficiency η is the expectation

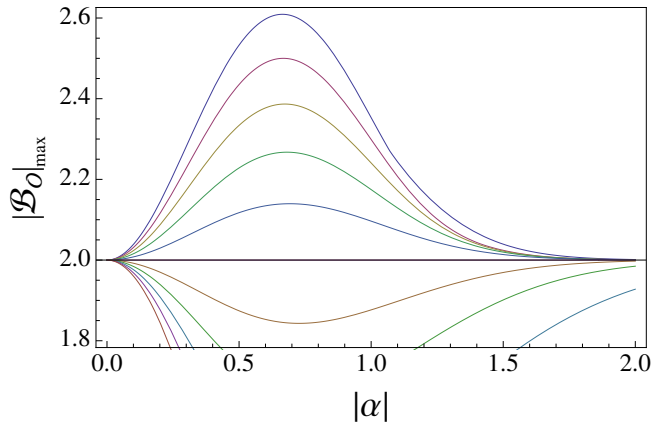

Figure 5: Numerically optimized values of Bell functions $\mathcal{B}_O$ with displaced on/off measurements against amplitude α of state (3.1). The detection efficiency ranges in value from $\eta = 0$ (lower curve) to $\eta = 1$ (upper curve), with intervals of 0.1 shown by the family of curves. The horizontal line corresponds to the case of $\eta = 0.5$, which coincides with the classical limit of the Bell-CHSH inequality.

value of $\hat{\Gamma}_A(\zeta) \otimes \hat{O}_C(\beta)$ for state (3.8) as

$$\begin{aligned} E_O(\zeta,\beta;\eta) =& \mathrm{Tr}\left[\rho_{AC}^{\eta}\hat{\Gamma}_A(\zeta)\otimes\hat{O}_C(\beta)\right] \\ =& -e^{-|\beta|^2-|\alpha|^2\eta-2|\alpha||\beta|\sqrt{\eta}\cos\Phi}\cos\frac{\theta}{2} \\ &+e^{-|\beta|^2-|\alpha|^2\eta+2|\alpha||\beta|\sqrt{\eta}\cos\Phi}\cos\frac{\theta}{2} \\ &+e^{-2|\alpha|^2}\cos\phi\sin\frac{\theta}{2} \\ &-2e^{-2|\alpha|^2-|\beta|^2+|\alpha|^2\eta}\cos\left(\phi-2|\alpha||\beta|\sqrt{\eta}\sin\Phi\right)\sin\frac{\theta}{2}, \end{aligned} \tag{3.9}$$

where $\alpha = |\alpha|e^{i\Phi_\alpha}$, $\beta = |\beta|e^{i\Phi_\beta}$, and $\Phi = \Phi_\beta - \Phi_\alpha$ with real phase parameters Φ_α and Φ_β. The Bell function is immediately obtained using Eqs. (3.3) and (3.9).

Using the method of steepest descent [78], we numerically find optimized val-

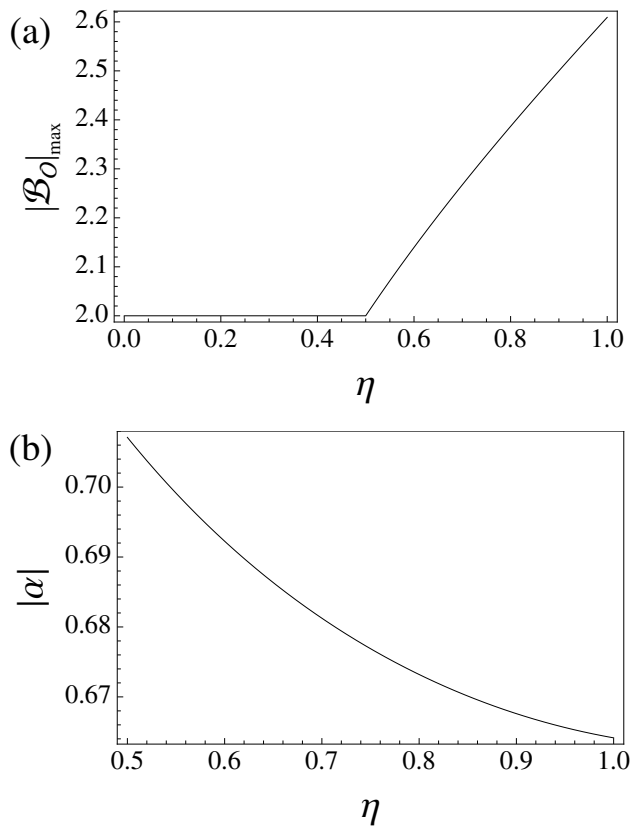

Figure 6: (a) Numerically optimized values of Bell function $\mathcal{B}_O$ with displaced on/off measurements against detection efficiency η. The local realistic bound, 2, is violated for $\eta \geq 0.5$. (b) Plot of optimizing values of $|\alpha|$ with respect to η.

ues, $|\mathcal{B}_O|_{\max}$, *i.e.*, absolute values of the Bell function maximized over variables ζ, ζ', β and β'. We plot the results against amplitude $|\alpha|$ for various choices of the detection efficiency from $\eta = 0$ to $\eta = 1$ (from bottom to top), where η differs by 0.1 between closest curves in Fig. 5. Assuming a real positive value of α, we find that the optimizing conditions can also be obtained as

$$\zeta = \frac{\pi}{2}, \;\; \zeta' = 0, \;\; \beta = -\beta' = |\beta|, \tag{3.10}$$

where $|\beta|$ satisfies

$$2|\beta| e^{2(\eta-1)|\alpha|^2} = e^{-2|\alpha||\beta|\sqrt{\eta}} \left(|\beta| + |\alpha|\sqrt{\eta}\right) - e^{2|\alpha||\beta|\sqrt{\eta}} \left(|\beta| - |\alpha|\sqrt{\eta}\right). \tag{3.11}$$

As expected, the perfect detection efficiency, $\eta = 1$, gives the higher violation up to $|\mathcal{B}_O|_{\max} \approx 2.61$ when $|\alpha| \approx 0.664$. A Bell violation of $|\mathcal{B}_O|_{\max} \approx 2.39$ ($|\mathcal{B}_O|_{\max} \approx 2.14$) is obtained for $\eta = 0.8$ ($\eta = 0.6$) when $|\alpha| \approx 0.673$ ($|\alpha| \approx 0.692$).

When $|\alpha| = 0$, no violation occurs because state (3.1) contains no entanglement. As $|\alpha|$ increases, the Bell violation becomes higher until $|\alpha| \sim 0.7$. However, as shown in Fig. 5, as $|\alpha|$ keeps increasing, the degree of the Bell violation decreases towards zero even though the state has larger entanglement. This result is due to the fact that when $|\alpha|$ is large, the probability of detecting the vacuum for the field mode diminishes. Obviously, if photon on/off detection excludes one of the two possible results, violation of the Bell-CHSH inequality will not occur regardless of the degree of entanglement. This is in agreement with a previous result in Ref. [68] where the Bell-CHSH inequality with entangled coherent states, $|\alpha\rangle|-\alpha\rangle - |-\alpha\rangle|\alpha\rangle$ (without normalization), was considered with on/off detection.

It should be noted that in Fig. 5, the Bell functions for $\eta = 0.5$ overlaps with the horizontal line that indicates the classical limit 2. In fact, the photon detector efficiency should be higher than 0.5 in order to see a Bell violation as shown in Fig. 6(a). Figure 6(b) shows that the optimizing values of $|\alpha|$ are within the range of $0.66 < |\alpha| < 0.71$ for any of $\eta \geq 0.5$. We also note a previous result [55] that efficiency of 0.43 can be tolerated if a different type of Bell inequality [79] is used with a nonmaximally entangled state and a perfect atomic measurement.

3.3.2 Photon Number Parity Measurement for Field Mode

We now consider the displaced photon number parity measurement for the field mode

$$\hat{\Pi}_C(\beta) = \hat{\mathcal{D}}_C(\beta)\Big(\sum_{n=0}^{\infty} |2n\rangle\langle 2n| - |2n+1\rangle\langle 2n+1|\Big)\hat{\mathcal{D}}_C^{\dagger}(\beta). \tag{3.12}$$

Using Eq. (3.1) and the measurement operators defined above, it is straightforward to get

$$\begin{aligned} E_{\Pi}(\zeta,\beta) &= \langle \hat{\Gamma}_A(\zeta) \otimes \hat{\Pi}_C(\beta)\rangle \\ &= e^{-2|\beta|^2}\sin\theta\cos[4|\alpha||\beta|\sin\Phi - \phi] \\ &\quad + e^{-2(|\alpha|^2+|\beta|^2)}\cos\theta\sinh[4|\alpha||\beta|\cos\Phi], \end{aligned} \tag{3.13}$$

and the corresponding Bell function, $\mathcal{B}_{\Pi}$. We present the numerically optimized Bell function, $|\mathcal{B}_{\Pi}|_{\max}$, against $|\alpha|$ in Fig. 7, where Bell violation occurs for any nonzero α. Note that the atomic displacement operator corresponds to a single-qubit rotation for the atomic mode. It was argued that the field displacement plays a similar role to approximately rotate a coherent-state qubit [68]. If we restrict the atomic displace-

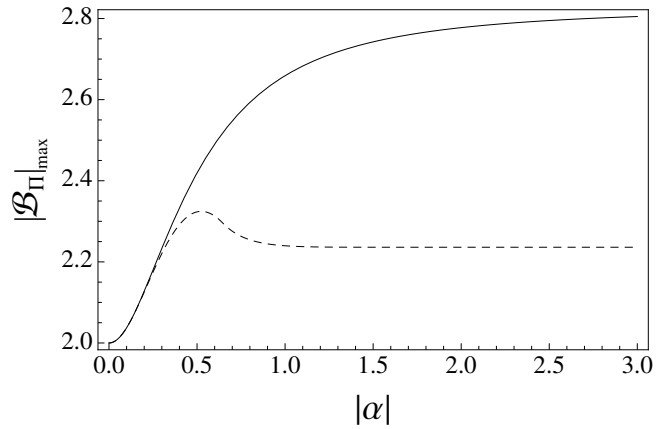

Figure 7: Numerically optimized values of Bell function $\mathcal{B}_\Pi$ with displaced parity measurements against $|\alpha|$. The solid curve corresponds to the absolute values of the Bell function maximized over arbitrary ζ, ζ', β and β', while the dashed curve corresponds to those values maximized over arbitrary β and β', but real ζ and ζ'.

ment parameters (ζ and ζ') to be real, our test becomes identical to the one in Ref. [59] and the result corresponds to the dashed curve in Fig. 7. However, it is not sufficient to reveal the maximal violation of the atom-field entangled state (3.1). In our numerical analysis, $\mathcal{B}_\Pi$ is optimized with respect to complex ζ, ζ', β, and β' that results in the solid curve in Fig. 7. Assuming that α is a real positive value, the optimizing conditions for $\mathcal{B}_\Pi$ are found as

$$\zeta = -\pi/4, \;\; \zeta' = i\pi/4, \;\; \beta = -\beta' = i|\beta|, \tag{3.14}$$

where $|\beta|$ satisfies

$$(|\alpha| - |\beta|)/(|\alpha| + |\beta|) = \tan 4|\alpha||\beta| \tag{3.15}$$

and is nearest to zero. As amplitude $|\alpha|$ increases, the degree of Bell violation rapidly gets larger up to Cirel'son's bound $2\sqrt{2}$.

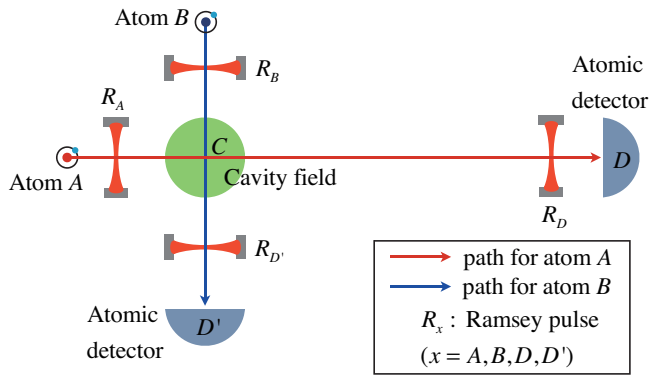

Figure 8: Schematic of the proposal. The horizontal arrow is to describe the entangled state (3.1) generation (with R_A and C) and measurement for atom A. The vertical arrow depicts the indirect parity measurement of the cavity field using ancillary atom B.

3.4 Approach Using Indirect Measurement

In this section, we discuss physical implementations of the Bell-CHSH inequality test using displaced parity measurements in a 'circular Rydberg atom'-'microwave cavity' configuration. Generation schemes for atom-field entangled states (3.1) have been theoretically studied and experimentally implemented [80, 81, 75, 82]. In the case of a scheme based on the off-resonant interaction [75], the required interaction Hamiltonian is

$$\hat{H}_I = \hbar\chi[(\hat{a}^\dagger\hat{a}+1)\,|e\rangle\langle e| - \hat{a}^\dagger\hat{a}\,|g\rangle\langle g|], \tag{3.16}$$

and $\chi = \Omega^2/(4\delta)$ is the coupling constant determined by the vacuum Rabi frequency Ω and detuning δ [75]. As shown in Fig. 8, $\pi/2$ Ramsey pulse with phase $-\pi/2$ (R_A) is applied to a circular Rydberg atom (A) prepared in the excited state $|e\rangle_A$ [83], which

results in an atomic superposition state:

$$|\phi_{-i}\rangle_A = (|e\rangle_A - i|g\rangle_A)/\sqrt{2}. \tag{3.17}$$

Then, a strong dispersive interaction in Eq. (3.16) between atom A and the cavity field produces the atom-field entangled state (3.1) for interaction time $t = \pi/(2\chi)$ [75].

Direct measurements of the light field in the microwave cavity are difficult to achieve, while indirect methods for parity measurements of the cavity field may be more feasible [84, 51, 75, 62]. A circular Rydberg atom (B) in Fig. 8 initially prepared in state $|e\rangle_B$ evolves to a superposition state $|\phi_{-i}\rangle_B$ by $\pi/2$ Ramsey pulse with phase $-\pi/2$ (R_B), and the total state is $|\Psi_{tot}\rangle_{ABC} = |\Psi\rangle_{AC}|\phi_{-i}\rangle_B$. The displacement operation, $\hat{\mathcal{D}}_C^\dagger(\beta) = \hat{\mathcal{D}}_C(-\beta)$, is then applied to the field right before atom B enters the cavity, and the same type of interaction as Eq. (3.16) between modes B and C follows. One may indirectly detect the cavity field by appropriately choosing the interaction time $t = \pi/(2\chi)$ between atom B and the field before detecting the atom. The interaction time may be controlled by selecting the velocity of atom B. The final measurement for atom A, represented by $\hat{\Gamma}_A(-\pi e^{-i\phi}/4)$, is performed using $\pi/2$ Ramsey pulse of phase $\pi - \phi$ (R_D) and atomic detector D. The measurement on atom B, *i.e.*, $\hat{\Gamma}_B(-\pi/4)$, for indirect probing is performed with the help of $\pi/2$ Ramsey pulse with π phase ($R_{D'}$) and atomic detector D'. The measurement operator is then represented as

$$\hat{\Upsilon}_{B,C}(\beta,t) = \hat{\mathcal{U}}_{B,C}(\beta,t)^\dagger \hat{O}_{B,C} \hat{\mathcal{U}}_{B,C}(\beta,t), \tag{3.18}$$

where and $|\pm\rangle = (|e\rangle \pm |g\rangle)/\sqrt{2}$. The correlation function

$$E(\zeta,\beta,t) = \left\langle \hat{\Gamma}_A(\zeta) \otimes \hat{\Upsilon}_{B,C}(\beta,t) \right\rangle \tag{3.19}$$

is calculated using state $|\Psi_{tot}\rangle_{ABC}$ as

$$
\begin{aligned}
E(\zeta,\,\beta,\,t) =& \frac{1}{2}\cos\theta e^{(|\alpha|^2+|\beta|^2-2|\alpha||\beta|\cos\Phi)(-1+\cos 2\chi t)} \\
& \times \cos[(|\alpha|^2+|\beta|^2-2|\alpha||\beta|\cos\Phi)\sin 2\chi t] \\
& - \frac{1}{2}\cos\theta e^{(|\alpha|^2+|\beta|^2+2|\alpha||\beta|\cos\Phi)(-1+\cos 2\chi t)} \\
& \times \cos[(|\alpha|^2+|\beta|^2+2|\alpha||\beta|\cos\Phi)\sin 2\chi t] \\
& + \frac{1}{2}\sin\theta e^{-|\alpha|^2-|\beta|^2-(|\alpha|^2-|\beta|^2)\cos 2\chi t-2|\alpha||\beta|\sin\Phi\sin 2\chi t} \\
& \times \cos[\phi-(|\alpha|^2-|\beta|^2)\sin 2\chi t+2|\alpha||\beta|\sin\Phi(-1+\cos 2\chi t)] \\
& + \frac{1}{2}\sin\theta e^{-|\alpha|^2-|\beta|^2-(|\alpha|^2-|\beta|^2)\cos 2\chi t+2|\alpha||\beta|\sin\Phi\sin 2\chi t} \\
& \times \cos[\phi+(|\alpha|^2-|\beta|^2)\sin 2\chi t+2|\alpha||\beta|\sin\Phi(-1+\cos 2\chi t)]
\end{aligned}
\tag{3.20}
$$

and the Bell function, $\mathcal{B}_{\Upsilon}$, is accordingly obtained. As expected, the optimizing conditions for $|\mathcal{B}_{\Upsilon}|_{\max}$ are identical to those for $|\mathcal{B}_O|_{\max}$ in Eqs. (3.14) and (3.15) with an additional condition, $t = t' = \pi/2\chi$. Our numerical study confirms that the optimized Bell function $|\mathcal{B}_{\Upsilon}|_{\max}$ plotted with the abovementioned conditions in Fig. 9 exactly overlaps with the solid curve in Fig. 7 as shown . This result is due to the fact that the indirect measurement (3.18) is basically equivalent to the displaced parity measurement (3.12) on the cavity field when t is chosen to be $\pi/(2\chi)$ [84]. *I.e.*, the measurement on atom B in the basis $\{|+\rangle,\ |-\rangle\}$ after the interaction time $t = \pi/(2\chi)$ is equivalent to the parity measurement on the cavity-field. In fact, it can be shown that the correlation functions (3.20) with $t = \pi/(2\chi)$ and (3.13) are identical. Of course, if we restrict ζ to be real, the optimized plot of the Bell function $|\mathcal{B}_{\Upsilon}|_{\max}$ approaches the dashed curve in Fig. 7.

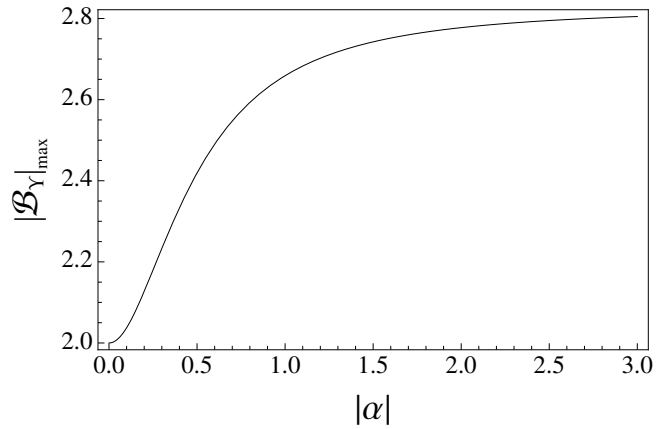

Figure 9: Numerically optimized values of Bell function $\mathcal{B}_Y$ with indirect measurements against $|\alpha|$. The result is found to be identical to the one using direct parity measurements shown as the solid curve in Fig. 7.

3.5 Decoherence and Loopholes

It is not difficult to predict that decoherence effects due to the cavity-field dissipation and the spontaneous emission of the atoms will obstruct Bell violations. This is particularly important when one intends to demonstrate a Bell violation free from the loopholes. In this section, we consider decoherence effects with realistic conditions for the Bell-CHSH inequality test using parity measurements and suggest quantitative requirements to perform a loophole-free Bell test.

3.5.1 Decoherence Effects in the Cavity-Atom System

There are two main effects that cause decoherence in our Bell inequality test, *i.e.*, spontaneous emissions from atoms and cavity field dissipations. In the atom-cavity system under consideration, one (or both) of these two effects may occur. The master equation which determines the time-evolution of the density operator, $\hat{\rho}(t)$, under the

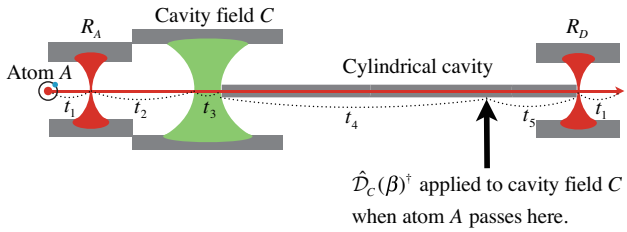

Figure 10: Sideview of the atom A's path with intervals of time. Each interval denotes an amount of time required for atom A to pass through the region related with atomic velocity v. We note that the distance $l = v \times (t_4 + t_5)$, which corresponds to the length of the cylindrical cavity, is a crucial factor in a loohole-free Bell inequality test.

atom-field interaction with spontaneous emissions and cavity dissipations is

$$\frac{d\hat{\rho}(t)}{dt} = \frac{1}{i\hbar}[\hat{H}_I, \hat{\rho}(t)] + \mathcal{L}\hat{\rho}(t), \tag{3.21}$$

with the Linblad decohering term $\mathcal{L}$ defined as

$$\begin{aligned} \mathcal{L}\hat{\rho} \equiv & \kappa(2\hat{a}\hat{\rho}\hat{a}^\dagger - \hat{a}^\dagger\hat{a}\hat{\rho} - \hat{\rho}\hat{a}^\dagger\hat{a}) \\ & + \gamma(2\hat{\sigma}_-\hat{\rho}\hat{\sigma}_+ - \hat{\sigma}_+\hat{\sigma}_-\hat{\rho} - \hat{\rho}\hat{\sigma}_+\hat{\sigma}_-), \end{aligned} \tag{3.22}$$

where κ is the dissipation rate of cavity field, and γ is the spontaneous emission rate.

It is known that the spontaneous emission rate of an atom can be significantly reduced by engineering the shape of the cavity that contains the atom [85, 86]. A complete inhibition of spontaneous emission was suggested using a cylindrical metal cavity with a diameter shorter than $1.8412c/\omega_0$, where ω_0 is the transition rate between atomic states $|e\rangle$ and $|g\rangle$ and c is the speed of light [86]. For our setup, the transition rate can be taken from Ref. [62] as $\omega_0 = 51.1$GHz. This means that the diameter should be smaller than 3.44mm that is experimentally achievable. As seen in Fig. 10, a long cylindrical cavity may be used between cavity C and Ramsey zone

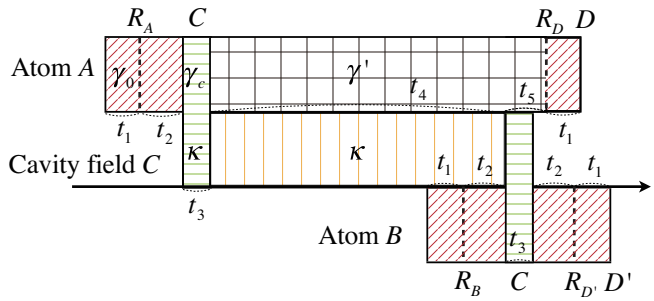

Figure 11: A timeline for decoherence with dynamical parameters related in each regions (from left to right). The top line is for atom A, the middle for cavity field C, and the bottom for atom B. The times when Ramsey pulses are applied are described as vertical dashed lines. We consider a Ramsey pulse application as an instant event as a Ramsey pulse lasts as short as 1 μs order. Regions are differently hatched depending on the types of dynamics. In the diagonally hatched regions, atoms A and B travel in free spaces with the spontaneous emission rate γ_0 before and after Ramsey pulses as shown in Fig. 8. In the cross-hatched region, atom A travels in a cylindrical cavity with the inhibited spontaneous emission rate γ'. In the vertically hatched region, the cavity dissipation with rate κ occurs in the cavity (C) field. The horizontally hatched regions correspond to the dynamics of the atom-field interaction $\hat{H}_I$ in the main cavity C together with spontaneous emission γ_c and cavity dissipation κ. Abbreviations C, D, D', R_A, R_B, R_D, and $R_{D'}$ are consistent with those in Fig. 8.

R_D to inhibit spontaneous emission.

The spontaneous emission rate γ_c inside the cavity C in Fig. 8 is also generally different from the spontaneous emission rate γ_0 in the vacuum. It is known that γ_c can be calculated by approximating the cavity in the one dimension while considering the effect of the atomic motion as described in Ref. [87]. In our case, $\gamma_c = 4.08$ Hz is obtained based on the result of Ref. [87] from the spontaneous emission rate in the vacuum, $\gamma_0 = 1/(2T_0)$ ($T_0 = 36$ ms is the atomic life time in the vacuum [75]) and related realistic parameters in a recent experiment [62].

Considering the discussions above, we present a timeline of decoherence effects in Fig. 11 together with time intervals defined in Table 1. Let us first consider the

Table 1: Definitions of time intervals

t_1	$\frac{1}{2}\times$ time required for an atom to pass through a cavity used for Ramsey pulse application
t_2	$t_1 + \frac{1}{2}\times$ time required for an atom to pass through the main cavity (C) without cavity waist
t_3	time required for an atom to pass through the main cavity(C)'s waist, $\pi/(2\chi)$
t_4	time required for atom A to pass through the long cylindrical cavity before the field displacement operation is applied to the cavity field
t_5	time required for atom A to pass through the remainder of the long cavity after the field displacement operation is applied
t_6	time required for atomic detection at D or D'

pathway of atom A, which corresponds to the top line of Fig. 11. Atom A undergoes spontaneous emission before and after the Ramsey pulse R_A with rate γ_0 (diagonally hatched part). Atom A then interacts with the cavity field with disspation rate κ under spontaneous emission (γ_c), which is represented by the horizontally hatched part. After the atom-field interaction, atom A passes through the cylindrical cavity experiencing inhibited spontaneous emission (γ'). Finally, atom A comes out of Ramsey pulse R_D experiencing spontaneous emission (γ_0), and is registered at detector D. In the mean while, cavity field C which have interacted with atom A undergoes field dissipation (κ) while atom A is passing through cylindrical cavity. Then, cavity field C begins to interacts with atom B under spontaneous emission (γ_c) and field dissipation (κ) after displacement operation on it. Atom B, used for an indirect measurement, experiences spontaneous emission (γ_0) around Ramsey pulse R_B, interaction with the cavity field (C) with spontaneous emmission (γ_c), and spontaneous emission (γ_0) before detection D'.

Here, we take the photon storage time $T_C = 0.13$ s ($\kappa = 1/(2T_C)$), $\Omega = 2\pi\cdot$

49 kHz and $\delta = 2\pi \cdot 65$ kHz ($\chi = \Omega^2/(4\delta) \approx 58$kHz) from recent experiments [62]. The solution of the master equation for the cavity dissipation alone with H_I, was examined in Ref. [88]. In next Sec. 3.6 , we obtain the solution of Eq. (3.21) and find an explicit form of the density operator and the correlation function. The Bell function can be constructed using the correlation function in Eq. (3.56) of Sec. 3.6. Note that we have assumed perfect Ramsey pulses during the procedures. Considering cavity dissipation, we employ the same optimizing conditions (3.14) except that $|\beta|$ is chosen to be the values that satisfy

$$\frac{|\alpha|e^{-\kappa(t_4+t_3)} - |\beta|}{|\alpha|e^{-\kappa(t_4+t_3)} + |\beta|} = \tan(4|\alpha|e^{-\kappa(t_4+t_3)}|\beta|), \tag{3.23}$$

and is nearest to zero.

3.5.2 Bell Violation and Separations under Practical Conditions without a Cylindrical Cavity

Let us first consider Bell violation depending on the separation $l = v \times (t_4 + t_5)$ between both parties *without* using a cylindrical cavity (thus $\gamma' = \gamma_0$). We choose some practical time-interval parameters as $t_1 = 80.0\,\mu$s, $t_2 = 166.5\,\mu$s, $t_3 = 27.1\,\mu$s, $t_6 = 20\,\mu$s and velocity of an atom $v = 250$ m/s [62, 89]. The Bell function with several choices of l are plotted in Fig. 12. The Bell function approaches the value near 2.7 when $l = 0.1$(meter), but it decreases as l gets larger. Clear Bell violations appear for $l \lesssim 2$(meter), however, this is insufficient for a space-like separation as we shall discuss in the next subsection.

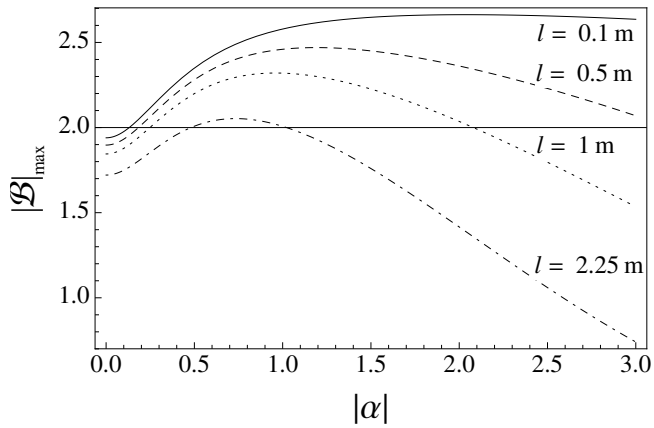

Figure 12: The Bell function under realistic conditions discussed in Sec. 3.5.2 are plotted with optimizing conditions in Eqs. (3.14) and (3.23) for several different cases of separation l. As the separation l gets larger, the maximum values of the Bell function decrease. The decoherence effects become heavier as $|\alpha|$ gets larger.

3.5.3 Requirements for a Bell Test Free from the Locality Loophole with a Cylindrical Cavity

In principle, a Bell test free from the locality loophole can be performed using a long cylindrical cavity with a low spontaneous emission rate (γ') and the main caivity with a low dissipation rate (κ). In order to close the locality loophole, the measurement event for atom A should not affect the measurement event for the cavity field C, and *vice versa* [50]. In other words, the measurement event for atom A should be outside of the "back light cone" from the detection event D' in Fig. 8. In the same manner, the measurement event for the cavity field C should not be in the back light cone from the detection event D. For simplicity, let us first suppose that each measurement process takes place at a single location (D and D'). In our Bell test, the time t_A required to measure atom A is smaller than the time required to measure field C (t_C) due to the indirect measurement scheme for field C. We assume that the measurement event for

the field C precedes to the measurement event for atom A by T (the opposite case will require a longer separation between the two parties). Then the conditions required to close the locality loophole are

$$\begin{aligned} d &\geq c(T + t_A), \\ d &\geq c(t_C - T), \end{aligned} \tag{3.24}$$

where d is the distance between D and D' and c is the speed of light.

In order to apply the locality-loophole-free conditions (3.24) to our Bell test setup in a more rigorous manner, one needs to consider locations of the local measurement elements. In Fig. 11, one can find that the measurement time for atom A (t_A) consists of the times for R_D (t_1) and D (t_6) and that for the field (t_C) consists of the times for C (t_3), R'_D ($t_2 + t_1$), and D' (t_6). A measurement event for each party actually does not take place at a single location, and both of the measurements are not even on a straight line. Therefore the distance d in Eqs. (3.24) needs to be replaced with the distances from the final detector of one party to the location where the measurement of the other party begins. A careful consideration leads to the conclusion that the following inequalities should be satisfied:

$$\begin{aligned} & v(t_3/2 + t_4 + t_5 + t_1 + t_6) \geq c(t_5 + t_1 + t_6), \\ & v\sqrt{(t_3/2 + t_2 + t_1 + t_6)^2 + (t_3/2 + t_4 + t_5)^2} \\ & \qquad \geq c(t_3 + t_2 + t_1 + t_6 - t_5). \end{aligned} \tag{3.25}$$

Using the feasible values of t_1, t_2, t_3, t_6 and v in the previous subsection, we find the minimum values $t_4 = 236.0\ s$ and $t_5 = 96.8\ \mu$s with which the equalities hold for Eqs. (3.25). Then, the minimum distance required for a Bell test free from the locality

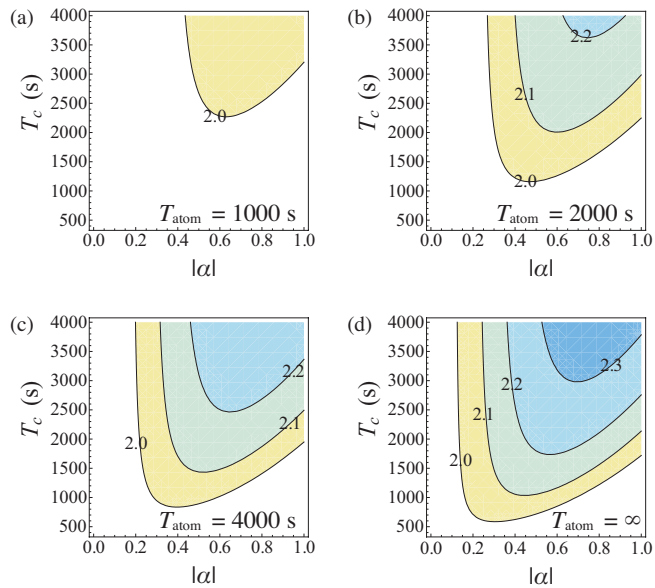

Figure 13: Contour plots of the Bell function with respect to photon storage time T_C in the main cavity and aplitude $|\alpha|$ of the entangled state. The atomic life time in cylindrical cavity $T_{\rm atom}$ is fixed at 1000, 2000, 4000 and ∞ (seconds). The minimum distance condition $l = 52.99$ (km) for a loophole-free Bell test was assumed. Higher inhibition of spontaneous emission in the cylindrical cavity reduces the required photon storage time in the main cavity.

loophole is found to be $l = 52.99$ km [62].

We finally consider conditions of the atomic life time $T_{\rm atom} = 1/(2\gamma')$ and the photon storage time $T_c = 1/(2\kappa)$ required for a Bell test free from the locality loohole. In Fig. 13, we plot the Bell function constructed using Eq. (3.56) in Sec. 3.6 with respect to the photon storage time in the main cavity and amplitude $|\alpha|$ of the atom-field entanglement. Here, the extended lifetime of the atom in the cylindrical cavity was assumed to be $T_{\rm atom}$ =1000, 2000, 4000, and ∞ (seconds). The distance l was assumed to be the minimum distance required for a loophole-free Bell test (52.99 km). For example, when $T_{\rm atom} = 2000$ (seconds), the photon storage time $T_C \sim 1160$

(seconds) at $|\alpha| \sim 0.47$ is required to see a Bell violation. If complete inhibition of the spontaneous emission in the cylindrical cavity is possible, (*i.e.*, $T_{\text{atom}} = \infty$), $T_C \sim 590$ at $|\alpha| \sim 0.3$ is required. Obviously, the stronger inhibition of the spontaneous emission in the cylindrical cavity relaxes the requirement of the photon storage time in the main cavity to see Bell violations. However, it still requires at least a few hundreds of seconds for the photon storage time to demonstrate a loophole-free Bell violation, while it is only about 0.13 s at present [90]. It would also be extremely challenging to build a long cylindrical cavity that strongly inhibits the spontaneous emission of atom A during such a long life time.

3.6 Solutions of the Master Equation for Matrix Elements

We first find general solutions of the master equation (3.21) for three types of decoherence processes step by step, *i.e.*, spontaneous emission of an atom, cavity dissipation, and atom-field interaction with spontaneous emission and cavity dissipation.

3.6.1 Spontaneous Emission for Atom

A density operator of a two-level atom, $\hat{\rho}_A(t)$, can be expressed as a matrix form

$$\hat{\rho}_A(t) = \begin{pmatrix} \rho_{A,ee}(t) & \rho_{A,eg}(t) \\ \rho_{A,ge}(t) & \rho_{A,gg}(t) \end{pmatrix}, \tag{3.26}$$

where $\rho_{A,ij}(t) = \langle i|\,\hat{\rho}_A(t)\,|j\rangle$. When an atom with a initial density matrix, $\hat{\rho}_A(0)$, goes through the spontaneous emission process for time t, its density matrix is straightfor-

wardly obatained using Eq. (3.21) with $\chi = 0$ and $\kappa = 0$ as

$$\begin{aligned}\hat{\rho}_A(t) =& \hat{S}_A(\gamma,t)[\hat{\rho}_A(0)] \\ =& \begin{pmatrix} e^{-2\gamma t}\rho_{A,ee}(0) & e^{-\gamma t}\rho_{A,eg}(0) \\ e^{-\gamma t}\rho_{A,ge}(0) & \rho_{A,gg}(0) - \rho_{A,ee}(0)(e^{-2\gamma t} - 1) \end{pmatrix},\end{aligned} \tag{3.27}$$

where superoperator $\hat{S}(\gamma,t)$ is defined for later use.

3.6.2 Dissipation for Cavity Field

In order to find the time evolution of the coherent-state part the density operator, it is sufficient to find the time evolution of an operator component $|\mu\rangle\langle\nu|$, where $|\mu\rangle$ and $|\nu\rangle$ are coherent states of amplitudes μ and ν. This solution for time t under the master equation (3.21) with $\chi = 0$ and $\gamma = 0$ is well known as [91, 92]

$$\exp[-\frac{(|\mu|^2 + |\nu|^2 - 2\nu^*\mu)(1 - \exp(-2\kappa t))}{2}] \left|\mu e^{-\kappa t}\right\rangle \left\langle \nu e^{-\kappa t}\right|. \tag{3.28}$$

3.6.3 Atom-Field Interaction with Spontaneous Emission and Cavity Dissipation

The density matrix $\hat{\rho}(t)$ for an atom-field state can be considered in a $2 \times \infty$ dimensional space, since we assume a two-level atom. It is possible to decompose the master equation (3.21) in $\{|e\rangle,\ |g\rangle\}$ basis with the density matrix elements $\hat{\rho}_{C,ij}(t) =$

$\langle i|\,\hat{\rho}(t)\,|j\rangle$. We then obtain equations

$$\begin{aligned}\frac{d}{dt}\hat{\rho}_{C,ee} =&\hat{\mathcal{L}}_{ee}\hat{\rho}_{C,ee} - 2\gamma\hat{\rho}_{C,ee}\\ =&-i\chi[\hat{a}^\dagger\hat{a},\hat{\rho}_{C,ee}] + \kappa(2\hat{a}\hat{\rho}_{C,ee}\hat{a}^\dagger - \hat{a}^\dagger\hat{a}\hat{\rho}_{C,ee} - \hat{\rho}_{C,ee}\hat{a}^\dagger\hat{a})\\ &-2\gamma\hat{\rho}_{C,ee},\end{aligned} \tag{3.29}$$

$$\begin{aligned}\frac{d}{dt}\hat{\rho}_{C,gg} =&\hat{\mathcal{L}}_{gg}\hat{\rho}_{C,gg} + 2\gamma\hat{\rho}_{C,ee}\\ =&i\chi[\hat{a}^\dagger\hat{a},\hat{\rho}_{C,gg}] + \kappa(2\hat{a}\hat{\rho}_{C,gg}\hat{a}^\dagger - \hat{a}^\dagger\hat{a}\hat{\rho}_{C,gg} - \hat{\rho}_{C,gg}\hat{a}^\dagger\hat{a})\\ &+2\gamma\hat{\rho}_{C,ee},\end{aligned} \tag{3.30}$$

$$\begin{aligned}\frac{d}{dt}\hat{\rho}_{C,eg} =&\hat{\mathcal{L}}_{eg}\hat{\rho}_{C,eg} - i\chi\hat{\rho}_{C,eg} - \gamma\hat{\rho}_{C,eg}\\ =&-i\chi(\hat{a}^\dagger\hat{a}+1)\hat{\rho}_{C,eg} - i\chi\hat{\rho}_{C,eg}\hat{a}^\dagger\hat{a}\\ &+\kappa(2\hat{a}\hat{\rho}_{C,eg}\hat{a}^\dagger - \hat{a}^\dagger\hat{a}\hat{\rho}_{C,eg} - \hat{\rho}_{C,eg}\hat{a}^\dagger\hat{a}) - \gamma\hat{\rho}_{C,eg},\end{aligned} \tag{3.31}$$

$$\begin{aligned}\frac{d}{dt}\hat{\rho}_{C,ge} =&\hat{\mathcal{L}}_{ge}\hat{\rho}_{C,ge} + i\chi\hat{\rho}_{C,ge} - \gamma\hat{\rho}_{C,ge}\\ =&i\chi\hat{\rho}_{C,ge}(\hat{a}^\dagger\hat{a}+1) + i\chi\hat{a}^\dagger\hat{a}\hat{\rho}_{C,ge}\\ &+\kappa(2\hat{a}\hat{\rho}_{C,ge}\hat{a}^\dagger - \hat{a}^\dagger\hat{a}\hat{\rho}_{C,ge} - \hat{\rho}_{C,ge}\hat{a}^\dagger\hat{a}) - \gamma\hat{\rho}_{C,ge}.\end{aligned} \tag{3.32}$$

We define the following superoperators for simplicity: $\hat{\mathcal{M}} = \hat{a}^\dagger\hat{a}\ \cdot\ $, $\hat{\mathcal{P}} = \ \cdot\ \hat{a}^\dagger\hat{a}$, and $\hat{\mathcal{J}} = \hat{a}\ \cdot\ \hat{a}^\dagger$. Then $\hat{\mathcal{L}}_{ee}$, $\hat{\mathcal{L}}_{gg}$, $\hat{\mathcal{L}}_{eg}$, and $\hat{\mathcal{L}}_{ge}$ can be expressed as,

$$\hat{\mathcal{L}}_{ee} \equiv 2\kappa\hat{\mathcal{J}} - r\hat{\mathcal{M}} - r^*\hat{\mathcal{P}}, \tag{3.33a}$$

$$\hat{\mathcal{L}}_{eg} \equiv 2\kappa\hat{\mathcal{J}} - r\hat{\mathcal{M}} - r\hat{\mathcal{P}}, \tag{3.33b}$$

where $r \equiv \kappa + i\chi$, and $\hat{\mathcal{L}}_{gg}$ and $\hat{\mathcal{L}}_{ge}$ are obtained by substituting χ with $-\chi$ in $\hat{\mathcal{L}}_{ee}$, and $\hat{\mathcal{L}}_{eg}$, respectively. A master equation of the form $d\hat{\rho}/dt = \hat{\mathcal{L}}\hat{\rho} + c\hat{\rho}$, where c is a constant and $\hat{\mathcal{L}}$ is a superoperator, can be solved with a usual exponential form $\exp[(\hat{\mathcal{L}} + c)t]\hat{\rho}$.

Solution for $\hat{\rho}_{C,ee}$

The solution of Eq. (3.29) is

$$\hat{\rho}_{C,ee}(t) = \exp[(\hat{\mathcal{L}}_{ee} - 2\gamma)t]\hat{\rho}_{C,ee}(0) = e^{-2\gamma t} e^{\hat{\mathcal{L}}_{ee}t} \hat{\rho}_{C,ee}(0). \tag{3.34}$$

where the factorization can be done by the similarity transformation [93]. Now we need to factorize $e^{\hat{\mathcal{L}}_{ee}t}$. This is solved with an ansatz (a technique can be found in Ref. [92])

$$\hat{\rho}_{C,ee}(t) = \exp[-2\gamma t] \exp[(-r\hat{\mathcal{M}} - r^*\hat{\mathcal{P}})t] \exp[f(t)2\kappa\hat{\mathcal{J}}]\hat{\rho}_{C,ee}(0), \tag{3.35}$$

where $f(t) = (1 - e^{-2\kappa t})/(2\kappa)$. For an initial state $\hat{\rho}_{C,ee}(0) = |\mu\rangle\langle\nu|$,

$$\hat{\rho}_{C,ee}(t) = \exp[-2\gamma t + \Theta(\kappa, 0, \mu, \nu, t)] \left|\mu e^{-rt}\right\rangle \left\langle \nu e^{-rt}\right| \tag{3.36}$$

with

$$\Theta(\kappa, \chi, \mu, \nu, t) := -\frac{1}{2}(|\nu|^2 + |\mu|^2)(1 - e^{-2\kappa t}) + \frac{\kappa}{r}(1 - e^{-2rt})\nu^*\mu. \tag{3.37}$$

Solution for $\hat{\rho}_{C,gg}$

In order to solve Eq. (3.30), we first assume $\gamma = 0$. A homogeneous solution is obtained from Eq. (3.36) by substituting χ with $-\chi$ as

$$\hat{\rho}^{h}_{C,gg}(t) = \exp[\Theta(\kappa, 0, \mu, \nu, t)] \left|\mu e^{-r^* t}\right\rangle \left\langle \nu e^{-r^* t}\right|. \tag{3.38}$$

Then it is obvious to see that the general solution $\hat{\rho}_{C,gg}(t)$ with $\gamma \neq 0$ is

$$\begin{aligned}\hat{\rho}_{C,gg}(t) &= \hat{\rho}^{h}_{C,gg}(t) + 2\gamma \int_0^t dt' \hat{\rho}_{C,ee}(t') \\ &= \exp[\Theta(\kappa, 0, \mu, \nu, t)] \left|\mu e^{-r^* t}\right\rangle \left\langle \nu e^{-r^* t}\right| \\ &+ 2\gamma \int_0^t dt' \exp[-2\gamma t' + \Theta(\kappa, 0, \mu, \nu, t')] \left|\mu e^{-rt'}\right\rangle \left\langle \nu e^{-rt'}\right|.\end{aligned} \tag{3.39}$$

Solution for $\hat{\rho}_{C,ge}$

The solution of Eq. (3.32) is

$$\hat{\rho}_{C,ge}(t) = \exp[(\hat{\mathcal{L}}_{ge} + i\chi - \gamma)t]\hat{\rho}_{C,ge}(0) = e^{(i\chi-\gamma)t} e^{\hat{\mathcal{L}}_{ge} t} \hat{\rho}_{C,ge}(0). \tag{3.40}$$

Factoring $e^{\hat{\mathcal{L}}_{eg} t}$ with an ansatz

$$\hat{\rho}_{C,ge}(t) = \exp[(i\chi - \gamma)t] \exp[(-r\hat{\mathcal{M}} - r^* \hat{\mathcal{P}})t] \exp[g(t) 2\kappa \hat{\mathcal{J}}] \hat{\rho}_{C,ee}(0), \tag{3.41}$$

where $g(t) = (1 - e^{-2r^* t})/(2r^*)$. For $\hat{\rho}_{C,ge}(0) = |\mu\rangle \langle \nu|$,

$$\hat{\rho}_{C,ge}(t) = \exp[(i\chi - \gamma)t + \Theta(\kappa, -\chi, \mu, \nu, t)] \left|\mu e^{-r^* t}\right\rangle \left\langle \nu e^{-rt}\right|. \tag{3.42}$$

Solution for $\hat{\rho}_{C,eg}$

The solution of Eq. (3.31) is obtained from Eq. (3.42) by substituting χ with $-\chi$ as

$$\hat{\rho}_{C,eg}(t) = \exp[(-i\chi-\gamma)t + \Theta(\kappa,\chi,\mu,\nu,t)] \left|\mu e^{-rt}\right\rangle \left\langle \nu e^{-r^* t}\right|. \tag{3.43}$$

3.7 Derivation of the Density Matrices for Atom-Field Entanglement and the Correlation Function

3.7.1 Atom-field Entanglement Generated Under Decoherence Effects

First, atom A initially prepared in $|e\rangle_A$ undergoes the spontaneous emission for the time t_1. After applying the first Ramsey pulse, $R_A = \hat{D}_A(-i\pi/4)$, explained in Sec. 3.4, atom A again undergoes the spontaneous emission for time t_2. Using Eqs. (3.27) again, it becomes

$$\begin{aligned}
&\hat{\mathcal{S}}_A(\gamma_0,t_2)\left[\hat{D}_A(-i\pi/4)|\left\{\hat{\mathcal{S}}_A(\gamma_0,t_1)[(|e\rangle\langle e|)_A]\right\}\hat{D}_A^\dagger(-i\pi/4)\right] \\
&= \begin{pmatrix} \frac{1}{2}e^{-2\gamma_0 t_2} & (-\frac{i}{2}+ie^{-2\gamma_0 t_1})e^{-\gamma_0 t_2} \\ (\frac{i}{2}-ie^{-2\gamma_0 t_1})e^{-\gamma_0 t_2} & (1-\frac{1}{2}e^{-2\gamma_0 t_2}) \end{pmatrix}.
\end{aligned} \tag{3.44}$$

Then atom A interacts with the cavity field C prepared in state $|i\alpha\rangle_C$. Using Eqs. (3.36), (3.39), (3.42) and (3.43), we find the state after the interaction time t_3 as $\hat{\rho}_{AC}^{(3)}$ with its matrix elements:

$$\hat{\rho}_{AC,ee}^{(3)} = \frac{1}{2}e^{-2\gamma_0 t_2 - 2\gamma_c t_3}\left|i\alpha e^{-rt_3}\right\rangle\left\langle i\alpha e^{-rt_3}\right|, \tag{3.45a}$$

$$\hat{\rho}^{(3)}_{AC,eg} = (-\frac{i}{2} + ie^{-2\gamma_0 t_1}) \exp[-\gamma_0 t_2 + (-i\chi - \gamma_c)t_3 + \Theta(\kappa, \chi, \alpha, \alpha, t_3)] \left|i\alpha e^{-rt_3}\right\rangle \left\langle i\alpha e^{-r^* t_3}\right|, \tag{3.45b}$$

$$\hat{\rho}^{(3)}_{AC,ge} = (\frac{i}{2} - ie^{-2\gamma_0 t_1}) \exp[-\gamma_0 t_2 + (i\chi - \gamma_c)t_3 + \Theta(\kappa, -\chi, \alpha, \alpha, t_3)] \left|i\alpha e^{-r^* t_3}\right\rangle \left\langle i\alpha e^{-rt_3}\right|, \tag{3.45c}$$

$$\hat{\rho}^{(3)}_{AC,gg} = (1 - \frac{1}{2}e^{-2\gamma_0 t_2}) \left|i\alpha e^{-r^* t_3}\right\rangle \left\langle i\alpha e^{-r^* t_3}\right| + 2\gamma_c \int_0^{t_3} dt \frac{1}{2} e^{-2\gamma_0 t_2 - 2\gamma_c t} \left|i\alpha e^{-rt}\right\rangle \left\langle i\alpha e^{-rt}\right|. \tag{3.45d}$$

3.7.2 Atom-Field Entanglement after Traveling for the Space-like Separation

We now derive the total density matrix right before $\hat{\mathcal{D}}^{\dagger}_{C}(\beta)$ is applied. The state $\hat{\rho}^{(3)}_{AC}$ undergoes spontaneous emission inside the cylindrical cavity and dissipation inside the cavity field C. The calculation can be done using the results in Sec. 3.6.3 with $\chi = 0$. Then the state becomes $\hat{\rho}^{(4)}_{AC}$, where

$$\hat{\rho}^{(4)}_{AC,ee} = \frac{1}{2} e^{-2\gamma_0 t_2 - 2\gamma_c t_3 - 2\gamma' t_4} \left|i\alpha e^{-rt_3 - \kappa t_4}\right\rangle \left\langle i\alpha e^{-rt_3 - \kappa t_4}\right|, \tag{3.46a}$$

$$\hat{\rho}^{(4)}_{AC,eg} = (-\frac{i}{2} + ie^{-2\gamma_0 t_1}) \exp[-\gamma_0 t_2 + (-i\chi - \gamma_c)t_3 - \gamma' t_4 + \Theta(\kappa, \chi, \alpha, \alpha, t_3) + \Theta(\kappa, 0, \alpha e^{-rt_3}, \alpha e^{-r^* t_3}, t_4)] \left|i\alpha e^{-rt_3 - \kappa t_4}\right\rangle \left\langle i\alpha e^{-r^* t_3 - \kappa t_4}\right|, \tag{3.46b}$$

$$\hat{\rho}^{(4)}_{AC,ge} = (\frac{i}{2} - ie^{-2\gamma_0 t_1}) \exp[-\gamma t_2 + (i\chi - \gamma_c)t_3 - \gamma' t_4 + \Theta(\kappa, -\chi, \alpha, \alpha, t_3) + \Theta(\kappa, 0, \alpha e^{-r^* t_3}, \alpha e^{-rt_3}, t_4)] \left| i\alpha e^{-r^* t_3 - \kappa t_4} \right\rangle \left\langle i\alpha e^{-rt_3 - \kappa t_4} \right| , \tag{3.46c}$$

$$\begin{aligned}\hat{\rho}^{(4)}_{AC,gg} = {} & (1 - \frac{1}{2}e^{-2\gamma_0 t_2}) \left| i\alpha e^{-r^* t_3 - \kappa t_4} \right\rangle \left\langle i\alpha e^{-r^* t_3 - \kappa t_4} \right| \\ & + 2\gamma_c \int_0^{t_3} dt \frac{1}{2} e^{-2\gamma_0 t_2 - 2\gamma_c t} \left| i\alpha e^{-rt - \kappa t_4} \right\rangle \left\langle i\alpha e^{-rt - \kappa t_4} \right| \\ & + 2\gamma' \int_0^{t_4} dt \frac{1}{2} e^{-2\gamma_0 t_2 - 2\gamma_c t_3 - 2\gamma' t} \left| i\alpha e^{-rt_3 - \kappa t} \right\rangle \left\langle i\alpha e^{-rt_3 - \kappa t} \right| ,\end{aligned} \tag{3.46d}$$

and here the subscripts are consistent with the previous ones.

3.7.3 Effects with Atom *B* for Indirect Measurement

After applying the displacement operation $\hat{\mathcal{D}}^{\dagger}_C(\beta)$, the total state becomes $\hat{\rho}^{\beta}_{AC} = \hat{\mathcal{D}}^{\dagger}_C(\beta)\hat{\rho}^{l}_{AC}\hat{\mathcal{D}}_C(\beta)$. Now, the probe atom B, which is in the same state as that of atom A in Eq. (3.44), goes into the cavity field of state $\hat{\rho}^{\beta}_{AC}$. The atom-field interaction H_I with the coupling constant χ occurs between atom B and field C for time t_3. When solving the master equation, it is convenient if one notes that the field-part of state $\hat{\rho}^{\beta}_{AC}$ can be expressed by coheren-state dyadics such as $|\mu\rangle\langle\nu|$. If the component of the cavity field, initially prepared as $|\mu\rangle\langle\nu|$, interacts with an atomic state (3.44) for time t_3, the resulting density operator element is obtained as $\hat{\Omega}_{BC}(\mu, \nu, t_3)$ with

$$\hat{\Omega}_{BC,ee}(\mu, \nu, t_3) = \frac{1}{2} e^{-2\gamma_0 t_2 - 2\gamma_c t_3 + \Theta(\kappa, 0, \mu, \nu, t_3)} \left| \mu e^{-rt_3} \right\rangle \left\langle \nu e^{-rt_3} \right| , \tag{3.47a}$$

$$\begin{aligned}\hat{\Omega}_{BC,eg}(\mu, \nu, t_3) = {} & (-\frac{i}{2} + ie^{-2\gamma_0 t_1}) \exp[-\gamma_0 t_2 + (-i\chi - \gamma_c)t_3 \\ & + \Theta(\kappa, \chi, \mu, \nu, t_3)] \left| \mu e^{-rt_3} \right\rangle \left\langle \nu e^{-r^* t_3} \right| ,\end{aligned} \tag{3.47b}$$

$$\hat{\Omega}_{BC,ge}(\mu,\nu,t_3) = (\frac{i}{2} - ie^{-2\gamma_0 t_1})\exp[-\gamma_0 t_2 + (i\chi-\gamma_c)t_3 + \Theta(\kappa,-\chi,\mu,\nu,t_3)]\left|\mu e^{-r^* t_3}\right\rangle\left\langle \nu e^{-rt_3}\right|, \tag{3.47c}$$

$$\hat{\Omega}_{BC,gg}(\mu,\nu,t_3) = (1-\frac{1}{2}e^{-2\gamma_0 t_2})e^{\Theta(\kappa,0,\mu,\nu,t_3)}\left|\mu e^{-r^* t_3}\right\rangle\left\langle \nu e^{-r^* t_3}\right| + 2\gamma_c\int_0^{t_3} dt\frac{1}{2}e^{-2\gamma_0 t_2 - 2\gamma_c t + \Theta(\kappa,0,\mu,\nu,t)}\left|\mu e^{-rt}\right\rangle\left\langle \nu e^{-rt}\right|. \tag{3.47d}$$

We used Eqs. (3.36), (3.39), (3.42) and (3.43) again to find Eqs. (3.47a)-(3.47d). Therefore, $\hat{\rho}_{AC}^{\beta}$ interacts with atom B and evolves to

$$\hat{\rho}_{ABC} = (|e\rangle\langle e|)_A \otimes \hat{\rho}_{BC,ee} + (|e\rangle\langle g|)_A \otimes \hat{\rho}_{BC,eg} + (|g\rangle\langle e|)_A \otimes \hat{\rho}_{BC,ge} + (|g\rangle\langle g|)_A \otimes \hat{\rho}_{BC,gg}, \tag{3.48}$$

where

$$\hat{\rho}_{BC,ee} = \frac{1}{2}e^{-2\gamma_0 t_2 - 2\gamma_c t_3 - 2\gamma'(t_4+t_3)} \hat{\Omega}_{BC}(i\alpha e^{-rt_3-\kappa t_4} - \beta, i\alpha e^{-rt_3-\kappa t_4} - \beta, t_3), \tag{3.49a}$$

$$\hat{\rho}_{BC,eg} = (-\frac{i}{2} + ie^{-2\gamma_0 t_1})\exp[-\gamma_0 t_2 + (-i\chi-\gamma_c)t_3 - \gamma'(t_4+t_3) + \Theta(\kappa,\chi,\alpha,\alpha,t_3) + \Theta(\kappa,0,\alpha e^{-rt_3},\alpha e^{-r^* t_3},t_4) - 2ie^{-\kappa(t_4+t_3)}\sin(\chi t_3)\mathrm{Im}(\alpha^*\beta)] \hat{\Omega}_{BC}(i\alpha e^{-rt_3-\kappa t_4} - \beta, i\alpha e^{-r^* t_3-\kappa t_4} - \beta, t_3) \tag{3.49b}$$

$$\hat{\rho}_{BC,ge} = (\frac{i}{2} - ie^{-2\gamma_0 t_1})\exp[-\gamma_0 t_2 + (i\chi-\gamma_c)t_3 - \gamma'(t_4+t_3) + \Theta(\kappa,-\chi,\alpha,\alpha,t_3) + \Theta(\kappa,0,\alpha e^{-r^* t_3},\alpha e^{-rt_3},t_4) + 2ie^{-\kappa(t_4+t_3)}\sin(\chi t_3)\mathrm{Im}(\alpha^*\beta)] \hat{\Omega}_{BC}(i\alpha e^{-r^* t_3-\kappa t_4} - \beta, i\alpha e^{-rt_3-\kappa t_4} - \beta, t_3) \tag{3.49c}$$

$$
\begin{aligned}
\hat{\rho}_{BC,gg} &= (1-\frac{1}{2}e^{-2\gamma_0 t_2})\hat{\Omega}_{BC}(i\alpha e^{-r^* t_3-\kappa t_4}-\beta, i\alpha e^{-r^* t_3-\kappa t_4}-\beta, t_3) \\
&+ 2\gamma_c \int_0^{t_3} dt \frac{1}{2} e^{-2\gamma_0 t_2 - 2\gamma_c t}\hat{\Omega}_{BC}(i\alpha e^{-rt-\kappa t_4}-\beta, i\alpha e^{-rt-\kappa t_4}-\beta, t_3) \\
&+ 2\gamma' \int_0^{t_4} dt \frac{1}{2} e^{-2\gamma_0 t_2 - 2\gamma_c t_3 - 2\gamma' t}\hat{\Omega}_{BC}(i\alpha e^{-rt_3-\kappa t}-\beta, i\alpha e^{-rt_3-\kappa t}-\beta, t_3) \\
&+ \frac{1}{2} e^{-2\gamma_0 t_2 - 2\gamma_c t_3 - 2\gamma' t_4}\hat{\Omega}_{BC}(i\alpha e^{-rt_3-\kappa t_4}-\beta, i\alpha e^{-rt_3-\kappa t_4}-\beta, t_3) \\
&\times (1-e^{-2\gamma' t_3}).
\end{aligned}
\tag{3.49d}
$$

Spontaneous emissions of atom A and B that may occur after this point shall be taken into account when we derive the correlation function. Since the field state is not considered any more from this point before the final measurements, the cavity dissipation can be ignored. By tracing out the cavity field, we get

$$
\hat{\rho}_{AB} = \mathrm{Tr}_C \hat{\rho}_{ABC} = \sum_{i,j=e,g} (|i\rangle\langle j|)_A \otimes \hat{\sigma}_{B,ij}, \tag{3.50}
$$

where

$$
\begin{aligned}
\hat{\sigma}_{B,ee} =& \mathrm{Tr}_C \hat{\rho}_{BC,ee} \\
=& \frac{1}{2} e^{-2\gamma_0 t_2 - 2\gamma_c t_3 - 2\gamma'(t_4+t_3)} \\
& \hat{\upsilon}_B(i\alpha e^{-rt_3-\kappa t_4}-\beta, i\alpha e^{-rt_3-\kappa t_4}-\beta, t_3),
\end{aligned}
\tag{3.51a}
$$

$$
\begin{aligned}
\hat{\sigma}_{B,eg} =& (-\frac{i}{2} + ie^{-2\gamma_0 t_1}) \exp[-\gamma_0 t_2 + (-i\chi-\gamma_c)t_3 - \gamma'(t_4+t_3) \\
& + \Theta(\kappa,\chi,\alpha,\alpha,t_3) + \Theta(\kappa,0,\alpha e^{-rt_3}, \alpha e^{-r^* t_3}, t_4) \\
& - 2ie^{-\kappa(t_4+t_3)} \sin(\chi t_3)\mathrm{Im}(\alpha^*\beta)] \\
& \hat{\upsilon}_B(i\alpha e^{-rt_3-\kappa t_4}-\beta, i\alpha e^{-r^* t_3-\kappa t_4}-\beta, t_3),
\end{aligned}
\tag{3.51b}
$$

$$\begin{aligned}\hat{\sigma}_{B,ge} =&(\frac{i}{2}-ie^{-2\gamma_0 t_1})\exp[-\gamma_0 t_2+(i\chi-\gamma_c)t_3-\gamma'(t_4+t_3)\\&+\Theta(\kappa,-\chi,\alpha,\alpha,t_3)+\Theta(\kappa,0,\alpha e^{-r^* t_3},\alpha e^{-rt_3},t_4)\\&+2ie^{-\kappa(t_4+t_3)}\sin(\chi t_3)\mathrm{Im}(\alpha^*\beta)]\\&\hat{\mho}_B(i\alpha e^{-r^* t_3-\kappa t_4}-\beta,i\alpha e^{-rt_3-\kappa t_4}-\beta,t_3),\end{aligned}\tag{3.51c}$$

$$\begin{aligned}&\hat{\sigma}_{B,gg}=(1-\frac{1}{2}e^{-2\gamma_0 t_2})\hat{\mho}_B(i\alpha e^{-r^* t_3-\kappa t_4}-\beta,i\alpha e^{-r^* t_3-\kappa t_4}-\beta,t_3)\\&+2\gamma_c\int_0^{t_3}dt\frac{1}{2}e^{-2\gamma_0 t_2-2\gamma_c t}\hat{\mho}_B(i\alpha e^{-rt-\kappa t_4}-\beta,i\alpha e^{-rt-\kappa t_4}-\beta,t_3)\\&+2\gamma'\int_0^{t_4}dt\frac{1}{2}e^{-2\gamma_0 t_2-2\gamma_c t_3-2\gamma' t}\hat{\mho}_B(i\alpha e^{-rt_3-\kappa t}-\beta,i\alpha e^{-rt_3-\kappa t}-\beta,t_3)\\&+\frac{1}{2}e^{-2\gamma_0 t_2-2\gamma_c t_3-2\gamma' t_4}\hat{\mho}_B(i\alpha e^{-rt_3-\kappa t_4}-\beta,i\alpha e^{-rt_3-\kappa t_4}-\beta,t_3)\\&\times(1-e^{-2\gamma' t_3}),\end{aligned}\tag{3.51d}$$

and operator $\hat{\mho}_B(\mu,\nu,t_3)=\mathrm{Tr}_C\hat{\Omega}_{BC}(\mu,\nu,t_3)$ is determined as

$$\mho_{B,ee}(\mu,\nu,t_3)=\frac{1}{2}e^{-2\gamma_0 t_2-2\gamma_c t_3+\Theta(\kappa,0,\mu,\nu,t_3)-\frac{1}{2}(|\mu|^2+|\nu|^2-2\mu\nu^*)\exp(-2\kappa t_3)},\tag{3.52a}$$

$$\begin{aligned}\mho_{B,eg}(\mu,\nu,t_3)=&(-\frac{i}{2}+ie^{-2\gamma_0 t_1})\exp[-\gamma_0 t_2+(-i\chi-\gamma_c)t_3\\&+\Theta(\kappa,\chi,\mu,\nu,t_3)-\frac{1}{2}(|\mu|^2+|\nu|^2-2\mu\nu^* e^{-2i\chi t_3})e^{-2\kappa t_3}],\end{aligned}\tag{3.52b}$$

$$\begin{aligned}\mho_{B,ge}(\mu,\nu,t_3)=&(\frac{i}{2}-ie^{-2\gamma_0 t_1})\exp[-\gamma_0 t_2+(i\chi-\gamma_c)t_3\\&+\Theta(\kappa,-\chi,\mu,\nu,t_3)-\frac{1}{2}(|\mu|^2+|\nu|^2-2\mu\nu^* e^{2i\chi t_3})e^{-2\kappa t_3}],\end{aligned}\tag{3.52c}$$

$$\begin{aligned}&\mho_{B,gg}(\mu,\nu,t_3)=(1-\frac{1}{2}e^{-2\gamma t_2})e^{\Theta(\kappa,0,\mu,\nu,t_3)-\frac{1}{2}(|\mu|^2+|\nu|^2-2\mu\nu^*)\exp(-2\kappa t_3)}\\&+2\gamma_c\int_0^{t_3}dt\frac{1}{2}e^{-2\gamma_0 t_2-2\gamma_c t+\Theta(\kappa,0,\mu,\nu,t)-\frac{1}{2}(|\mu|^2+|\nu|^2-2\mu\nu^*)\exp(-2\kappa t)}.\end{aligned}\tag{3.52d}$$

3.7.4 Decoherence Right before Final Measurements and the Correlation Function

We now consider the last measurement process for both parties. Atom A experiences spontaneous emission for time $t_5 - t_3$ with rate γ', then atomic displacement operation $\hat{D}_A^\dagger(-e^{-i\phi}\pi/4)$ is applied. After the displacement operation, atom A evolves again under the spontaneous emission for time t_1 with rate γ_0. We define superoperator $\hat{\mathcal{X}}$ to describe this process as

$$\begin{aligned}&\hat{\mathcal{X}}_A(\gamma', \gamma_0, t_5 - t_3, t_1, \phi)\left[\hat{\rho}_A\right] \\ &= \hat{\mathcal{S}}_A(\gamma_0, t_1)\left[\hat{D}_A^\dagger(-e^{-i\phi}\pi/4)\left\{\hat{\mathcal{S}}_A(\gamma', t_5 - t_3)\left[\hat{\rho}_A\right]\right\}\hat{D}_A(-e^{-i\phi}\pi/4)\right]\end{aligned} \tag{3.53}$$

Atom B undergoes spontaneous emission for time t_2 with rate γ_0, and displacement operation $\hat{D}_B^\dagger(-\pi/4)$ is applied. Then, it experiences spontaneous emission for time t_1 with rate γ_0 just before the final measurement. This process can be expressed as

$$\begin{aligned}&\hat{\mathcal{X}}_B(\gamma_0, \gamma_0, t_2, t_1, 0)\left[\hat{\rho}_B\right] \\ &= \hat{\mathcal{S}}_B(\gamma_0, t_1)\left[\hat{D}_B^\dagger(-\pi/4)\left\{\hat{\mathcal{S}}_B(\gamma_0, t_2)\left[\hat{\rho}_B\right]\right\}\hat{D}_B(-\pi/4)\right]\end{aligned} \tag{3.54}$$

The final density operator used to obtain the correlation function is then obtained using state $\hat{\rho}_{AB}$ in Eq. (3.50) with $\hat{\mathcal{X}}_A$ and $\hat{\mathcal{X}}_B$ as

$$\hat{\rho}_{AB}^{\text{final}} = \hat{\mathcal{X}}_A(\gamma', \gamma_0, t_5 - t_3, t_1, \phi) \otimes \hat{\mathcal{X}}_B(\gamma_0, \gamma_0, t_2, t_1, 0)\left[\hat{\rho}_{AB}\right]. \tag{3.55}$$

The correlation function is obtained as the expectation value of dichotomic measurements (3.4) performed by both the parties:

$$
\begin{aligned}
&E(\phi,\beta,t_1,t_2,t_3,t_4,t_5) = \mathrm{Tr}[\hat{\rho}_{AB}^{\mathrm{final}}\hat{\Gamma}_A \otimes \hat{\Gamma}_B] \\
=&\frac{1}{2}e^{-2\gamma_0 t_2 - 2\gamma_c t_3 - 2\gamma' t_4}(e^{-2\gamma_0 t_1}-1)(1-e^{-2\gamma' t_3}+e^{-2\gamma' t_5})\xi_B(\Lambda_1,\Lambda_1,t_3) \\
&+\mathcal{Z}\,\xi_B(\Lambda_1,\Lambda_2,t_3)+\mathcal{Z}^*\xi_B(\Lambda_2,\Lambda_1,t_3) \\
&+(e^{-2\gamma_0 t_1}-1)\{(1-\frac{1}{2}e^{-2\gamma_0 t_2})\xi_B(\Lambda_2,\Lambda_2,t_3) \\
&+2\gamma_c\int_0^{t_3}dt\frac{1}{2}e^{-2\gamma_0 t_2-2\gamma_c t}\xi_B(i\alpha e^{-rt-\kappa t_4}-\beta, i\alpha e^{-rt-\kappa t_4}-\beta,t_3) \\
&+2\gamma'\int_0^{t_4}dt\frac{1}{2}e^{-2\gamma_0 t_2-2\gamma_c t_3-2\gamma' t}\xi_B(i\alpha e^{-rt_3-\kappa t}-\beta, i\alpha e^{-rt_3-\kappa t}-\beta,t_3)\},
\end{aligned}
\tag{3.56}
$$

where

$$
\begin{aligned}
\xi_B(\mu,\nu,t_3) =&(\mho_{B,ee}(\mu,\nu,t_3)+\mho_{B,gg}(\mu,\nu,t_3))(e^{-2\gamma_0 t_1}-1) \\
&+(\mho_{B,eg}(\mu,\nu,t_3)+\mho_{B,ge}(\mu,\nu,t_3))e^{-\gamma_0 t_5-2\gamma_0 t_1}, \\
\mathcal{Z} =&(-\frac{i}{2}+ie^{-2\gamma_0 t_1}) \\
&\exp\Big\{-\gamma_0(t_2+2t_1)+(-i\chi-\gamma_c)t_3-\gamma'(t_4+t_5)+\Theta(\kappa,\chi,\alpha,\alpha,t_3) \\
&+\Theta(\kappa,0,\alpha e^{-rt_3},\alpha e^{-r^*t_3},t_4)-2ie^{-\kappa(t_4+t_3)}\sin(\chi t_3)\mathrm{Im}(\alpha^*\beta)+i\phi\Big\},
\end{aligned}
\tag{3.57}
$$

$\Lambda_1 = i\alpha e^{-rt_3-\kappa t_4}-\beta$ and $\Lambda_2 = i\alpha e^{-r^*t_3-\kappa t_4}-\beta$. Using this correlation function, one can eventually construct the Bell function using Eq. (3.3).

3.8 Remarks

We have investigated Bell-CHSH inequality tests with entanglement between a two-level atom and a coherent-state field in a cavity. In order to detect the cavity field for these tests, photon on/off measurements and photon number parity measurements, respectively, have been attempted. When photon on/off measurements with the perfect efficiency are used, the maximum value of the Bell violation is $\mathcal{B}_O \approx 2.61$ at $|\alpha| \approx 0.664$. In order to see a violation of the Bell-CHSH inequality, at least 50% of detection efficiency is required. When photon parity measurements are used, the value of the Bell-CHSH violation rapidly increases as α gets larger, and it approaches Cirel'son's bound for $\alpha \gg 1$. Although precise direct measurements of cavity fields are experimentally difficult, photon number parity measurements for the cavity field can be effectively performed using ancillary probe atoms and atomic detectors. We have fully analyzed decoherence effects in both field and atomic modes and discuss conditions required to perform a Bell inequality test free from the locality loophole.

Our proposal may be considered an attempt to analyze a Bell inequality test using entanglement between a microscopic system and a mesoscopic classical system. Since atomic detectors are known to be highly efficient [94], it may also be a reasonable target to perform this type of experiment in a way free from the detection loophole. In principle, a Bell inequality test free from the locality loophole in our framework using atom-field entanglement may be performed using a long cylindrical cavity for the atom with a low spontaneous emission rate [86]. However, our analysis shows that it would be extremely demanding to perform a Bell inequality test free from both the locality and detection loopholes in this framework since the main cavity for field with a low dissipation rate would be necessary together with

a long cylindrical cavity. Our mathematical scheme but which uses different system (superconducting qubit and microwave cavity photon) was implemented by Ref. [95]

Chapter 4

EPR Steering with Entangled Coherent States

4.1 Introduction

The so called, EPR paradox [30], was the first example which caught the nonlocal property of the quantum theory. However, Schrödinger was the first one who caught the idea of EPR steering[35]. Later, the concept of EPR steering was rigorously define by [9], which also revealed the hierarchy between Bell nonlocality, entanglement, and EPR steering. The idea of the coherent state also had been developed by Schrödinger [96]. Entangled coherent states (ECSs) are often called as Schrödinger's cat states, because when the amplitude of ECSs is large, they are in the superposition of distinct macroscopic states. Thus, it is very intriguing to demonstrate nonlocal characteristic of Schrödinger's cat states. Studies under the similar goal had been conducted with Bell nonlocality [67, 68]. However, since EPR-steering is in the form weaker nonlocality than Bell nonlocality [9]. In fact, loophole-free demonstration of EPR-steering was realized [10], whereas that of Bell nonlocality have not been reported. Note that there is a similarl approach which studies EPR-steering of ECSs with entropic steering inequalities [97]. Our work is motivated from Jones *et al.* [98] and their EPR-steering inequality for single-photon entanglement.

4.2 EPR-Steering Inequalities with Entangled Coherent States

Steering scenario requires two spatially separated parties, namely, Alice and Bob. Throughout this chapter, we assume that Alice is the party who is trying to demonstrate her nonlocal ability to steer the other party, Bob. Bob first, asks Alice to perform his randomly chosen measurements. With her results reported, Bob checks whether his conditioned states can be explained by local hidden state (LHS) models. If his states cannot be explained by any LHS model, then Alice is said to have the ability steer Bob, demonstrating the EPR steering.

Jones *et al.* derived the following inequality to demonstrate EPR-steering of a single-photon entangled state [98]

$$|\psi\rangle_{AB} = \frac{1}{2}\left(|0\rangle|1\rangle - |1\rangle|0\rangle\right): \tag{4.1}$$

$$\mathcal{S} = \frac{1}{\pi}\int_{-\pi/2}^{\pi/2} d\theta \mathcal{E}(\theta) - \frac{2}{\pi}\mathcal{P} \leqslant 0 \tag{4.2}$$

is composed of expectation values of equatorial measurement $\mathcal{E}(\theta) = \left\langle \hat{A}_\theta \otimes \hat{\sigma}_\theta \right\rangle$ and polar measurement $\mathcal{P}$, where $\hat{\sigma}_\theta = e^{-i\theta}|1\rangle\langle 0| + e^{i\theta}|0\rangle\langle 1|$ is Bob's equatorial dichotomic measurement on the Bloch sphere, and $\hat{A}_\theta$ is Alice's equatorial-like measurement chosen accordingly.

$$\mathcal{P} = E_{A_z}\left[\sqrt{1 - \langle\hat{\sigma}_z\rangle^2_{a_z}}\right] \tag{4.3}$$

is Bob's conditional expectation value of $\sqrt{1 - \langle\hat{\sigma}_z\rangle^2_{a_z}}$ averaged over outcome results a_z's from Alice's polar-like measurement $\hat{A}_z$, where $\hat{\sigma}_z = |1\rangle\langle 1| - |0\rangle\langle 0|$ is Bob's polar measurement on the Bloch sphere. They also have come up with the finite

version of the inequality (4.2) as the following:

$$\mathcal{S}_n = \frac{1}{n}\sum_{i=1}^{n}\mathcal{E}(\theta_i) - f(n)\mathcal{P} \leqslant 0, \tag{4.4}$$

where

$$f(n) = \frac{1}{n}\left(\left|\sin(\frac{n\pi}{2})\right| + 2\sum_{k=1}^{[n/2]}\sin\left[(2k-1)\frac{\pi}{2n}\right]\right) \tag{4.5}$$

and $\theta_i = -\pi/2 + i\pi/n$. It is worth to note that $\mathcal{S}_n$ converges to $\mathcal{S}$ as n approaches to ∞. In order to demonstrate EPR-steering, $\mathcal{S}(\mathcal{S}_n)$ is required to exceed the bound 0, while the maximum bound 1 can be achieved by exploiting the property of anti-correlated state (4.1), such that Alice's measurement strategy is chosen as $\hat{A}_\theta = -\sigma_\theta$ and $\hat{A}_z = \sigma_z$.

We are interested in testing the EPR-steering inequalities (4.2) and (4.4) with the following entangled coherent state with negative phase:

$$|\Psi\rangle_{AB} = \frac{1}{\sqrt{2-2e^{-4|\alpha|^2}}}\Big(|-\alpha\rangle|\alpha\rangle - |\alpha\rangle|-\alpha\rangle\Big). \tag{4.6}$$

The entangled coherent state $|\Psi\rangle_{AB}$ is generated by passing a superposition coherent state

$$|\phi\rangle = \frac{1}{\sqrt{2-2e^{-4|\alpha|^2}}}\Big(|-\sqrt{2}\alpha\rangle - |\sqrt{2}\alpha\rangle\Big) \tag{4.7}$$

through the beam splitter with the intensity transmission coefficient $T = \frac{1}{2}$ (intensity reflection coefficient $R = 1 - T$), where $|\pm\alpha\rangle$ is a coherent state with an amplitude $\pm\alpha$ ($\alpha \geq 0$). The entangled coherent state $|\Psi\rangle_{AB}$ becomes the single photon entangled state $|\psi\rangle_{AB}$ as α decreases to 0 with $T = 1/2$ [71]. The bound of steering inequality

is dependent not on the state being measured but only on the Bob's measurement operators, hence we may change his basis such that $\left|\frac{1\pm1}{2}\right\rangle \rightarrow$

$$\begin{aligned}\left|\pm_\gamma\right\rangle :=& \frac{1}{2}\left(\frac{1}{\sqrt{1+e^{-2|\gamma|^2}}} \pm \frac{1}{\sqrt{1-e^{-2|\gamma|^2}}}\right)|\gamma\rangle \\ &+ \frac{1}{2}\left(\frac{1}{\sqrt{1+e^{-2|\gamma|^2}}} \mp \frac{1}{\sqrt{1-e^{-2|\gamma|^2}}}\right)|-\gamma\rangle\end{aligned} \tag{4.8}$$

while keeping Bob's measurements unitarily equivalent as

$$\hat{\sigma}_z = |+_\alpha\rangle\langle+_\alpha| - |-_\alpha\rangle\langle-_\alpha|, \tag{4.9}$$

$$\hat{\sigma}_\theta = e^{-i\theta}|+_\alpha\rangle\langle-_\alpha| + e^{i\theta}|-_\alpha\rangle\langle+_\alpha|. \tag{4.10}$$

In the EPR steering scenario, Bob's measurements may be done indirectly by state tomography (e.g. homodyne tomography). However, it enforces Alice to report the specific measurement results (±1) in a direct way so that Bob can test whether his conditioned states violate local hidden state model. Unfortunately, Alice's measurement strategy for anti-correlated states, $\hat{A}_\theta = -\hat{\sigma}_\theta$ and $\hat{A}_z = \hat{\sigma}_z$ in the basis $|\pm_\alpha\rangle$, cannot be exactly performed but only be approximated as in the Ref [99, 100, 101].

In the following subsections, we investigate three steering inequalities adopting different equatorial-like measurements for Alice, $\hat{A}_\theta$, while Alice's polar-like measurement is identically approximated by the following homodyne measurement

$$\hat{A}_z = \int_0^\infty dr\,|r\rangle\langle r| - \int_{-\infty}^0 dr\,|r\rangle\langle r|, \tag{4.11}$$

where $|r\rangle$ is a quadrature eigenstate.

4.2.1 Homodyne Measurement with Nonlinear Interaction and Displacement Operation

Alice's equatorial-like measurements can be approximated by using homodyne measurement $\hat{A}_z$ preceded by Kerr nonlinear interaction $\hat{U}_{NL} = \exp(-i\hat{\mathcal{H}}_{NL}t/\hbar)$ and displacement operation

$$\hat{D}(\frac{i\chi_\theta}{4\alpha^*}) = \exp\left[\frac{i\chi_\theta}{4}\left(\frac{\hat{a}_A^\dagger}{\alpha^*} + \frac{\hat{a}_A}{\alpha}\right)\right],$$

where $\hat{\mathcal{H}}_{NL} = \hbar\Omega(\hat{a}_A^\dagger\hat{a}_A)^2$ is the hamiltonian with nonlinear susceptibility of the medium denoted as Ω, the interaction time $t = \pi/\Omega$ is chosen to perform x-axis $\pi/2$ rotation as in the Ref. [99], and $\hat{a}_A$ is the field annihilation operator for the Alice's mode. Corresponding steering inequality to Eq. (4.2) is

$$\mathcal{S}_\mathcal{F} = \frac{1}{\pi}\int_{-\pi/2}^{\pi/2} d\theta \mathcal{E}_\mathcal{F}(\theta) - \frac{2}{\pi}\mathcal{P} \leqslant 0, \tag{4.12}$$

where

$$\mathcal{E}_\mathcal{F}(\theta) = \left\langle \mathrm{sgn}\theta \hat{D}^\dagger(\chi_\theta)\hat{U}_{NL}^\dagger \hat{A}_z \hat{U}_{NL}\hat{D}(\chi_\theta) \otimes \hat{\sigma}_\theta \right\rangle. \tag{4.13}$$

The efficiency of the homodyne measurement can be simulated by introducing a perfect homodyne detection with a beam splitter of the intensity transmission coefficient η_h in front of it, which mixes the vacuum state in the idler mode $|0\rangle_i$ and the Alice's mode [76]. By replacing $\hat{A}_z$ with $\hat{B}_{Ai}^\dagger \hat{A}_z \hat{B}_{Ai}$ in the inequality (4.12) where $\hat{B}_{Ai} = \exp[(\cos^{-1}\sqrt{\eta})(\hat{a}_A^\dagger\hat{a}_i - \hat{a}_A\hat{a}_i^\dagger)]$ is the beam splitter operator with efficiency η_h ($\hat{a}_i$ is the field annihilation operator for the idler mode), the efficiency considered steering inequality is obtained from the expectation values of the state $|\Psi\rangle_{AB}|0\rangle_i$ as

the following:

$$\begin{aligned}\mathcal{S}_{\mathcal{F}}^{\eta_h} &= \frac{1}{\pi}\int_{-\pi/2}^{\pi/2} d\theta \mathcal{E}_{\mathcal{F}}^{\eta_h}(\theta) - \frac{2}{\pi}\mathcal{P}^{\eta_h} \\ &\leqslant 0,\end{aligned} \tag{4.14}$$

where

$$\begin{aligned}\mathcal{E}_{\mathcal{F}}^{\eta_h}(\theta) =& \frac{1}{4}e^{-\frac{\chi_\theta{}^2}{8|\alpha|^2}}(\coth|\alpha|^2 - 1)\Big\{2\cos\theta\,\mathrm{erfi}\left(\frac{\chi_\theta}{2\sqrt{2/\eta_h}|\alpha|}\right) \\ &+ 2\mathrm{Re}\Big[e^{2|\alpha|^2+i\chi_\theta}\mathrm{erf}\left(\frac{4|\alpha|^2+i\chi_\theta}{2\sqrt{2/\eta_h}|\alpha|}\right)\times \\ &\left(\sin\theta\sqrt{1-e^{-4|\alpha|^2}}+i\cos\theta\right)\Big]\Big\},\end{aligned} \tag{4.15}$$

$$\mathcal{P}^{\eta_h} = \sqrt{1+\frac{1}{4}e^{2|\alpha|^2}\left(e^{-4|\alpha|^2}-1\right)\mathrm{csch}^2|\alpha|^2\ \ \mathrm{erf}^2(\sqrt{\eta_h})} \tag{4.16}$$

correspond to the terms $\mathcal{E}_{\mathcal{F}}(\theta)$, $\mathcal{P}$ respectively with $\hat{A}_z$ replaced by $\hat{B}_{Ai}^\dagger \hat{A}_z \hat{B}_{Ai}$.

$\mathcal{S}_{\mathcal{F}}^{\eta_h}$ is plotted as the solid curve in Fig. 14. $|\alpha| > 0.27$ is required to see the violation of the inequality (4.12). As $|\alpha|$ increases, $\mathcal{S}_{\mathcal{F}}$ reaches the maximum bound 1. This is due to the fact that displacement operators are able to perform perfect qubit phase rotations as $|\alpha|$ increases [99].

4.2.2 Photon Parity Measurement with Displacement Operation

Photon parity measurement

$$\hat{\Pi} = \sum_{n=0}^{\infty} |2n+1\rangle\langle 2n+1| - |2n\rangle\langle 2n| \tag{4.17}$$

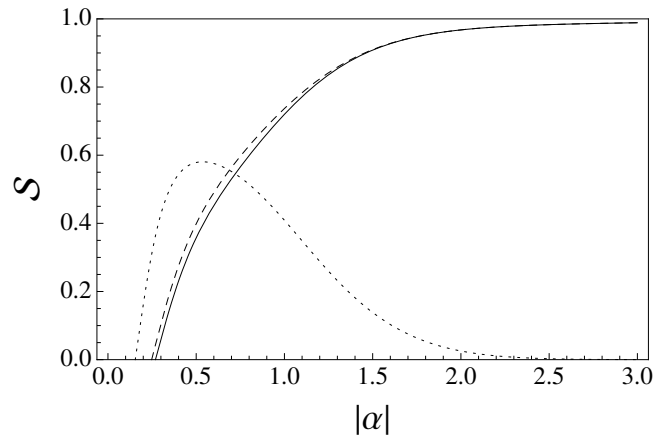

Figure 14: Values of $\mathcal{S}$ in the inequality (4.2) are plotted with respect to $|\alpha|$. The solid curve ($\mathcal{S}_{\mathcal{F}}$), dashed curve ($\mathcal{S}_{\Pi}$), and dotted curve ($\mathcal{S}_{O}$) correspond to the case when homodyne measurement, parity measurement, and on/off measurement is chosen respectively. Demonstration of steering is achieved for $\mathcal{S} > 0$, while the maximum being 1.

preceded by displacement operation $\hat{D}(\chi_\theta)$ can approximate $-\hat{\sigma}_\theta$ as well.

$$\hat{\Pi}_\theta = \hat{D}^\dagger(\frac{i\chi_\theta}{4\alpha^*})\hat{\Pi}\hat{D}(\frac{i\chi_\theta}{4\alpha^*}), \tag{4.18}$$

Corresponding steering inequality to Eq. (4.2) is

$$\mathcal{S}_\Pi = \frac{1}{\pi}\int_{-\pi/2}^{\pi/2} d\theta \mathcal{E}_\Pi(\theta) - \frac{2}{\pi}\mathcal{P} \leqslant 0, \tag{4.19}$$

The efficiency of the parity measurement can be also simulated by introducing a perfect photon detector with a beam splitter of the intensity transmission coefficient η_p in front of it. Then the following steering inequality is obtained by following

identical procedures in the previous subsection.

$$\begin{aligned}\mathcal{S}_{\Pi}^{\eta_p,\eta_h} &= \frac{1}{\pi}\int_{-\pi/2}^{\pi/2} d\theta \mathcal{E}_{\Pi}^{\eta_p}(\theta) - \frac{2}{\pi}\mathcal{P}^{\eta_h} \\ &\leqslant 0,\end{aligned} \tag{4.20}$$

where

$$\begin{aligned}\mathcal{E}_{\Pi}^{\eta_p}(\theta) =& \frac{1}{2}\left(\coth|\alpha|^2 - 1\right)\exp\left(-\frac{\eta_p\chi_\theta{}^2}{8|\alpha|^2} - 2|\alpha|^2(\eta_p - 1)\right)\times \\ & \Big\{\sin\theta\sqrt{1-e^{-4|\alpha|^2}}\sin(\eta_p\chi_\theta)e^{2|\alpha|^2\eta_p} \\ & + \cos\theta\left(\cos(\eta_p\chi_\theta)e^{2|\alpha|^2\eta_p} - 1\right)\Big\}.\end{aligned} \tag{4.21}$$

$\mathcal{S}_{\Pi}$ is plotted as the dashed curve in Fig. 14. $|\alpha| > 0.25$ is required to see the violation of the inequality (4.12). As $|\alpha|$ increases, $\mathcal{S}_{\Pi}$ reaches the maximum bound 1 due to the same reason for $\mathcal{S}_{\mathcal{F}}$.

4.2.3 Photon On/Off Measurement with Displacement Operation

In practical experiments, photon parity measurement is quite sensitive to its efficiency. Alternatively, let us consider photon on/off measurement, as it act as parity measurement when average photon number of the state examined is small. Photon on/off measurement $\hat{O}$ preceded by displacement operation $\hat{D}(\frac{i\theta}{4\alpha^*})$ is defined as

$$\hat{O}_\theta = \hat{D}^\dagger(\frac{i\chi_\theta}{4\alpha^*})\hat{O}\hat{D}(\frac{i\chi_\theta}{4\alpha^*}), \tag{4.22}$$

where

$$\hat{O} = \sum_{n=1}^{\infty} |n\rangle\langle n| - |0\rangle\langle 0|.$$

The identical treatments in the previous subsection gives the following efficiency considered steering inequality

$$\begin{aligned} \mathcal{S}_O^{\eta_p,\eta_h} &= \frac{1}{\pi}\int_{-\pi/2}^{\pi/2} d\theta \mathcal{E}_O^{\eta_p}(\theta) - \frac{2}{\pi}\mathcal{P}^{\eta_h} \\ &\leqslant 0, \end{aligned} \tag{4.23}$$

where

$$\begin{aligned} \mathcal{E}_O^{\eta_p}(\theta) = \big(\coth|\alpha|^2 - 1\big)\exp\left(-\frac{\eta_p{\chi_\theta}^2}{16|\alpha|^2} - 2|\alpha|^2\left(\frac{\eta_p}{2}-1\right)\right)\times \\ \left\{\cos\theta\left(\cos\left(\frac{\eta_p\chi_\theta}{2}\right)e^{2|\alpha|^2((\eta_p-2)/2+1)} - 1\right)\right. \\ \left. + \sin\theta\sqrt{1-e^{-2|\alpha|^2}}\sin\left(\frac{\eta_p\chi_\theta}{2}\right)e^{|\alpha|^2\eta_p}\right\}. \end{aligned} \tag{4.24}$$

$\mathcal{S}_O$ is plotted as the dotted curve in Fig. 14. $|\alpha| > 0.15$ is required to see the violation of the inequality (4.12). $\mathcal{S}_O$ reaches its maximum 0.58 at $|\alpha| \sim 0.53$.

$\mathcal{S}_O$ has higher violation then $\mathcal{S}_\Pi$, when $|\alpha|$ is small. This is due to the fact that average success probability of detecting an eigenstate of $\hat{\sigma}_\theta$ with eigenvalue -1

$$|\psi_\theta^-\rangle = \frac{1}{\sqrt{2}}\left(|-\alpha\rangle - e^{-i\theta}|+\alpha\rangle\right) \tag{4.25}$$

by displaced on measurements,

$$\mathcal{P}_-^O = \frac{1}{\pi}\int_{-\pi/2}^{\pi/2} d\theta\ \mathrm{Tr}\Big[\sum_{n=1}^{\infty} D^\dagger\left(\frac{i\theta}{4\alpha^*}\right)|n\rangle\langle n|D\left(\frac{i\theta}{4\alpha^*}\right)|\psi_\theta^-\rangle\langle\psi_\theta^-|\Big], \tag{4.26}$$

is quite higher than by displaced odd measurements'

$$\mathcal{P}_{-}^{\Pi} = \frac{1}{\pi}\int_{-\pi/2}^{\pi/2} d\theta \, \mathrm{Tr}\Big[\sum_{n=0}^{\infty} D^{\dagger}(\frac{i\theta}{4\alpha^*})|2n+1\rangle\langle 2n+1|D(\frac{i\theta}{4\alpha^*})|\psi_{\theta}^{-}\rangle\langle\psi_{\theta}^{-}|\Big] \tag{4.27}$$

for small $|\alpha|$ as in the Fig. 15 (a). However, $\mathcal{S}_{\Pi}$ has higher violation then $\mathcal{S}_O$ for $|\alpha|$ is large. Likewise, this is due to the fact that the success probability of detecting an eigenstate of $\hat{\sigma}_{\theta}$ with eigenvalue +1

$$|\psi_{\theta}^{+}\rangle = \frac{1}{\sqrt{2}}\left(|-\alpha\rangle + e^{-i\theta}|+\alpha\rangle\right) \tag{4.28}$$

by displaced even measurements

$$\mathcal{P}_{+}^{\Pi} = \frac{1}{\pi}\int_{-\pi/2}^{\pi/2} d\theta \, \mathrm{Tr}\Big[\sum_{n=0}^{\infty} D^{\dagger}(\frac{i\theta}{4\alpha^*})|2n\rangle\langle 2n|D(\frac{i\theta}{4\alpha^*})|\psi_{\theta}^{+}\rangle\langle\psi_{\theta}^{+}|\Big] \tag{4.29}$$

approaches 1, while displaced vacuum measurements'

$$\mathcal{P}_{+}^{O} = \frac{1}{\pi}\int_{-\pi/2}^{\pi/2} d\theta \, \mathrm{Tr}\Big[D^{\dagger}(\frac{i\theta}{4\alpha^*})|0\rangle\langle 0|D(\frac{i\theta}{4\alpha^*})|\psi_{\theta}^{+}\rangle\langle\psi_{\theta}^{+}|\Big], \tag{4.30}$$

drops to 0 due to low average photon number as in the Fig. 15 (b).

4.2.4 Finite-Setting EPR Steering

As mentioned in the previous section, we are always constrained by finite number of measurement settings in practical experiments. Therefore, it is important to consider the finite version of steering inequality (4.4). Steering value with n-finite measurement settings $\mathcal{S}_n$ can be trivially calculated as explained, which is plotted in the Fig.

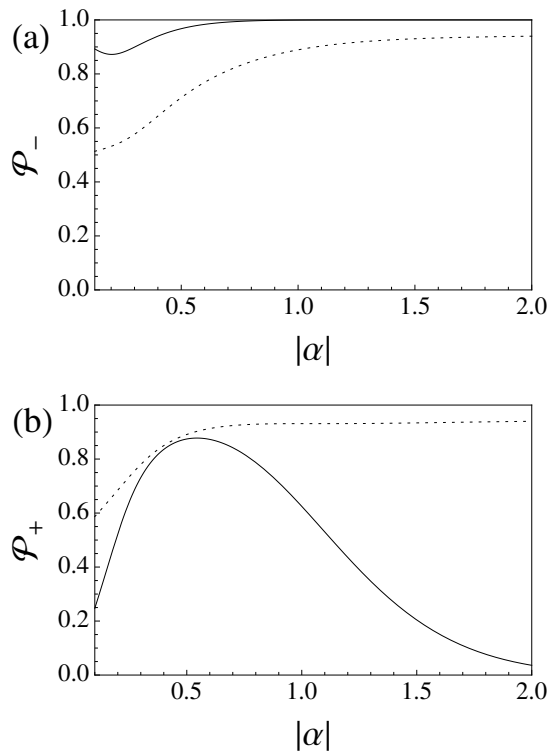

Figure 15: Average success probabilities $\mathcal{P}_-$ ($\mathcal{P}_+$) of detecting eigenstates of $\hat{\sigma}_\theta$ with eigenvalues -1 (+1) by using on/off and parity measurements are plotted with respect to α. Solid curves corresponds to the case when on/off measurements are used, and dotted curves corresponds to the case when parity measurements are used. For small $|\alpha|$, $\mathcal{P}_+$ of the parity measurements being lower than the on/off measurements' are responsible for lower $\mathcal{S}_\Pi$ than $\mathcal{S}_O$. Whereas, nearly vanishing $\mathcal{P}_-$ of the on/off measurements is responsible for vanishing $\mathcal{S}_O$ for large $|\alpha|$.

16. Mostly fewer measurement settings mean less violation of steering inequality, but as the number of measurement settings increases, $\mathcal{S}_n$ approaches $\mathcal{S}(=\mathcal{S}_\infty)$ quite rapidly. Therefore, the number of the measurement settings is not a big obstacle to demonstrate steering in our case.

4.3 On/Off Steering with Efficiency

In this section, we reinvestigate steering inequality in the subsection 4.2.3, where on/off measurement is chosen for Alice supplemented by homodyne measurement. However non perfect efficiencies for on/off measurement and homodyne measurement (η_p, η_h) will be considered. Bob does not need to consider his detection efficiency, as he trusts his device in the steering scenario [9]. Both detectors with non perfect efficiencies η can be modeled by a perfect detector together with a beam splitter of transmissivity $\sqrt{\eta}$ in front of it [76]. The signal field A is mixed with the vacuum state $|0\rangle_C$ at a beam splitter. The beam splitter operator between modes A and C is $\hat{B}_{AC} = \exp[(\cos^{-1}\sqrt{\eta})(\hat{a}_A^\dagger \hat{a}_C - \hat{a}_A \hat{a}_C^\dagger)]$ [77], where $\hat{a}_C$ ($\hat{a}_C^\dagger$) is the field annihilation (creation) operator for the ancilla mode C. After passing through the beam splitter, the entangled coherent state $|\Psi\rangle_{AB}$ is changed to a mixed state as

$$\begin{aligned}
\rho_{AB}^{\eta} =& \mathrm{Tr}_C\left[\hat{B}_{AC}\Big(|\Psi\rangle\langle\Psi|\Big)_{AB} \otimes \Big(|0\rangle\langle 0|\Big)_C \hat{B}_{AC}^\dagger\right] \\
=& \frac{1}{2-2e^{-4|\alpha|^2}}\Big\{|-\sqrt{\eta}\alpha\rangle\langle -\sqrt{\eta}\alpha| \otimes |\alpha\rangle\langle\alpha| \\
&+ |\sqrt{\eta}\alpha\rangle\langle\sqrt{\eta}\alpha| \otimes |-\alpha\rangle\langle -\alpha| \\
&- e^{-2(1-\eta)|\alpha|^2}|-\sqrt{\eta}\alpha\rangle\langle\sqrt{\eta}\alpha| \otimes |\alpha\rangle\langle -\alpha| \\
&- e^{-2(1-\eta)|\alpha|^2}|\sqrt{\eta}\alpha\rangle\langle -\sqrt{\eta}\alpha| \otimes |-\alpha\rangle\langle\alpha|\Big\}_{AB}.
\end{aligned} \tag{4.31}$$

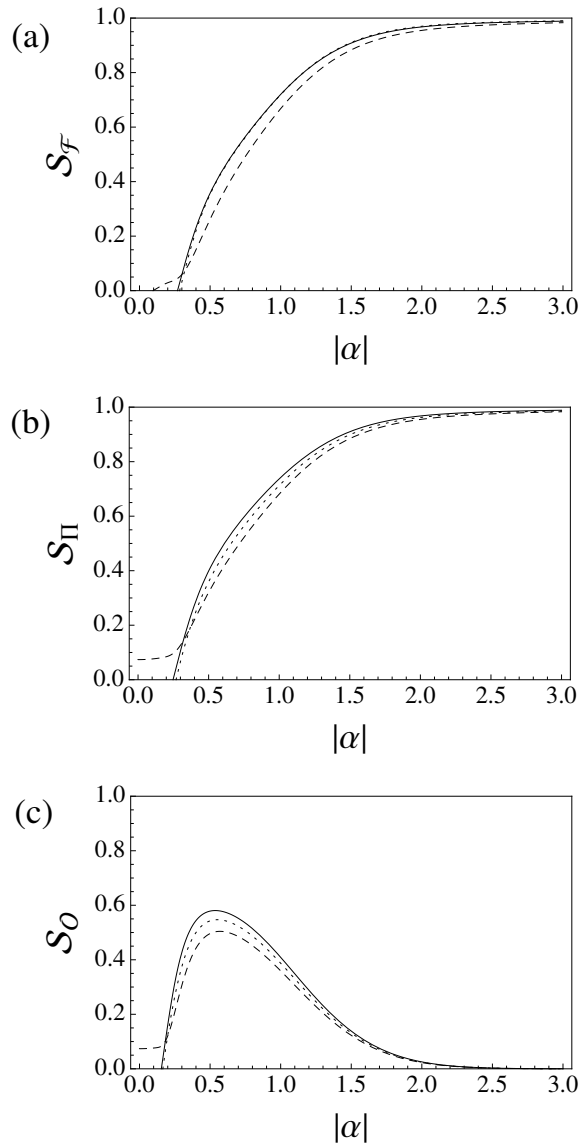

Figure 16: Values of steering $\mathcal{S}_n$ in the inequality (4.4), when n-finite measurement settings are used, are plotted with respect to $|\alpha|$. Finite versions of steering value with homodyne measurement ($\mathcal{S}_{\mathcal{F}}$), parity measurement ($\mathcal{S}_{\Pi}$), and on/off measurement ($\mathcal{S}_{O}$) are plotted at (a), (b), and (c) respectively Each dashed curve, dotted curve and solid curve corresponds to the case when the number of measurement settings is chosen as $n = 2$, $n = 3$, and $n = \infty$ respectively.

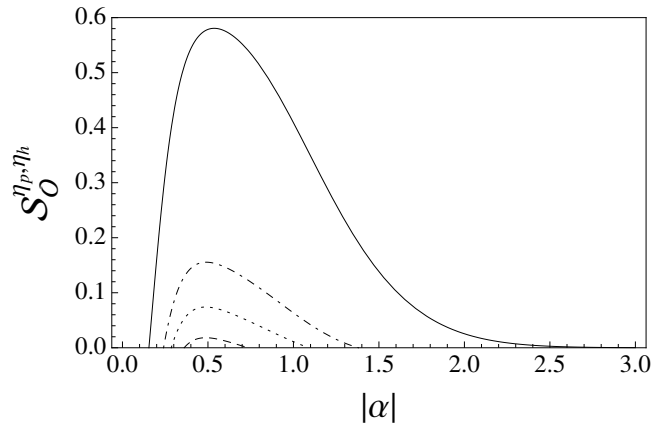

Figure 17: Values of $\mathcal{S}_O^{\eta_p,\eta_h}$ in the inequality (4.32) are plotted with respect to $|\alpha|$. Curves with different values of photon detection efficiency η_p while realistic efficiency of homodyne measurement being fixed at $\eta_h = 0.9$ are plotted. Dashed curve, dotted curve, dot-dashed curve correspond to the case when the efficiency of on/off measurement is chosen as $\eta_p = \frac{1}{3}$, $\eta_p = 0.4$, and $\eta_p = 0.5$ respectively. Solid curve corresponds to the ideal case when efficiencies of both measurements are perfect.

Then the steering inequality becomes

$$\mathcal{S}_O^{\eta_p,\eta_h} = \frac{1}{\pi}\int_{-\pi/2}^{\pi/2} d\theta \mathrm{Tr}\left[\hat{O}_\theta \hat{\sigma}_\theta \rho_{AB}^{\eta_p}\right] - \frac{2}{\pi}\mathcal{N}_{\eta_h} \leqslant 0, \tag{4.32}$$

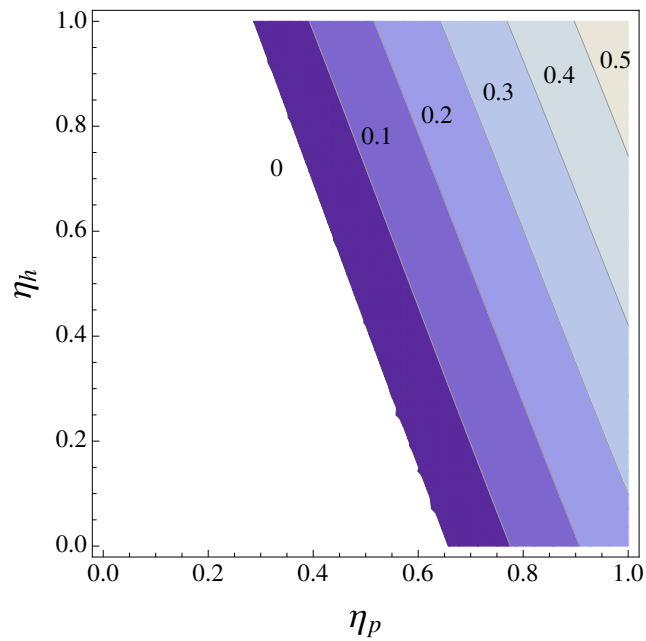

Figure 18: Maximum values of $\mathcal{S}_O^{\eta_p,\eta_h}$ optimized for $|\alpha|$ are plotted with respect to η_p, η_h. Contour lines are drawn for $\mathcal{S}$ above 0 with 0.1 intervals. When homodyne detection efficiency is $\eta_h = 1$, required photon detection efficiency is $\eta_p = 0.28$, while $\eta_p = 0.65$ is required for $\eta_h = 0$.

where

$$
\begin{aligned}
&\frac{1}{\pi}\int_{-\pi/2}^{\pi/2} d\theta \mathrm{Tr}\left[\hat{O}_\theta \hat{\sigma}_\theta \rho_{AB}^{\eta_p}\right] \\
=&\frac{2\sqrt{\pi}|\alpha|}{e^{4|\alpha|^2}-1}\Big[\sqrt{1-e^{-4|\alpha|^2}}e^{-|\alpha|^2\left(4\sqrt{\eta_p}+2\right)} \\
&\Big\{e^{8|\alpha|^2\sqrt{\eta_p}}\Big(\mathrm{erf}\left(\frac{\pi}{8|\alpha|}+i|\alpha|\left(\sqrt{\eta_p}-2\right)\right) \\
&+\mathrm{erf}\left(\frac{\pi}{8|\alpha|}-i|\alpha|\left(\sqrt{\eta_p}-2\right)\right)\Big)+\mathrm{erfc}\left(\frac{\pi}{8|\alpha|}+i|\alpha|\left(\sqrt{\eta_p}+2\right)\right) \\
&+\mathrm{erfc}\left(\frac{\pi}{8|\alpha|}-i|\alpha|\left(\sqrt{\eta_p}+2\right)\right)-2\Big\} \\
&+e^{-2|\alpha|^2\left(2\sqrt{\eta_p}+1\right)}\Big\{e^{8|\alpha|^2\sqrt{\eta_p}}\Big(\mathrm{erf}\left(\frac{\pi}{8|\alpha|}+i|\alpha|\left(\sqrt{\eta_p}-2\right)\right) \\
&+\mathrm{erf}\left(\frac{\pi}{8|\alpha|}-i|\alpha|\left(\sqrt{\eta_p}-2\right)\right)\Big)+\mathrm{erf}\left(\frac{\pi}{8|\alpha|}+i|\alpha|\left(\sqrt{\eta_p}+2\right)\right) \\
&+\mathrm{erf}\left(\frac{\pi}{8|\alpha|}-i|\alpha|\left(\sqrt{\eta_p}+2\right)\right)\Big\} \\
&-2ie^{-|\alpha|^2(\eta p+2)}\Big\{\mathrm{erfi}\left(2|\alpha|-\frac{i\pi}{8|\alpha|}\right)-\mathrm{erfi}\left(2|\alpha|+\frac{i\pi}{8|\alpha|}\right)\Big\}\Big]
\end{aligned}
\tag{4.33}
$$

and

$$
\mathcal{N}_{\eta_h}=\sqrt{1-\frac{\mathrm{erf}\left(\sqrt{2\eta_h}|\alpha|\right)^2}{1-e^{-4|\alpha|^2}}}. \tag{4.34}
$$

Steering values $\mathcal{S}_O^{\eta_p,\eta_h}$ are plotted in the Fig. 17 and Fig. 18. Demonstration of steering is achievable with practical experimental detection efficiencies $\eta_p = 1/3$, $\eta_h = 0.9$. For small $|\alpha|$, an entangled coherent state can be approximated by Schrödinger's kitten state, which is generated by photon subtracted squeezed vacuum or squeezed single photon state [102, 103]. But in real experiment, it is quite challenging to generate the Schrödinger's kitten state with high fidelity [104]. Therefore, experimental demonstration of EPR-steering may be possible when the high generation fidelity is achieved with improved photon detection efficiency.

4.4 Remarks

EPR Steering of ECS without detection loophole seems possible, if ECS can be generated with high fidelity. Demonstration of ECS steering is required for secure oneside-device-independent QKD. However, demonstration of EPR steering of ECS without detection loophole seems harder than the single photon singlet states.

Chapter 5

Noiseless Linear Amplification of Superpositions of Coherent States Using Photon Addition and Subtraction

5.1 Introduction

Quantum noise is a fundamental property which forbids quantum cloning [45], superluminal communication [105], and violation of generalized uncertainty principle [106]. Quantum theory prohibits deterministic linear amplification of bosonic system to be noiseless [18]. The one way to circumvent this fundamental restriction is to adopt probabilistic amplification, which is heralded from successful measurements [107, 27, 108].

Noiseless amplification can be used for many quantum information tasks such as entanglement distillation [19], continuous variable quantum key distribution [20, 21], loss suppression [22], quantum repeater [23], phase estimation [24], error correction [25], high-accuracy homodyne detection with low-efficiency detector [26], and nonlocality tests [16, 17].

Implementing noiseless amplification is however the state-of-the-art technique. Photon subtraction and addition operations, $\hat{a}$ and $\hat{a}^{\dagger}$, which construct the basic building blocks of noiseless amplification scheme [27], have been independently realized in Refs. [109, 110]. A superposition of these operations has been implemented by Mach-Zehnder interferometer (MZI) [111]. It is only recently that the first order ap-

proximation of the noiseless amplification $\hat{a}\hat{a}^\dagger$ is implemented [28]. Considering the difficulties of mode matching in MZI and photon resolving detection, the noiseless amplifications considered here are in-line-approximated amplifications, $\hat{a}\hat{a}^\dagger$ and $a^{\dagger 2}$, which all show a noiseless property in our study. The $\hat{a}\hat{a}^\dagger$ operation as the first order approximation of the ideal noiseless amplification is appropriate for small-amplitude coherent states [27, 28]. It was pointed out that n-photon addition operations, $(a^\dagger)^n$, may be used used to amplify coherent states [112].

Theoretical and experimental studies are devoted to the imperfect noiseless amplification of coherent states [113, 28], while a little is known for practical (imperfect) amplification of superpositions of coherent states (SCSs). Thus, we also discuss the amplification of SCSs in a manner analgous to the amplification of coherent state. Note that deterministic amplification of SCS in circuit quantum electrodynamics has been proposed in [114]. Large amplitude SCSs are important quantum states both in fundamental and practical aspects, which are frequently referred to as "Schrödinger's cat states", as they are in the superposition of two marcoscopically distinct opposite phases. Fault-tolerant coherent state quantum computing can be achieved via large amplitude SCSs($\alpha > 1.2$) [115]. Large amplitude SCSs can be also used to generate entangled coherent states with large amplitude which are beneficial for demonstrating Bell nonlocality [116, 117, 67, 118, 68, 72, 119, 120, 73, 70, 101, 121, 122, 123, 124, 125] and precision measurement [126, 127, 128, 129, 130, 131, 132, 133, 134]. There are different approaches for generating large amplitude SCS [102, 135, 136]. However, quadrature squeezing is often used for approximating SCSs in linear optics[135, 137, 138], whereas practically implementable high squeezing level is often restricted to be near 10 dB [139, 140, 141]. Besides, these implementations are only approximations, which exhibits low fidelity to large SCSs [135]. Thus, it is also intriguing

to investigate whether the fidelity to large SCS increases under the practical amplification processes. In this study, we show that the amplification of the squeezed states exhibits higher fidelity than the states without the amplification and requires less squeezing. A similar but different approach which requires back squeezing for approximating SCS can be found in [103]. Studies about the nonclassical properties of similarly engineered states can be found in [142, 143].

Our aim in this work is to scrutinize in-line-approximated amplifications of coherent states and SCSs, and to find efficient amplification strategies depending on various conditions. Here we find that the $a^{\dagger 2}$ operation is an effective noiseless amplifier for states with relatively larger amplitudes. Figures of merit examined here are the state fidelity, the amplitude gain, and the equivalent input noise (EIN) [144]. The noiseless property of the amplification is assessed by the EIN of the amplifier, which is affected by both the state fidelity and the amplitude gain.

The remainder of this chapter is organized as follows. In Sec. 5.2, we examine one- and two- cycle amplification of coherent states. The fidelity, amplitude-gain, and noiseless property after the amplifications are studied. Sec. 5.3 is devoted into the amplification of SCSs, which behaves in an analogous manner to coherent states. Concluding remarks are followed in Sec. 5.4.

5.2 Amplification of Coherent States

5.2.1 One-Cycle Amplification

Applying the amplification operator $\hat{A} \in \{\hat{a}\hat{a}^\dagger, \hat{a}^{\dagger 2}\}$ to a coherent state of amplitude α_i, the amplified state is expressed as

$$\frac{1}{N^{\hat{A}}(\alpha_i)}\hat{A}\left|\alpha_i\right\rangle, \tag{5.1}$$

where the normalization factors are given respectively as

$$N^{\hat{a}\hat{a}^\dagger}(\alpha_i) = (|\alpha_i|^4 + 3|\alpha_i|^2 + 1)^{\frac{1}{2}}, \tag{5.2}$$

$$N^{\hat{a}^{\dagger 2}}(\alpha_i) = (|\alpha_i|^4 + 4|\alpha_i|^2 + 2)^{\frac{1}{2}}. \tag{5.3}$$

Throughout this chapter, all the parameters are assumed to be reals. The fidelity between the $\hat{A}$-amplified coherent state of initial amplitude α_i and the coherent state of amplitude α_f is

$$F^{\hat{A}} = \frac{\left|\left\langle\alpha_f\right|\hat{A}\left|\alpha_i\right\rangle\right|^2}{|N^{\hat{A}}(\alpha_i)|^2}. \tag{5.4}$$

The analytic results for $\hat{A} \in \{\hat{a}\hat{a}^\dagger, \hat{a}^{\dagger 2}\}$ are expressed as

$$F^{\hat{a}\hat{a}^\dagger} = \frac{e^{-|\alpha_f+\alpha_i|^2}\left|e^{2\alpha_f\alpha_i}(\alpha_f\alpha_i+1)\right|^2}{\left|N^{\hat{a}\hat{a}^\dagger}(\alpha_i)\right|^2}, \tag{5.5}$$

$$F^{\hat{a}^{\dagger 2}} = \frac{|\alpha_f|^4 e^{-|\alpha_i-\alpha_f|^2}}{\left|N^{\hat{a}^{\dagger 2}}(\alpha_i)\right|^2}. \tag{5.6}$$

We take the maximum fidelity of the $\hat{A}$-amplified coherent state of initial amplitude α_i to the initial coherent state as

$$_{\max}F^{\hat{A}}(\alpha_i) = \max_{\alpha_f} F^{\hat{A}} \tag{5.7}$$

where the maximum is taken over the amplitude α_f.

The results of numerical maximization are presented in Fig. 19(a). The $(\hat{a}\hat{a}^\dagger)$-amplification always exhibits higher maximum fidelity than the $(\hat{a}^\dagger)^2$-amplification while it is the opposite for the amplitude gain. The amplitude gain from the amplification $\hat{A}$ can be defined as the ratio of the expectation values of the quadrature operator with phase λ [28]:

$$g_\lambda^{\hat{A}} = \frac{\left|\langle\alpha_i|\hat{A}^\dagger x_\lambda \hat{A}\,|\alpha_i\rangle\right|}{|N^{\hat{A}}(\alpha_i)|^2|\langle\alpha_i|x_\lambda\,|\alpha_i\rangle|}, \tag{5.8}$$

where the results for $\hat{A}$ are followed as

$$g_\lambda^{\hat{a}\hat{a}^\dagger} = \frac{\alpha_i^2+1}{\alpha_i^4+3\alpha_i^2+1}+1, \tag{5.9}$$

$$g_\lambda^{\hat{a}^{\dagger 2}} = \frac{2\left(\alpha_i^2+2\right)}{\alpha_i^4+4\alpha_i^2+2}+1. \tag{5.10}$$

The amplitude gains are independent of λ for the amplifications of coherent states considered here. The gain monotonically decreases to unity with respect to $|\alpha_i|$ (Fig. 19(b)), since $\hat{a}\hat{a}^\dagger$ or $\hat{a}^{\dagger 2}$ merely alters the ratios of the superposition of Fock states for large-amplitude coherent states. The maximum fidelity in Fig. 19(a) reaches unity for large $|\alpha_i|$ with the same reason.

We now employ the equivalent input noise (EIN) [144] for comparison between

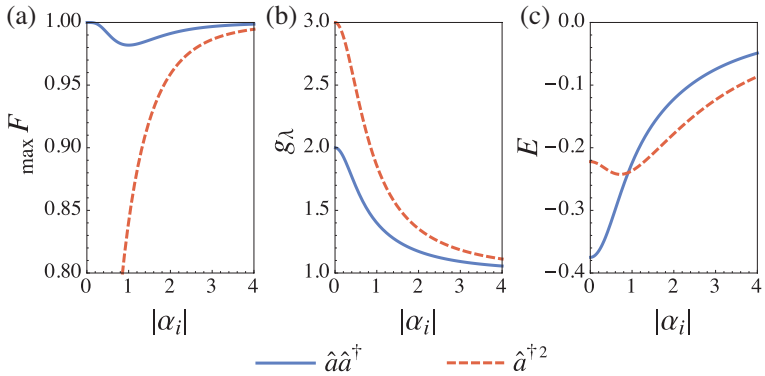

Figure 19: (a) Maximum fidelities, (b) amplitude gains, and (c) average EINs when the amplification methods $\hat{a}\hat{a}^\dagger$ (solid curve) and $\hat{a}^{\dagger 2}$ (dashed curve) are applied to the coherent state of initial amplitude $|\alpha_i|$. (a) The fidelity of the $\hat{a}\hat{a}^\dagger$-amplified coherent states are higher than $_{\max}F > 0.98$, which are close to 1 for small and large $|\alpha_i|$. The fidelity of the $\hat{a}^{\dagger 2}$-amplified coherent state approaches 1 for large $|\alpha_i|$. (b) The higher gain is obtained when the amplification is performed by $\hat{a}^{\dagger 2}$ rather than $\hat{a}\hat{a}^\dagger$. The gains from $\hat{a}\hat{a}^\dagger$ and $\hat{a}^{\dagger 2}$ are initiated at 2 and 3 as $|\alpha_i| \to 0$, and are dropped to 1 as $|\alpha_i| \to \infty$. (c) The $\hat{a}^{\dagger 2}$-amplification exhibits lower EINs than the $\hat{a}\hat{a}^\dagger$-amplification with large amplitude $|\alpha_i| \gtrsim 0.91$, while the opposite is true for $|\alpha_i| \lesssim 0.91$. As $|\alpha_i| \to 0$, the average EIN approaches to $-3/8$ for $\hat{a}\hat{a}^\dagger$, and $-2/9$ for $\hat{a}^{\dagger 2}$. The average EIN approaches zero as $|\alpha_i|$ increases for both cases.

the two amplification schemes. The EIN of an amplifier is defined as

$$E_\lambda^{\hat{A}} = \frac{\langle \Delta x_\lambda \rangle_{\text{out}}^2}{(g_\lambda^{\hat{A}})^2} - \langle \Delta x_\lambda \rangle_{\text{in}}^2 , \tag{5.11}$$

where $\langle \Delta x_\lambda \rangle_{\text{in}}^2$ and $\langle \Delta x_\lambda \rangle_{\text{out}}^2$ is the expectation values of quadrature variance operator with phase λ for input and output states. It represents the level of noise added into the input signal to mimic the output signal in the quadrature x_λ. The EIN from $\hat{A}$ is

determined as

$$
\begin{aligned}
E_{\lambda}^{\hat{a}\hat{a}^{\dagger}}(\alpha_i) &= \frac{\alpha_i^8 + 6\alpha_i^6 + 13\alpha_i^4 - 2\left(\alpha_i^3 + \alpha_i\right)^2 \cos(2\lambda) + 6\alpha_i^2 + 1}{2\left(\alpha_i^4 + 3\alpha_i^2 + 1\right)^2}, \\
E_{\lambda}^{\hat{a}^{\dagger 2}}(\alpha_i) &= \frac{\alpha_i^8 + 8\alpha_i^6 + 28\alpha_i^4 + 32\alpha_i^2 - 4\left(\alpha_i^4 + 4\alpha_i^2 + 6\right)\alpha_i^2 \cos(2\lambda) + 20}{2\left(\alpha_i^4 + 4\alpha_i^2 + 2\right)^2}.
\end{aligned}
\tag{5.12}
$$

The λ-averaged EINs, $E^{\hat{a}\hat{a}^{\dagger}}(\alpha_i)$, $E^{a^{\dagger 2}}(\alpha_i)$, are plotted in Fig. 19(c). All average EINs are negative, which indicates the characteristic of noiseless amplification; negative EIN cannot be obtained by the classical amplification. As the $\hat{a}\hat{a}^{\dagger}$-amplification has much higher fidelity than $\hat{a}^{\dagger 2}$ for small $|\alpha_i|$, $\hat{a}\hat{a}^{\dagger}$ has lower EIN for small $|\alpha_i|$, while $\hat{a}^{\dagger 2}$ has lower EIN for large $|\alpha_i|$ due to higher gains.

The $\hat{a}\hat{a}^{\dagger}$-amplification of the coherent state shows higher fidelity to the coherent state than the $\hat{a}^{\dagger 2}$-amplification. However, when the initial amplitude is large enough to approach a sufficiently high fidelity, the $\hat{a}^{\dagger 2}$-amplification is advantageous in terms of amplitude gain and EIN.

5.2.2 Two-Cycle Amplification

We consider four possible combinatorial two-cycle amplifications, $\hat{A} \in \{(\hat{a}\hat{a}^{\dagger})^2, \hat{a}^{\dagger 4}, \hat{a}^{\dagger 2}\hat{a}\hat{a}^{\dagger}, \hat{a}\hat{a}^{\dagger}\hat{a}^{\dagger 2}\}$. The normalization factors $N^{\hat{A}}$ in Eq. (5.1) are presented as

$$
\begin{aligned}
N^{(\hat{a}\hat{a}^{\dagger})^2}(\alpha_i) &= \sqrt{{\alpha_i}^8 + 10{\alpha_i}^6 + 25{\alpha_i}^4 + 15{\alpha_i}^2 + 1}, \\
N^{\hat{a}^{\dagger 4}}(\alpha_i) &= \sqrt{{\alpha_i}^8 + 16{\alpha_i}^6 + 72{\alpha_i}^4 + 96{\alpha_i}^2 + 24}, \\
N^{\hat{a}\hat{a}^{\dagger}\hat{a}^{\dagger 2}}(\alpha_i) &= \sqrt{{\alpha_i}^8 + 15{\alpha_i}^6 + 63{\alpha_i}^4 + 78{\alpha_i}^2 + 18}, \\
N^{\hat{a}^{\dagger 2}\hat{a}\hat{a}^{\dagger}}(\alpha_i) &= \sqrt{{\alpha_i}^8 + 11{\alpha_i}^6 + 31{\alpha_i}^4 + 22{\alpha_i}^2 + 2}.
\end{aligned}
\tag{5.13}
$$

The fidelities of the $\hat{A}$-amplified coherent state to the coherent state of amplitude $|\alpha_f|$ are

$$\begin{aligned}
F^{(\hat{a}\hat{a}^\dagger)^2} &= \frac{e^{-(\alpha_i-\alpha_f)^2}(\alpha_i{}^2\alpha_f^2+3\alpha_i\alpha_f+1)^2}{\left|N^{(\hat{a}\hat{a}^\dagger)^2}(\alpha_i)\right|^2}, \\
F^{\hat{a}^{\dagger 4}} &= \frac{\alpha_i{}^8 e^{-(\alpha_i-\alpha_f)^2}}{\left|N^{\hat{a}^{\dagger 4}}(\alpha_i)\right|^2}, \\
F^{\hat{a}\hat{a}^\dagger\hat{a}^{\dagger 2}} &= \frac{\alpha_f^4 e^{-(\alpha_i-\alpha_f)^2}(\alpha_i\alpha_f+3)^2}{\left|N^{\hat{a}\hat{a}^\dagger\hat{a}^{\dagger 2}}(\alpha_i)\right|^2}, \\
F^{\hat{a}^{\dagger 2}\hat{a}\hat{a}^\dagger} &= \frac{\alpha_f^4 e^{-(\alpha_i-\alpha_f)^2}(\alpha_i\alpha_f+1)^2}{\left|N^{\hat{a}^{\dagger 2}\hat{a}\hat{a}^\dagger}(\alpha_i)\right|^2}.
\end{aligned} \tag{5.14}$$

The maximum fidelity ${}_{\max}F^{\hat{A}}(\alpha_i)$ in terms of the initial amplitude $|\alpha_i|$ is numerically obtained and plotted in Fig. 20(a). Among the two-cycle amplifications, the $(\hat{a}\hat{a}^\dagger)^2$-amplification exhibits the highest maximum fidelity to the coherent state, although the fidelity is slightly lower than one-cycle amplification, $\hat{a}\hat{a}^\dagger$. The order of the fidelity performance is

$${}_{\max}F^{\hat{a}^{\dagger 4}}(\alpha_i) < {}_{\max}F^{\hat{a}^{\dagger 2}\hat{a}\hat{a}^\dagger}(\alpha_i) < {}_{\max}F^{\hat{a}\hat{a}^\dagger\hat{a}^{\dagger 2}}(\alpha_i) < {}_{\max}F^{(\hat{a}\hat{a}^\dagger)^2}(\alpha_i). \tag{5.15}$$

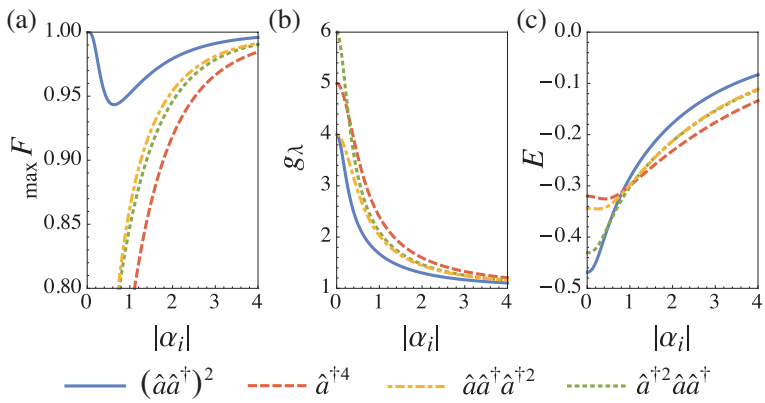

Figure 20: (a) Maximum fidelities, (b) amplitude gains, and (c) average EINs after two-cycle amplifications $(\hat{a}\hat{a}^\dagger)^2$ (solid curve), $\hat{a}^{\dagger 4}$ (dashed curve), $\hat{a}\hat{a}^\dagger\hat{a}^{\dagger 2}$ (dot-dashed curve), and $\hat{a}^{\dagger 2}\hat{a}\hat{a}^\dagger$ (dotted curve). (a) The maximum fidelity of the $(\hat{a}\hat{a}^\dagger)^2$-amplified coherent states approaches 1 for small and large $|\alpha_i|$'s, which is the highest among the two-cycle amplifications. All the maximum fidelities become perfect as the initial amplitude $|\alpha_i|$ increases. (b) The higher gain is obtained by the two-cycle amplifications compared to the one-cycle amplifications. The gains from $(\hat{a}\hat{a}^\dagger)^2$, $\hat{a}^{\dagger 4}$, $\hat{a}^{\dagger 2}\hat{a}\hat{a}^\dagger$, and $\hat{a}\hat{a}^\dagger\hat{a}^{\dagger 2}$ become 4, 5, 4, and 6 for $|\alpha_i| \to 0$, respectively, and drop to 1 as $|\alpha_i|$ increases. (c) In the regions of $|\alpha_i| \lesssim 0.51$, $0.51 \lesssim |\alpha_i| \lesssim 1.05$, and $|\alpha_i| \gtrsim 1.05$, $(\hat{a}\hat{a}^\dagger)^2$, $\hat{a}^{\dagger 4}$, and $\hat{a}^{\dagger 2}\hat{a}\hat{a}^\dagger$ show the lowest EIN, respectively, which are all lower than EINs obtained by the one-cycle amplifications.

The gains from the amplification $\hat{A}$ are expressed as

$$
\begin{aligned}
g_{\lambda}^{(\hat{a}\hat{a}^{\dagger})^2} &= \frac{\left(2{\alpha_i}^2+3\right)\left({\alpha_i}^4+5{\alpha_i}^2+1\right)}{\left({\alpha_i}^2\left({\alpha_i}^2+5\right)^2+15\right){\alpha_i}^2+1}+1, \\
g_{\lambda}^{\hat{a}^{\dagger 4}} &= \frac{4\left({\alpha_i}^2\left({\alpha_i}^2+6\right)^2+24\right)}{{\alpha_i}^8+16{\alpha_i}^6+72{\alpha_i}^4+96{\alpha_i}^2+24}+1, \\
g_{\lambda}^{\hat{a}\hat{a}^{\dagger}\hat{a}^{\dagger 2}} &= \frac{3\left({\alpha_i}^2+3\right)\left({\alpha_i}^4+8{\alpha_i}^2+6\right)}{{\alpha_i}^8+15{\alpha_i}^6+63{\alpha_i}^4+78{\alpha_i}^2+18}+1, \\
g_{\lambda}^{\hat{a}^{\dagger 2}\hat{a}\hat{a}^{\dagger}} &= \frac{3{\alpha_i}^6+23{\alpha_i}^4+38{\alpha_i}^2+10}{{\alpha_i}^8+11{\alpha_i}^6+31{\alpha_i}^4+22{\alpha_i}^2+2}+1.
\end{aligned}
\tag{5.16}
$$

All the gains from the two-cycle amplifications (Eq. (5.16)) are higher than those from one-cycle amplification, which also monotonically decreases to unity with respect to $|\alpha_i|$ (Fig. 20(b)). The gain from $(\hat{a}\hat{a}^{\dagger})^2$ is the lowest among the two-cycle amplifications, although the fidelity is the highest. For sufficiently large amplitude ($|\alpha_i| \gtrsim 0.27$), the following relation holds for amplitude gains:

$$
g_{\lambda}^{(\hat{a}\hat{a}^{\dagger})^2}(\alpha_i) < g_{\lambda}^{\hat{a}\hat{a}^{\dagger}\hat{a}^{\dagger 2}}(\alpha_i) < g_{\lambda}^{\hat{a}^{\dagger 2}\hat{a}\hat{a}^{\dagger}}(\alpha_i) < g_{\lambda}^{\hat{a}^{\dagger 4}}(\alpha_i). \tag{5.17}
$$

The EINs are represented as

$$E_{\lambda}^{(\hat{a}\hat{a}^{\dagger})^2}(\alpha_i) = -\Big\{4{\alpha_i}^{14} + 62{\alpha_i}^{12} + 382{\alpha_i}^{10} + 1101{\alpha_i}^{8} + 1554{\alpha_i}^{6} + 955{\alpha_i}^{4} + 226{\alpha_i}^{2} + 2(2{\alpha_i}^{12} + 26{\alpha_i}^{10} + 125{\alpha_i}^{8} + 254{\alpha_i}^{6} + 225{\alpha_i}^{4} + 66{\alpha_i}^{2} + 7){\alpha_i}^{2}\cos(2\lambda) + 15\Big\} / \Big\{2\left({\alpha_i}^{8} + 12{\alpha_i}^{6} + 38{\alpha_i}^{4} + 32{\alpha_i}^{2} + 4\right)^2\Big\}, \tag{5.18}$$

$$E_{\lambda}^{\hat{a}^{\dagger 4}}(\alpha_i) = -4\Big\{{\alpha_i}^{14} + 26{\alpha_i}^{12} + 276{\alpha_i}^{10} + 1488{\alpha_i}^{8} + 4344{\alpha_i}^{6} + 6624{\alpha_i}^{4} + 4896{\alpha_i}^{2} + ({\alpha_i}^{12} + 24{\alpha_i}^{10} + 228{\alpha_i}^{8} + 1056{\alpha_i}^{6} + 2520{\alpha_i}^{4} + 2880{\alpha_i}^{2} + 1440){\alpha_i}^{2}\cos(2\lambda) + 1152\Big\} / \Big\{\left({\alpha_i}^{8} + 20{\alpha_i}^{6} + 120{\alpha_i}^{4} + 240{\alpha_i}^{2} + 120\right)^2\Big\}, \tag{5.19}$$

$$E_{\lambda}^{\hat{a}\hat{a}^{\dagger}\hat{a}^{\dagger 2}}(\alpha_i) = -3\Big\{2{\alpha_i}^{14} + 49{\alpha_i}^{12} + 486{\alpha_i}^{10} + 2421{\alpha_i}^{8} + 6432{\alpha_i}^{6} + 8784{\alpha_i}^{4} + 5688{\alpha_i}^{2} + 2({\alpha_i}^{12} + 22{\alpha_i}^{10} + 189{\alpha_i}^{8} + 780{\alpha_i}^{6} + 1626{\alpha_i}^{4} + 1584{\alpha_i}^{2} + 648){\alpha_i}^{2}\cos(2\lambda) + 1188\Big\} / \Big\{2\left({\alpha_i}^{8} + 18{\alpha_i}^{6} + 96{\alpha_i}^{4} + 168{\alpha_i}^{2} + 72\right)^2\Big\}, \tag{5.20}$$

$$E_{\lambda}^{\hat{a}^{\dagger 2}\hat{a}\hat{a}^{\dagger}}(\alpha_i) = -\Big\{6{\alpha_i}^{14} + 103{\alpha_i}^{12} + 714{\alpha_i}^{10} + 2395{\alpha_i}^{8} + 4128{\alpha_i}^{6} + 3344{\alpha_i}^{4} + 1192{\alpha_i}^{2} + 2(3{\alpha_i}^{12} + 46{\alpha_i}^{10} + 271{\alpha_i}^{8} + 716{\alpha_i}^{6} + 886{\alpha_i}^{4} + 400{\alpha_i}^{2} + 72){\alpha_i}^{2}\cos(2\lambda) + 124\Big\} / \Big\{2\left({\alpha_i}^{8} + 14{\alpha_i}^{6} + 54{\alpha_i}^{4} + 60{\alpha_i}^{2} + 12\right)^2\Big\}. \tag{5.21}$$

Integrating EINs to obtain λ-averaged EINs, $E^{(\hat{a}\hat{a}^{\dagger})^2}(\alpha_i)$, $E^{\hat{a}^{\dagger 2}\hat{a}\hat{a}^{\dagger}}(\alpha_i)$, $E^{\hat{a}\hat{a}^{\dagger}\hat{a}^{\dagger 2}}(\alpha_i)$, and $E^{\hat{a}^{\dagger 4}}(\alpha_i)$ are plotted in Fig. 20(c), which are all negative indicating the characteristic of noiseless amplification. The following two-cycle amplifications achieve the lowest

EINs, including one-cycle amplifications, in the corresponding regions: $(\hat{a}\hat{a}^\dagger)^2$ in $|\alpha_i| \lesssim 0.51$, $\hat{a}^{\dagger 4}$ in $0.51 \lesssim |\alpha_i| \lesssim 1.05$, and $\hat{a}^{\dagger 2}\hat{a}\hat{a}^\dagger$ in $|\alpha_i| \gtrsim 1.05$.

5.3 Amplification of Superpositions of Coherent States

5.3.1 Even and Odd Superposition of Coherent States

Even and odd SCSs are written as

$$|\pm_\alpha\rangle = \frac{1}{\sqrt{2(1 \pm e^{-2|\alpha|^2})}}(|\alpha\rangle \pm |-\alpha\rangle). \tag{5.22}$$

The "even"/"odd" is intended to signify that the state is in the superposition of only even/odd Fock states. Amplifying the even/odd SCS of amplitude α_i with the amplifier $\hat{A} \in \{\hat{a}\hat{a}^\dagger, \hat{a}^{\dagger 2}\}$, the amplified state is expressed as

$$\left|\pm^{\hat{A}}_{\alpha_i}\right\rangle = \frac{1}{N^{\hat{A}}_\pm(\alpha_i)}\hat{A}\,|\pm_{\alpha_i}\rangle\,, \tag{5.23}$$

with normalization factors,

$$\begin{aligned} N^{\hat{a}\hat{a}^\dagger}_\pm(\alpha_i) &= [2\{\pm e^{-2|\alpha_i|^2}\left(|\alpha_i|^4 - 3|\alpha_i|^2 + 1\right) + (|\alpha_i|^4 + 3|\alpha_i|^2 + 1)\}]^{\frac{1}{2}}, \\ N^{\hat{a}^{\dagger 2}}_\pm(\alpha_i) &= [2\{\pm e^{-2|\alpha_i|^2}\left(|\alpha_i|^4 - 4|\alpha_i|^2 + 2\right) + (|\alpha_i|^4 + 4|\alpha_i|^2 + 2)\}]^{\frac{1}{2}}. \end{aligned} \tag{5.24}$$

The maximum fidelity of the $\hat{A}$-amplified even/odd SCS with initial amplitude α_i is

$$_{\max}F^{\hat{A}}_\pm(\alpha_i) = \max_{\alpha_f}\left|\left\langle \pm_{\alpha_f}\middle|\pm^{\hat{A}}_{\alpha_i}\right\rangle\right|^2, \tag{5.25}$$

where the results of $F_{\pm}^{\hat{A}}$ are presented as

$$
\begin{aligned}
F_{\pm}^{\hat{a}\hat{a}^{\dagger}} &= \frac{2e^{-|\alpha_f+\alpha_i|^2}\left|e^{2\alpha_f\alpha_i}(\alpha_f\alpha_i+1)\mp(\alpha_f\alpha_i-1)\right|^2}{(\pm e^{-2|\alpha_f|^2}+1)\left|N_{\pm}^{\hat{a}\hat{a}^{\dagger}}(\alpha_i)\right|^2}, \\
F_{\pm}^{\hat{a}^{\dagger 2}} &= \frac{2|\alpha_f|^4\left(\pm e^{-\frac{1}{2}|\alpha_i+\alpha_f|^2}+e^{-\frac{1}{2}|\alpha_i-\alpha_f|^2}\right)^2}{(\pm e^{-2|\alpha_f|^2}+1)\left|N_{\pm}^{\hat{a}^{\dagger 2}}(\alpha_i)\right|^2}.
\end{aligned}
\tag{5.26}
$$

The $(\hat{a}\hat{a}^{\dagger})$-amplification illustrates higher maximum fidelity than the $(\hat{a}^{\dagger})^2$-amplification, which is numerically observed in Fig. 21(a), (d).

Unlike coherent states, which exhibit Gaussian probability distributions in measurement $\hat{x}_{\lambda}$, the identical definitions of gain (Eq. (5.8)) and EIN (Eq. (5.11)) can not be applied to the even and odd SCSs. Alternatively, amplitude gain can be defined as the ratio between the input amplitude of SCS and the output amplitude of SCS which maximizes the fidelity,

$$
g^{\hat{A}}(\alpha_i) = \frac{|\alpha_f|}{|\alpha_i|}, \tag{5.27}
$$

where α_f maximizes $F_{\pm}^{\hat{A}}$. It is numerically verified that the gain from $\hat{a}^{\dagger 2}$ is always higher than $\hat{a}\hat{a}^{\dagger}$ (Fig. 21(b), (e)).

Concerning the definition of EIN for SCSs, it is not trivial task to develop equivalent notions, as defining the concept of noise for SCSs is not straight forward. It was pointed in Ref. [131] that SCSs are useful resource for phase estimation. As the larger SCSs are more useful for phase estimation, the optimal phase estimation is closely related to the amplitude gain and the noiseless property of the amplifier, which is what EIN quantifies. Therefore, we have compared the optimal phase estimations obtained

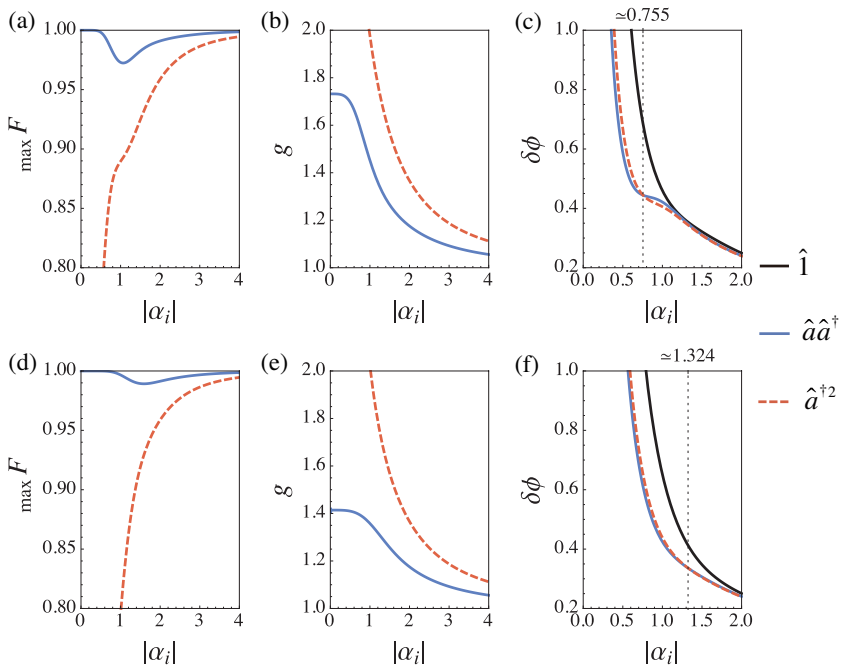

Figure 21: (a)/(d) Maximum fidelities, (b)/(e) amplitude gains, and (c)/(f) phase uncertainties when the amplification methods $\hat{a}\hat{a}^\dagger$ (solid curve) and $\hat{a}^{\dagger 2}$ (dashed curve) are applied to the even/odd SCS of initial amplitude $|\alpha_i|$. (a) The fidelity of the $\hat{a}\hat{a}^\dagger$-amplified even/odd SCSs are higher than '$F_{\max} > 0.97$' / '$F_{\max} > 0.98$', which are close to 1 for small and large $|\alpha_i|$. The fidelity of the $\hat{a}^{\dagger 2}$-amplified even/odd SCS approaches 1 for large $|\alpha_i|$. (b) The higher gain is obtained by $\hat{a}^{\dagger 2}$ than $\hat{a}\hat{a}^\dagger$. The gains from $\hat{a}\hat{a}^\dagger$ approaches '$\sqrt{3}$' / '$\sqrt{2}$' as $|\alpha_i| \to 0$. The gains from both of the amplifications approaches 1 as $|\alpha_i| \to \infty$. (c) The $\hat{a}^{\dagger 2}$-amplification exhibits lower phase uncertainties than the $\hat{a}\hat{a}^\dagger$-amplification with even/odd SCSs of large amplitude '$|\alpha_i| \gtrsim 0.755$' / '$|\alpha_i| \gtrsim 1.324$', while the opposite is true for lower $|\alpha_i|$. The phase uncertainties from both of the amplifications are lower than those from the original even/odd SCS (black curve).

from Cramér-Rao bound [145, 146],

$$\delta\phi = \frac{1}{\sqrt{\mathcal{F}}}, \tag{5.28}$$

where $\mathcal{F}$ is quantum Fisher information and can be expressed as the following for a pure state case:

$$\mathcal{F} = 4\langle(\Delta\hat{n})^2\rangle. \tag{5.29}$$

The quantum Fisher information after applying $\hat{A} \in \{\hat{1}, \hat{a}\hat{a}^\dagger, \hat{a}^{\dagger 2}\}$ to the SCS of amplitude α_i is

$$\begin{aligned}
\mathcal{F}_+^{\hat{1}}(\alpha_i) &= 4{\alpha_i}^2\left(4e^{2{\alpha_i}^2}{\alpha_i}^2 + e^{4{\alpha_i}^2} - 1\right)/\left(e^{2{\alpha_i}^2}+1\right)^2, \\
\mathcal{F}_+^{\hat{a}\hat{a}^\dagger}(\alpha_i) &= 16e^{-2{\alpha_i}^2}{\alpha_i}^2\Big\{(N_+^{\hat{a}\hat{a}^\dagger})^2\left(7\left(e^{2{\alpha_i}^2}+1\right){\alpha_i}^2 + e^{{\alpha_i}^2}{\alpha_i}^6\cosh{\alpha_i}^2\right. \\
&\quad \left. + 4e^{{\alpha_i}^2}\left(2{\alpha_i}^4+1\right)\sinh{\alpha_i}^2\right) - 4(\left({\alpha_i}^4+4\right)\alpha_i\sinh{\alpha_i}^2 \\
&\quad + 5{\alpha_i}^3\cosh{\alpha_i}^2)^2\Big\}/(N_+^{\hat{a}\hat{a}^\dagger})^4, \\
\mathcal{F}_+^{\hat{a}^{\dagger 2}}(\alpha_i) &= 16e^{-2{\alpha_i}^2}\Big\{e^{{\alpha_i}^2}(N_+^{\hat{a}^{\dagger 2}})^2(\left(13{\alpha_i}^4+46\right){\alpha_i}^2\sinh{\alpha_i}^2 \\
&\quad + \left({\alpha_i}^8+46{\alpha_i}^4+8\right)\cosh{\alpha_i}^2) \\
&\quad - 4\left(\left({\alpha_i}^4+14\right){\alpha_i}^2\sinh{\alpha_i}^2 + \left(8{\alpha_i}^4+4\right)\cosh{\alpha_i}^2\right)^2\Big\}/(N_+^{\hat{a}^{\dagger 2}})^4,
\end{aligned} \tag{5.30}$$

$$
\begin{aligned}
\mathcal{F}_{-}^{\hat{1}}(\alpha_i) &= 4{\alpha_i}^2\left(-4e^{2{\alpha_i}^2}{\alpha_i}^2+e^{4{\alpha_i}^2}-1\right)/\left(e^{2{\alpha_i}^2}-1\right)^2,\\
\mathcal{F}_{-}^{\hat{a}\hat{a}^\dagger}(\alpha_i) &= 16e^{-2{\alpha_i}^2}{\alpha_i}^2\\
&\quad\Big\{e^{{\alpha_i}^2}(N_{-}^{\hat{a}\hat{a}^\dagger})^2\left(\left({\alpha_i}^4+14\right){\alpha_i}^2\sinh{\alpha_i}^2+\left(8{\alpha_i}^4+4\right)\cosh{\alpha_i}^2\right)\\
&\quad-4\left(\left({\alpha_i}^4+4\right)\alpha_i\cosh{\alpha_i}^2+5{\alpha_i}^3\sinh{\alpha_i}^2\right)^2\Big\}/(N_{-}^{\hat{a}\hat{a}^\dagger})^4, \qquad (5.31)\\
\mathcal{F}_{-}^{\hat{a}^{\dagger 2}}(\alpha_i) &= 16e^{-2{\alpha_i}^2}\Big\{e^{{\alpha_i}^2}(N_{-}^{\hat{a}^{\dagger 2}})^2(\left(13{\alpha_i}^4+46\right){\alpha_i}^2\cosh{\alpha_i}^2\\
&\quad+\left({\alpha_i}^8+46{\alpha_i}^4+8\right)\sinh{\alpha_i}^2)\\
&\quad-4\left(4\left(2{\alpha_i}^4+1\right)\sinh{\alpha_i}^2+\left({\alpha_i}^4+14\right){\alpha_i}^2\cosh{\alpha_i}^2\right)^2\Big\}/(N_{-}^{\hat{a}^{\dagger 2}})^4.
\end{aligned}
$$

The enhancement in phase uncertainty is also witnessed for the amplification, which indicates the signature of noiseless amplification. As expected, the $\hat{a}^{\dagger 2}$-amplification is more efficient for large amplitude SCS to illustrate lower phase uncertainties than the $\hat{a}\hat{a}^\dagger$-amplification.

5.3.2 Squeezed States Approximation with Amplification

A squeezed vacuum state and a squeezed single-photon state can approximate the even and the odd SCSs of small amplitude [135], as the squeezed vacuum/single-photon state contains only even/odd number of the photons as the following expansion,

$$
\hat{S}(r)\,|(1\mp 1)/2\rangle=\sum_{n=0}^{\infty}\frac{(\tanh r)^n}{(\cosh r)^{1\mp 1/2}}\frac{\sqrt{(2n+(1\mp 1)/2)!}}{2^n n!}\,|2n+(1\mp 1)/2\rangle\,, \qquad (5.32)
$$

where $\hat{S}(r)=\exp[-r(\hat{a}^2-\hat{a}^{\dagger 2})/2]$ is the squeezing operator with a parameter r. When the even/odd SCS of amplitude $|\alpha_f|$ is desired, the maximum fidelity with which the

squeezed vacuum/single-photon state can approximate is

$$_{\max}F^{\hat{1}}_{\pm S}(\alpha_f) = \max_r \left|\langle \pm\alpha_f|\hat{S}(r)\,|(1\mp 1)/2\rangle\right|^2. \tag{5.33}$$

It is numerically verified in Fig. 22(a)/(b) that the maximum fidelity of the squeezed vacuum/single-photon state to the even/odd SCS of amplitude $|\alpha_f|$ approaches 1, as $|\alpha_f| \to 0$.

Applying the amplifier $\hat{A} \in \{\hat{a}\hat{a}^\dagger, \hat{a}^{\dagger 2}\}$, the amplified squeezed vacuum/single-photon states can be written as the following:

$$\left|\pm S^{\hat{A}}_r\right\rangle = \frac{1}{M^{\hat{A}}_{\pm}(r)}\hat{A}\hat{S}(r)\,|(1\mp 1)/2\rangle\,, \tag{5.34}$$

where the normalization factors are

$$\begin{aligned} M^{\hat{a}\hat{a}^\dagger}_{\pm}(r) &= \cosh^2 r\sqrt{\{(1\mp 1)\tanh^4 r + (3\mp 2)\tanh^2 r + 5\mp 3\}/2}, \\ M^{\hat{a}^{\dagger 2}}_{\pm}(r) &= \cosh^2 r\sqrt{(5\mp 4)\tanh^2 r + 4\mp 2}. \end{aligned} \tag{5.35}$$

The fidelity between the $\hat{A}$-amplified squeezed vacuum/single-photon states with initial squeeze level r and the even/odd SCS of amplitude $|\alpha_f|$ is

$$F^{\hat{A}}_{\pm S} = \left|\left\langle \pm\alpha_f\right| \pm S^{\hat{A}}_r\right\rangle\Big|^2. \tag{5.36}$$

The $\hat{a}\hat{a}^\dagger$- and $\hat{a}^{\dagger 2}$- amplified squeezed vacuum/single-photon states with initial squeez-

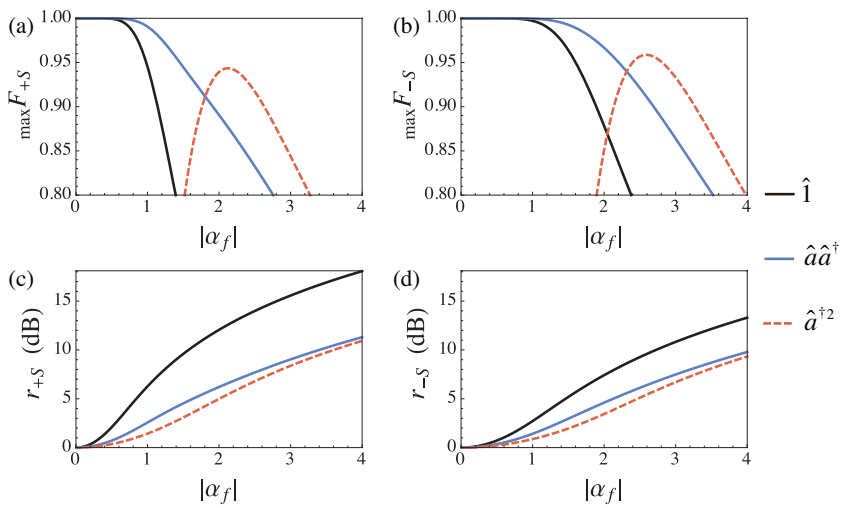

Figure 22: (a)/(b) Maximum fidelities and (c)/(d) required squeeze levels (dB) of squeezed vacuum/single-photon to approximate the even/odd SCS of amplitude $|\alpha_f|$. The maximum fidelities of the $\hat{a}\hat{a}^\dagger$-, $\hat{a}^{\dagger 2}$-amplified squeezed vacuum/single-photon states (solid blue and dashed red curves) and the squeezed vacuum/single-photon (solid black curve) are close to unity when $|\alpha_f|$ is near zero, while the fidelities begin to decrease as $|\alpha_f|$ increases. The $\hat{a}\hat{a}^\dagger$- and $\hat{a}^{\dagger 2}$- amplified squeezed vacuum/single-photon state have higher fidelities then the unamplifed state. The $\hat{a}\hat{a}^\dagger$-amplified squeezed vacuum/single-photon exhibits the highest fidelities for '$|\alpha_f| \lesssim 1.81$' / '$|\alpha_f| \lesssim 2.32$'. Although the $\hat{a}^{\dagger 2}$-amplified squeezed vacuum/single-photon state has low fidelity for small $|\alpha_f|$, the fidelity is the highest in the region peaked near '$|\alpha_f| \simeq 2.12$'/'$|\alpha_f| \simeq 2.59$' with the fidelity '$_{\max}F_{+S}^{\hat{a}^{\dagger 2}} \simeq 0.943$' / '$_{\max}F_{-S}^{\hat{a}^{\dagger 2}} \simeq 0.959$'. The $\hat{a}\hat{a}^\dagger$- and $\hat{a}^2$- amplified squeezed (c) vacuum/(d) single-photon states require less squeezing than the squeezed states in the entire $|\alpha_f|$, while the least amount of squeezing is required for the $\hat{a}^{\dagger 2}$-amplification.

ing r have the following fidelities to the even/odd SCS with target amplitude $|\alpha_f|$

$$\begin{aligned} F_{\pm S}^{\hat{a}\hat{a}^\dagger} &= \frac{2|\alpha_f|^{1\mp1} e^{-|\alpha_f|^2(\tanh r+1)} \left(|\alpha_f|^2 \tanh r - \frac{3\mp1}{2}\right)^2}{M_{\pm}^{\hat{a}\hat{a}^\dagger}(r)^2 \left(1 \pm e^{2|\alpha_f|^2}\right) \cosh^{2\mp1} r}, \\ F_{\pm S}^{\hat{a}^{\dagger 2}} &= \frac{2|\alpha_f|^{5\mp1} e^{-|\alpha_f|^2(\tanh r+1)}}{M_{\pm}^{\hat{a}^{\dagger 2}}(r)^2 \left(1 \pm e^{-2|\alpha_f|^2}\right) \cosh^{2\mp1} r}, \end{aligned} \tag{5.37}$$

The maximum fidelity with which $\hat{A}$-amplified squeezed vacuum/single-photon state can approximate the even/odd SCS of target amplitude $|\alpha_f|$ is denoted as

$$_{\max}F_{\pm S}^{\hat{A}}(\alpha_f) = \max_r \left| \left\langle \pm\alpha_f \right| \pm S_r^{\hat{A}} \right\rangle \Big|^2. \tag{5.38}$$

The maximum fidelities of the amplified squeezed vacuum and squeezed vacuum (amplified squeezed single photon and squeezed single photon) are numerically computed and plotted together in Fig. 22(a) (Fig. 22(b)) with respect to the desired amplitude of the even (odd) SCS, $|\alpha_f|$. Using the $\hat{a}\hat{a}^\dagger$-amplification on the squeezed vacuum/single-photon, the even/odd SCS of any amplitude can be better approximated with higher fidelity than the squeezed state. The fidelities to SCSs of small amplitudes are the most enhanced by the $\hat{a}\hat{a}^\dagger$-amplification. By contrast, $\hat{a}^{\dagger 2}$-amplfication best enhances the fidelity to SCSs of large amplitudes.

Required squeeze parameters $r_{\pm S}^{\hat{a}\hat{a}^\dagger}(\alpha_f)$, $r_{\pm S}^{a^{\dagger 2}}(\alpha_f)$ of the $\hat{a}\hat{a}^\dagger$-, $\hat{a}^{\dagger 2}$- amplified squeezed vacuum/single-photon states also significantly improve as shown in Fig. 22(c)/(d) ($r = r_{\pm S}^{\hat{A}}(\alpha_f)$ maximize the fidelity in Eq. (5.38)). The $\hat{a}^{\dagger 2}$-amplified squeezed vacuum/single-photon state requires the least squeezing to approximate the even/odd SCS of amplitude $|\alpha_f|$, while the $\hat{a}\hat{a}^\dagger$-amplfied squeezed vacuum/single-photon states also require the lesser squeezing than the squeezed state.

The $\hat{a}\hat{a}^\dagger$- and $\hat{a}^{\dagger 2}$- amplified squeezed vacuum/single-photon state exhibit higher

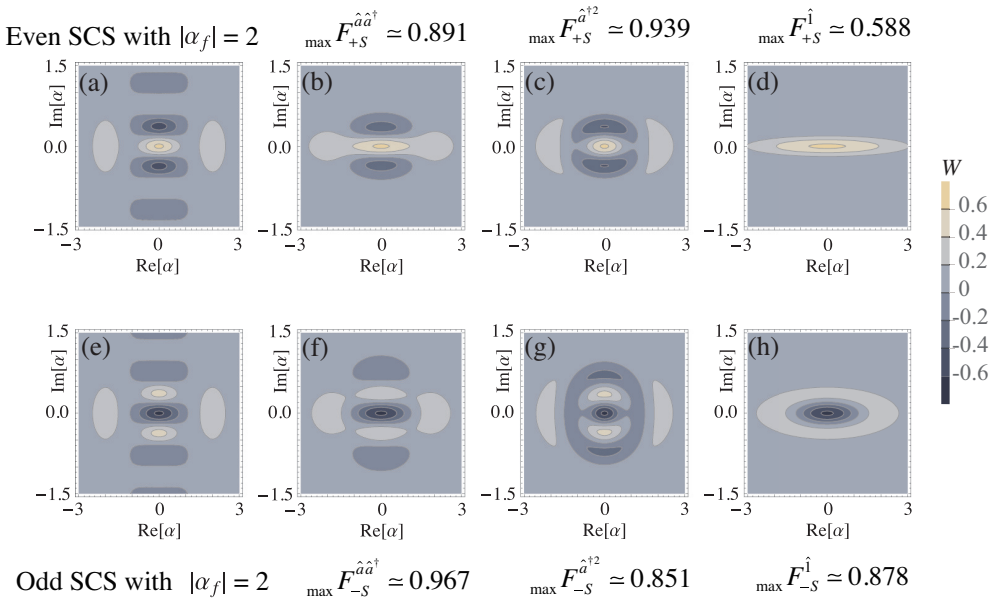

Figure 23: Contour plotted Wigner functions of the (b) $\hat{a}\hat{a}^\dagger$-amplified squeezed vacuum, (c) $\hat{a}^{\dagger 2}$-amplified squeezed vacuum, and (d) squeezed vacuum which approximate the (a) even SCS of amplitude $|\alpha_f| = 2$; (f) $\hat{a}\hat{a}^\dagger$-amplified squeezed single-photon, (g) $\hat{a}^{\dagger 2}$-amplified squeezed single-photon, and (h) squeezed single-photon which approximate which approximate the (e) odd SCS of amplitude $|\alpha_f| = 2$. Wigner function of the $\hat{a}^{\dagger 2}$-amplified squeezed vacuum can be visually verified to have the closest Wigner function to the even SCS of the amplitude $|\alpha_f| = 2$, which can be also inferred from the maximum fidelities. On the other hand, Wigner function of the $\hat{a}\hat{a}^\dagger$-amplified squeezed single-photon can be visually verified to have the closest Wigner function to the odd SCS of the amplitude $|\alpha_f| = 2$.

fidelity to the even/odd SCS than the squeezed state, not to mention of the required squeezing. The $\hat{a}\hat{a}^\dagger$-amplification shows the higher fidelity to the SCS with small target amplitude. However, when the even/odd SCS with a larger amplitude is desired, the $\hat{a}^{\dagger 2}$-amplification is more advantageous in terms of fidelity and required squeezing.

5.4 Remarks

In conclusion, $\hat{a}^{\dagger 2}$ is better than $\hat{a}\hat{a}^\dagger$ as a noiseless amplifier for coherent states as far as the initial amplitude is $|\alpha_i| \gtrsim 0.91$ in terms of EIN. Similarly, when $\hat{a}\hat{a}^\dagger$ and $\hat{a}^{\dagger 2}$ are successively applied with different possible orders, $\hat{a}^{\dagger 2}$ is found to serve as the best noiseless amplifier as far as the initial amplitude is $|\alpha_i| \gtrsim 1.05$. The analogous behavior is also observed for SCSs in terms of optimal phase uncertainty. Besides, the enhancement of maximum fidelities and squeeze levels are found when amplified squeezed states are used to approximate SCSs. In contrast to the previous studies [28], our work provides efficient schemes to implement a noiseless amplifier for light fields with medium and large amplitudes.

Chapter 6

Conclusion

In this thesis, we have proposed schemes to witness Bell nonlocality, EPR steering without loopholes, and have investigated the hierarchical relation between EPR steerable states and quantum teleportable states. We also have suggested and investigated an efficient noiseless amplification of light fields with large amplitudes, which may be used for enhancing nonlocal behaviors of quantum mechanics and quantum information processing.

There are two classes of nonlocality which entangled states can possess. The higher hierarchy is Bell nonlocality, and the lower hierarchy is EPR steering (Every Bell nonlocal states are EPR steerable). Quantum teleportation also uses nonlocality from the entangled channel. There had been researches about the hierarchy between two qubits Bell-CHSH nonlocal states, quantum teleportable state, and entangled states, and the hierarchical order is known as the following: Bell nonlocal states, quantum teleportable states, and entangled states (from high to low). We have shown that for a two qubit system quantum steerable states and quantum teleportable states have no subset relation. Since quantum teleportation can be regarded as a special case of remote state preparation, it might be interesting to find out hierarchical relation between EPR steerable states and remote state preparable states for a further study.

We have investigated Bell-CHSH inequality tests with entanglement between a two-level Rydberg atom and a coherent-state field in a cavity. Our aim was to avoid

loopholes in Bell-CHSH inequality tests using advantages of hybrid system which is composed of atoms and photons. We could reduce the decoherence effect using superconducting cylinder channel, which inhibits spontaneous emission in atomic system. We have fully analyzed decoherence effects from state generation process to measurement process, and derived conditions required to perform a Bell inequality test free from the locality loophole. Bell violation with about 2m of separation seems feasible with our scheme, although considerable improvement of cavity life time is required to close the detection loophole.

Subsequently, we also have investigated EPR Steering of ECSs. Demonstration of EPR steering without detection loophole seems feasible, if ECS can be generated with high fidelity. Demonstration of ECS steering is required for secure oneside-device-independent QKD. Although the required detection efficiency from our demonstration of EPR steering with ECS seems feasible to achieve, it is more demanding than the efficiency required in the previous study with single photon singlet states. As the loophole-free test of EPR steering requires precise detection efficiency and short measurement time for only one side of the system, demonstrating EPR steering is easier than Bell nonlocality. Therefore, it may be intriguing to consider EPR steering of cavity-atom entangled system which is the system we have considered previously for Bell nonlocality, and examine required experimental parameters to close loopholes.

Finally, we have suggested and investigated an efficient noiseless amplification scheme for coherent states with large amplitudes, while previous studies are suitable for amplification of coherent states with small amplitudes. We have proposed double-photon-addition operator as an amplifier for large amplitude coherent states, and have compared with photon-addition-then-subtraction operator which is an efficient amplifier for small coherent states. Both amplifiers can be constructed with series of

elementary photonics operations, which are not challenging to implement. Our study verifies that double-photon-addition is also more noiseless amplifier for large SCSs in terms of optimal phase uncertainty. Furthermore, the enhancement of maximum fidelities and squeeze levels are found when amplified squeezed vacuum/single-photon states are used to approximate SCSs. Our study motivates to develop a generalized measure of noiselessness of the amplifier for various types of non-Gaussian states.

We believe that our study has added some understanding of quantum nonlocality and quantum engineering, and expect our schemes can be realized with progresses in experiment. Combining the studies in this thesis, demonstration of EPR steering with atom-photon entangled states which is engineered by practical amplification scheme may be intriguing to investigate.

Bibliography

[1] M. Steiner, "Towards quantifying non-local information transfer: finite-bit non-locality," *Physics Letters A*, vol. 270, pp. 239–244, June 2000.

[2] S. J. Freedman and J. F. Clauser, "Experimental Test of Local Hidden-Variable Theories," *Physical Review Letters*, vol. 28, pp. 938–941, Apr. 1972.

[3] A. Aspect, P. Grangier, and G. Roger, "Experimental Tests of Realistic Local Theories via Bell's Theorem," *Physical Review Letters*, vol. 47, pp. 460–463, Aug. 1981.

[4] W. Tittel, J. Brendel, H. Zbinden, and N. Gisin, "Violation of Bell Inequalities by Photons More Than 10 km Apart," *Physical Review Letters*, vol. 81, pp. 3563–3566, Oct. 1998.

[5] G. Weihs, T. Jennewein, C. Simon, H. Weinfurter, and A. Zeilinger, "Violation of Bell's Inequality under Strict Einstein Locality Conditions," *Physical Review Letters*, vol. 81, pp. 5039–5043, Dec. 1998.

[6] M. A. Rowe, D. Kielpinski, V. Meyer, C. A. Sackett, W. M. Itano, C. Monroe, and D. J. Wineland, "Experimental violation of a Bell's inequality with efficient detection," *Nature Photonics*, vol. 409, pp. 791–794, Feb. 2001.

[7] D. N. Matsukevich, P. Maunz, D. L. Moehring, S. Olmschenk, and C. Monroe, "Bell Inequality Violation with Two Remote Atomic Qubits," *Physical Review Letters*, vol. 100, p. 150404, Apr. 2008.

[8] F. J. Tipler, "Quantum nonlocality does not exist.," *Proceedings of the National Academy of Sciences of the United States of America*, vol. 111, pp. 11281–11286, Aug. 2014.

[9] H. M. Wiseman, S. J. Jones, and A. C. Doherty, "Steering, Entanglement, Nonlocality, and the Einstein-Podolsky-Rosen Paradox," *Physical Review Letters*, vol. 98, p. 140402, Apr. 2007.

[10] B. Wittmann, S. Ramelow, F. Steinlechner, N. K. Langford, N. Brunner, H. M. Wiseman, R. Ursin, and A. Zeilinger, "Loophole-free Einstein–Podolsky–Rosen experiment via quantum steering," *New Journal of Physics*, vol. 14, p. 053030, May 2012.

[11] L. Masanes, S. Pironio, and A. Acín, "Secure device-independent quantum key distribution with causally independent measurement devices," *Nature Communications*, vol. 2, p. 238, Mar. 2011.

[12] C. Branciard, E. G. Cavalcanti, S. P. Walborn, V. Scarani, and H. M. Wiseman, "One-sided device-independent quantum key distribution: Security, feasibility, and the connection with steering," *Physical Review A*, vol. 85, p. 010301, Jan. 2012.

[13] C. H. Bennett, G. Brassard, C. Crépeau, R. Jozsa, A. Peres, and W. K. Wootters, "Teleporting an unknown quantum state via dual classical and Einstein-Podolsky-Rosen channels," *Physical Review Letters*, vol. 70, pp. 1895–1899, Mar. 1993.

[14] S. Popescu, "Bell's inequalities versus teleportation: What is nonlocality?," *Physical Review Letters*, vol. 72, pp. 797–799, Feb. 1994.

[15] R. Horodecki, M. Horodecki, and P. Horodecki, "Teleportation, Bell's inequalities and inseparability," *Physics Letters A*, vol. 222, pp. 21–25, Oct. 1996.

[16] J. Park, S.-Y. Lee, H.-W. Lee, and H. Nha, "Enhanced Bell violation by a coherent superposition of photon subtraction and addition," *Journal of the Optical Society of America B*, vol. 29, pp. 906–911, May 2012.

[17] G. Torlai, G. McKeown, P. Marek, R. Filip, H. Jeong, M. Paternostro, and G. D. Chiara, "Violation of Bell's inequalities with preamplified homodyne detection," *Physical Review A*, vol. 87, no. 5, p. 052112, 2013.

[18] C. Caves, "Quantum limits on noise in linear amplifiers," *Physical Review D*, vol. 26, pp. 1817–1839, Oct. 1982.

[19] G. Y. Xiang, T. C. Ralph, A. P. Lund, N. Walk, and G. J. Pryde, "Heralded noiseless linear amplification and distillation of entanglement," *Nature Photonics*, vol. 4, pp. 316–319, May 2010.

[20] S. Fossier, E. Diamanti, T. Debuisschert, R. Tualle-Brouri, and P. Grangier, "Improvement of continuous-variable quantum key distribution systems by using optical preamplifiers," *Journal of Physics B: Atomic, Molecular and Optical Physics*, vol. 42, p. 114014, June 2009.

[21] R. Blandino, A. Leverrier, M. Barbieri, J. Etesse, P. Grangier, and R. Tualle-Brouri, "Improving the maximum transmission distance of continuous-variable quantum key distribution using a noiseless amplifier," *Physical Review A*, vol. 86, p. 012327, July 2012.

[22] M. Mičuda, I. Straka, M. Miková, M. Dušek, N. J. Cerf, J. Fiurášek, and M. Ježek, "Noiseless Loss Suppression in Quantum Optical Communication," *Physical Review Letters*, vol. 109, p. 180503, Nov. 2012.

[23] L. M. Duan, M. D. Lukin, J. I. Cirac, and P. Zoller, "Long-distance quantum communication with atomic ensembles and linear optics," *Nature Photonics*, vol. 414, pp. 413–418, Nov. 2001.

[24] M. A. Usuga, C. R. Müller, C. Wittmann, P. Marek, R. Filip, C. Marquardt, G. Leuchs, and U. L. Andersen, "Noise-powered probabilistic concentration of phase information," *Nature Physics*, vol. 6, pp. 767–771, Aug. 2010.

[25] T. C. Ralph, "Quantum error correction of continuous-variable states against Gaussian noise," *Physical Review A*, vol. 84, p. 022339, Aug. 2011.

[26] U. Leonhardt and H. Paul, "High-Accuracy Optical Homodyne Detection with Low-Efficiency Detectors: "Preamplification" from Antisqueezing," *Physical Review Letters*, vol. 72, pp. 4086–4089, June 1994.

[27] J. Fiurášek, "Engineering quantum operations on traveling light beams by multiple photon addition and subtraction," *Physical Review A*, vol. 80, p. 053822, Nov. 2009.

[28] A. Zavatta, J. Fiurášek, and M. Bellini, "A high-fidelity noiseless amplifier for quantum light states," *Nature Photonics*, vol. 5, pp. 52–60, Jan. 2011.

[29] A. Einstein, M. Born, and H. Born, *The Born-Einstein letters: correspondence between Albert Einstein and Max and Hedwig Born from 1916-1955, with commentaries by Max Born*. Macmillan, 1971.

[30] A. Einstein, B. Podolsky, and N. Rosen, "Can Quantum-Mechanical Description of Physical Reality Be Considered Complete?," *Phys. Rev.*, vol. 47, pp. 777–780, May 1935.

[31] G. Brassard and A. A. Méthot, "CAN QUANTUM-MECHANICAL DESCRIPTION OF PHYSICAL REALITY BE CONSIDERED INCOMPLETE?," *International Journal of Quantum Information*, vol. 04, no. 01, pp. 45–54, 2006.

[32] W. . Heisenberg, "ber den anschaulichen Inhalt der quantentheoretischen Kinematik und Mechanik," *Zeitschrift fr Physik*, vol. 43, pp. 172–198, Mar. 1927.

[33] D. Bohm, *Quantum Theory*. Englewood Cliffs, New Jersey: Prentice Hall, 1951.

[34] J. S. Bell, "On the Einstein Podolsky Rosen paradox," *Physics*, vol. 1, no. 3, pp. 195–200, 1964.

[35] E. Schrödinger, "Die gegenwärtige Situation in der Quantenmechanik," *Naturwissenschaften*, vol. 23, no. 49, pp. 823–828, 1935.

[36] E. Schrödinger and M. Born, "Discussion of Probability Relations between Separated Systems," *Mathematical Proceedings of the Cambridge Philosophical Society*, vol. 31, p. 555, Oct. 2008.

[37] J. D. Trimmer, "The present situation in quantum mechanics: A TRANSLATION OF SCHRÖDINGER'S "CAT PARADOX" PAPER," in *Proceedings of the American Philosophical Society*, pp. 323–338, 1980.

[38] E. Schrödinger and P. A. M. Dirac, "Probability relations between separated systems," *Mathematical Proceedings of the Cambridge Philosophical Society*, vol. 32, p. 446, Oct. 2008.

[39] R. F. Werner, "Quantum states with Einstein-Podolsky-Rosen correlations admitting a hidden-variable model," *Physical Review A*, vol. 40, pp. 4277–4281, Oct. 1989.

[40] J. F. Clauser, M. A. Horne, A. Shimony, and R. A. Holt, "Proposed Experiment to Test Local Hidden-Variable Theories," *Physical Review Letters*, vol. 23, pp. 880–884, Oct. 1969.

[41] J. F. Clauser and M. A. Horne, "Experimental consequences of objective local theories," *Physical Review D*, vol. 10, pp. 526–535, July 1974.

[42] E. G. Cavalcanti, S. J. Jones, and H. Wiseman, "Experimental criteria for steering and the Einstein-Podolsky-Rosen paradox," *Physical Review A*, vol. 80, p. 032112, Sept. 2009.

[43] C. H. Bennett, H. J. Bernstein, S. Popescu, and B. Schumacher, "Concentrating partial entanglement by local operations," *Physical Review A*, vol. 53, pp. 2046–2052, Apr. 1996.

[44] C. H. Bennett, D. P. DiVincenzo, J. A. Smolin, and W. K. Wootters, "Mixed-state entanglement and quantum error correction," *Physical Review A*, vol. 54, pp. 3824–3851, Nov. 1996.

[45] W. K. Wootters and W. H. Zurek, "A single quantum cannot be cloned," *Nature Photonics*, vol. 299, pp. 802–803, Oct. 1982.

[46] H. Kim, J. Park, and H. Jeong, "Transfer of different types of optical qubits over a lossy environment," *Physical Review A*, vol. 89, p. 042303, Apr. 2014.

[47] M. Horodecki, P. Horodecki, and R. Horodecki, "General teleportation channel, singlet fraction, and quasidistillation," *Physical Review A*, vol. 60, pp. 1888–1898, Sept. 1999.

[48] J.-L. Chen, X. J. Ye, C. Wu, H.-Y. Su, A. Cabello, L. C. Kwek, and C. H. Oh, "All-Versus-Nothing Proof of Einstein-Podolsky-Rosen Steering," *Scientific Reports*, vol. 3, July 2013.

[49] P. M. Pearle, "Hidden-Variable Example Based upon Data Rejection," *Physical Review D*, vol. 2, pp. 1418–1425, Oct. 1970.

[50] J. S. Bell, "Bertlmann's socks and the nature of reality," *Le Journal de Physique Colloques*, vol. 42, pp. C2–41–C2–62, Mar. 1981.

[51] M. S. Kim and J. Lee, "Test of quantum nonlocality for cavity fields," *Physical Review A*, vol. 61, p. 042102, Mar. 2000.

[52] P. Milman, A. Auffeves, F. Yamaguchi, M. Brune, J.-M. Raimond, and S. Haroche, "A proposal to test Bell's inequalities with mesoscopic non-local states in cavity QED," *The European Physical Journal D*, vol. 32, pp. 233–239, Feb. 2005.

[53] C. Simon and W. T. M. Irvine, "Robust long-distance entanglement and a loophole-free Bell test with ions and photons," *Physical Review Letters*, 2003.

[54] J. Volz, M. Weber, D. Schlenk, W. Rosenfeld, J. Vrana, K. Saucke, C. Kurtsiefer, and H. Weinfurter, "Observation of Entanglement of a Single Photon with a Trapped Atom," *Physical Review Letters*, vol. 96, p. 030404, Jan. 2006.

[55] N. Brunner, N. Gisin, V. Scarani, and C. Simon, "Detection Loophole in Asymmetric Bell Experiments," *Physical Review Letters*, vol. 98, p. 220403, May 2007.

[56] N. Sangouard, J. D. Bancal, N. Gisin, W. Rosenfeld, P. Sekatski, M. Weber, and H. Weinfurter, "Loophole-free Bell test with one atom and less than one photon on average," *Physical Review A*, vol. 84, p. 052122, Nov. 2011.

[57] N. Spagnolo, C. Vitelli, M. Paternostro, F. De Martini, and F. Sciarrino, "Hybrid methods for witnessing entanglement in a microscopic-macroscopic system," *Physical Review A*, vol. 84, p. 032102, Sept. 2011.

[58] D. L. Moehring, M. J. Madsen, B. B. Blinov, and C. Monroe, "Experimental Bell Inequality Violation with an Atom and a Photon," *Physical Review Letters*, vol. 93, p. 090410, Aug. 2004.

[59] K. Wódkiewicz, "Nonlocality of the Schrödinger cat," *New Journal of Physics*, vol. 2, pp. 21–21, Sept. 2000.

[60] M. Brune, E. Hagley, J. Dreyer, X. Maître, A. Maali, C. Wunderlich, J.-M. Raimond, and S. Haroche, "Observing the Progressive Decoherence of the "Meter" in a Quantum Measurement," *Physical Review Letters*, vol. 77, pp. 4887–4890, Dec. 1996.

[61] C. Guerlin, J. Bernu, S. Deléglise, C. Sayrin, S. Gleyzes, S. Kuhr, M. Brune, J.-M. Raimond, and S. Haroche, "Progressive field-state collapse and quantum non-demolition photon counting," *Nature Photonics*, vol. 448, pp. 889–893, Aug. 2007.

[62] S. Deleglise, I. Dotsenko, C. Sayrin, J. Bernu, M. Brune, J.-M. Raimond, and S. Haroche, "Reconstruction of non-classical cavity field states with snapshots of their decoherence," *Nature Photonics*, 2008.

[63] T. C. Ralph and H. Jeong, "Transfer of nonclassical properties from a microscopic superposition to macroscopic thermal states in the high temperature limit," *Physical Review Letters*, 2006.

[64] F. De Martini, F. Sciarrino, and C. Vitelli, "Entanglement Test on a Microscopic-Macroscopic System," *Physical Review Letters*, vol. 100, p. 253601, June 2008.

[65] N. Spagnolo, C. Vitelli, F. Sciarrino, and F. De Martini, "Entanglement criteria for microscopic-macroscopic systems," *Physical Review A*, vol. 82, p. 052101, Nov. 2010.

[66] W. J. Munro, G. J. Milburn, and B. C. Sanders, "Entangled coherent-state qubits in an ion trap," *Physical Review A*, vol. 62, p. 052108, Oct. 2000.

[67] D. Wilson, H. Jeong, and M. S. Kim, "Quantum nonlocality for a mixed entangled coherent state," *Journal of Modern Optics*, vol. 49, pp. 851–864, Apr. 2002.

[68] H. Jeong, W. Son, and M. S. Kim, "Quantum nonlocality test for continuous-variable states with dichotomic observables," *Physical Review A*, vol. 67, p. 012106, Jan. 2003.

[69] H. Jeong, "Testing Bell inequalities with photon-subtracted Gaussian states," *Physical Review A*, 2008.

[70] H. Jeong and T. C. Ralph, "Failure of Local Realism Revealed by Extremely-Coarse-Grained Measurements," *Physical Review Letters*, vol. 102, p. 060403, Feb. 2009.

[71] H. Jeong and N. B. An, "Greenberger-Horne-Zeilinger–type and W-type entangled coherent states: Generation and Bell-type inequality tests without photon counting," *Physical Review A*, vol. 74, p. 022104, Aug. 2006.

[72] H. Jeong and T. C. Ralph, "Violation of Bell's inequality using classical measurements and nonlinear local operations," *Physical Review A*, vol. 75, p. 052105, May 2007.

[73] C. C. Gerry, J. Mimih, and A. Benmoussa, "Maximally entangled coherent states and strong violations of Bell-type inequalities," *Physical Review A*, vol. 80, p. 022111, Aug. 2009.

[74] B. S. Cirelson, "Quantum generalizations of Bell's inequality," *Letters in Mathematical Physics*, vol. 4, no. 2, pp. 93–100, 1980.

[75] S. Haroche and J.-M. Raimond, *Exploring the Quantum*. Atoms, Cavities, and Photons, Oxford University Press, Apr. 2013.

[76] H. Yuen and J. H. Shapiro, "Optical communication with two-photon coherent states–Part III: Quantum measurements realizable with photoemissive detectors," *IEEE Transactions on Information Theory*, vol. 26, pp. 78–92, Jan. 1980.

[77] R. A. Campos, B. E. A. Saleh, and M. C. Teich, "Quantum-mechanical lossless beam splitter: SU(2) symmetry and photon statistics," *Physical Review A*, vol. 40, pp. 1371–1384, Aug. 1989.

[78] W. H. Press, S. A. Teukolsky, W. T. Vetterling, and B. P. Flannery, ***Numerical Recipes in C***, vol. 1 of *The Art of Scientific Computing*. Cambridge University Press, Mar. 2003.

[79] N. Gisin and B. Gisin, "A local hidden variable model of quantum correlation exploiting the detection loophole," *Physics Letters A*, vol. 260, pp. 323–327, Sept. 1999.

[80] M. Brune, S. Haroche, J.-M. Raimond, L. Davidovich, and N. Zagury, "Manipulation of photons in a cavity by dispersive atom-field coupling: Quantum-nondemolition measurements and generation of ''Schrödinger cat'' states," *Physical Review A*, vol. 45, pp. 5193–5214, Apr. 1992.

[81] L. Davidovich, M. Brune, J.-M. Raimond, and S. Haroche, "Mesoscopic quantum coherences in cavity QED: Preparation and decoherence monitoring schemes," *Physical Review A*, vol. 53, pp. 1295–1309, Mar. 1996.

[82] J.-M. Raimond, M. Brune, and S. Haroche, "Manipulating quantum entanglement with atoms and photons in a cavity," *Reviews of Modern Physics*, vol. 73, pp. 565–582, Aug. 2001.

[83] P. Nussenzveig, F. Bernardot, M. Brune, J. Hare, J.-M. Raimond, S. Haroche, and W. Gawlik, "Preparation of high-principal-quantum-number ''circular'' states of rubidium," *Physical Review A*, vol. 48, pp. 3991–3994, Nov. 1993.

[84] B.-G. Englert, N. Sterpi, and H. Walther, "Parity states in the one-atom maser," *Optics Communications*, vol. 100, pp. 526–535, July 1993.

[85] R. G. Hulet, E. S. Hilfer, and D. Kleppner, "Inhibited Spontaneous Emission by a Rydberg Atom," *Physical Review Letters*, vol. 55, pp. 2137–2140, Nov. 1985.

[86] K. Kakazu and Y. S. Kim, "Field Quantization and Spontaneous Emission in Circular Cylindrical Cavities," *Progress of Theoretical Physics*, vol. 96, pp. 883–899, Nov. 1996.

[87] M. Wilkens, Z. Białynicka-Birula, and P. Meystre, "Spontaneous emission in a Fabry-Pérot cavity: The effects of atomic motion," *Physical Review A*, vol. 45, pp. 477–482, Jan. 1992.

[88] J. G. Peixoto de Faria and M. C. Nemes, "Dissipative dynamics of the Jaynes-Cummings model in the dispersive approximation: Analytical results," *Physical Review A*, vol. 59, pp. 3918–3925, May 1999.

[89] X. Zhou, C. Sayrin, S. Deléglise, J. Bernu, C. Guerlin, S. Gleyzes, S. Kuhr, I. Dotsenko, M. Brune, J.-M. Raimond, and S. Haroche, "Tools for fundamental cavity QED experiments," in *cqed.org*, 2009.

[90] S. Kuhr, S. Gleyzes, C. Guerlin, J. Bernu, U. B. Hoff, S. Deléglise, S. Osnaghi, M. Brune, J.-M. Raimond, S. Haroche, E. Jacques, P. Bosland, and B. Visentin, "Ultrahigh finesse Fabry-Pérot superconducting resonator," *Applied Physics Letters*, vol. 90, no. 16, p. 164101, 2007.

[91] S. J. D. Phoenix, "Wave-packet evolution in the damped oscillator," *Physical Review A*, vol. 41, pp. 5132–5138, May 1990.

[92] H. Moya-Cessa, "Decoherence in atom–field interactions: A treatment using superoperator techniques," *Physics Reports*, vol. 432, pp. 1–41, Sept. 2006.

[93] W. Witschel, "Ordered products of exponential operators by similarity transformations," *International Journal of Quantum Chemistry*, vol. 20, pp. 1233–1241, Dec. 1981.

[94] P. Maioli, T. Meunier, S. Gleyzes, A. Auffeves, G. Nogues, M. Brune, J.-M. Raimond, and S. Haroche, "Nondestructive Rydberg Atom Counting with Mesoscopic Fields in a Cavity," *Physical Review Letters*, vol. 94, p. 113601, Mar. 2005.

[95] B. Vlastakis, A. Petrenko, N. Ofek, L. Sun, Z. Leghtas, K. Sliwa, Y. Liu, M. Hatridge, J. Blumoff, L. Frunzio, M. Mirrahimi, L. Jiang, M. H. Devoret, and R. J. Schoelkopf, "Violating Bell's inequality with an artificial atom and a cat state in a cavity," *arxiv.com*, Apr. 2015.

[96] E. Schrödinger, "Der stetige Übergang von der Mikro- zur Makromechanik," *Naturwissenschaften*, vol. 14, pp. 664–666, July 1926.

[97] C.-W. Lee, S.-W. Ji, and H. Nha, "Quantum steering for continuous-variable states," *Journal of the Optical Society of America B*, vol. 30, no. 9, p. 2483, 2013.

[98] S. J. Jones and H. M. Wiseman, "Nonlocality of a single photon: Paths to an Einstein-Podolsky-Rosen-steering experiment," *Physical Review A*, vol. 84, p. 012110, July 2011.

[99] H. Jeong and M. S. Kim, "Efficient quantum computation using coherent states," *Physical Review A*, vol. 65, p. 042305, Mar. 2002.

[100] T. C. Ralph, A. Gilchrist, G. J. Milburn, W. J. Munro, and S. Glancy, "Quantum computation with optical coherent states," *Physical Review A*, vol. 68, p. 042319, Oct. 2003.

[101] M. Paternostro and H. Jeong, "Testing nonlocal realism with entangled coherent states," *Physical Review A*, vol. 81, p. 032115, Mar. 2010.

[102] A. P. Lund, H. Jeong, T. C. Ralph, and M. S. Kim, "Conditional production of superpositions of coherent states with inefficient photon detection," *Physical Review A*, vol. 70, p. 020101, Aug. 2004.

[103] P. Marek, H. Jeong, and M. S. Kim, "Generating "squeezed" superpositions of coherent states using photon addition and subtraction," *Physical Review A*, vol. 78, p. 063811, Dec. 2008.

[104] R. Tualle-Brouri, P. Grangier, A. Ourjoumtsev, and J. Laurat, "Generating optical Schrödinger kittens for quantum information processing," *Science*, 2006.

[105] N. Herbert, "FLASH—A superluminal communicator based upon a new kind of quantum measurement," *Foundations of Physics*, vol. 12, pp. 1171–1179, Dec. 1982.

[106] E. Arthurs and M. Goodman, "Quantum Correlations: A Generalized Heisenberg Uncertainty Relation," *Physical Review Letters*, vol. 60, pp. 2447–2449, June 1988.

[107] T. C. Ralph and A. P. Lund, "Nondeterministic Noiseless Linear Amplification of Quantum Systems," in *Proceedings of 9th International Conference on Quantum Communication, Measurement, and Computing* (A. Lvovsky, ed.), pp. 155–160, AIP, 2009.

[108] J. S. Neergaard-Nielsen, Y. Eto, C.-W. Lee, H. Jeong, and M. Sasaki, "Quantum tele-amplification with a continuous-variable superposition state," *Nature Photonics*, vol. 7, pp. 439–443, May 2013.

[109] J. Wenger, R. Tualle-Brouri, and P. Grangier, "Non-Gaussian Statistics from Individual Pulses of Squeezed Light," *Physical Review Letters*, vol. 92, p. 153601, Apr. 2004.

[110] A. Zavatta, S. Viciani, and M. Bellini, "Quantum-to-classical transition with single-photon-added coherent states of light.," *Science*, vol. 306, pp. 660–662, Oct. 2004.

[111] A. Zavatta, V. Parigi, M. S. Kim, H. Jeong, and M. Bellini, "Experimental Demonstration of the Bosonic Commutation Relation via Superpositions of Quantum Operations on Thermal Light Fields," *Physical Review Letters*, vol. 103, p. 140406, Oct. 2009.

[112] H. Jeong, A. Zavatta, M. Kang, S.-W. Lee, L. S. Costanzo, S. Grandi, T. C. Ralph, and M. Bellini, "Generation of hybrid entanglement of light," *Nature Photonics*, vol. 8, pp. 564–569, July 2014.

[113] H.-J. Kim, S.-Y. Lee, S.-W. Ji, and H. Nha, "Quantum linear amplifier enhanced by photon subtraction and addition," *Physical Review A*, vol. 85, p. 013839, Jan. 2012.

[114] J. Joo, M. Elliott, D. K. L. Oi, E. Ginossar, and T. P. Spiller, "Deterministic amplification of Schrödinger cat states in circuit quantum electrodynamics," *arxiv.com*, Feb. 2015.

[115] A. P. Lund, T. C. Ralph, and H. L. Haselgrove, "Fault-Tolerant Linear Optical Quantum Computing with Small-Amplitude Coherent States," *Physical Review Letters*, vol. 100, p. 030503, Jan. 2008.

[116] A. Mann, B. C. Sanders, and W. J. Munro, "Bell's inequality for an entanglement of nonorthogonal states," *Physical Review A*, vol. 51, pp. 989–991, Feb. 1995.

[117] R. Filip, J. Rehácek, and M. Dusek, "Entanglement of coherent states and decoherence," *Journal of Optics B: Quantum and Semiclassical Optics*, vol. 3, pp. 341–345, Oct. 2001.

[118] J. Wenger, M. Hafezi, F. Grosshans, R. Tualle-Brouri, and P. Grangier, "Maximal violation of Bell inequalities using continuous-variable measurements," *Physical Review A*, vol. 67, p. 012105, Jan. 2003.

[119] H. Jeong, "Testing Bell inequalities with photon-subtracted Gaussian states," *Physical Review A*, vol. 78, p. 042101, Oct. 2008.

[120] C.-W. Lee and H. Jeong, "Effects of squeezing on quantum nonlocality of superpositions of coherent states," *Physical Review A*, vol. 80, p. 052105, Nov. 2009.

[121] C.-W. Lee and H. Jeong, "Faithful test of nonlocal realism with entangled coherent states," *Physical Review A*, vol. 83, p. 022102, Feb. 2011.

[122] Y. Lim, M. Kang, J. Lee, and H. Jeong, "Using macroscopic entanglement to close the detection loophole in Bell-inequality tests," *Physical Review A*, vol. 85, p. 062112, June 2012.

[123] B. T. Kirby and J. D. Franson, "Nonlocal interferometry using macroscopic coherent states and weak nonlinearities," *Physical Review A*, vol. 87, p. 053822, May 2013.

[124] B. T. Kirby and J. D. Franson, "Macroscopic state interferometry over large distances using state discrimination," *Physical Review A*, vol. 89, p. 033861, Mar. 2014.

[125] C.-Y. Park and H. Jeong, "Bell-inequality tests using asymmetric entangled coherent states in asymmetric lossy environments," *Physical Review A*, vol. 91, p. 042328, Apr. 2015.

[126] C. Gerry and R. Campos, "Generation of maximally entangled photonic states with a quantum-optical Fredkin gate," *Physical Review A*, vol. 64, p. 063814, Nov. 2001.

[127] C. Gerry, A. Benmoussa, and R. Campos, "Nonlinear interferometer as a resource for maximally entangled photonic states: Application to interferometry," *Physical Review A*, vol. 66, p. 013804, July 2002.

[128] T. C. Ralph, "Coherent superposition states as quantum rulers," *Physical Review A*, vol. 65, p. 042313, Apr. 2002.

[129] W. J. Munro, K. Nemoto, G. J. Milburn, and S. Braunstein, "Weak-force detection with superposed coherent states," *Physical Review A*, vol. 66, p. 023819, Aug. 2002.

[130] R. Campos, C. Gerry, and A. Benmoussa, "Optical interferometry at the Heisenberg limit with twin Fock states and parity measurements," *Physical Review A*, vol. 68, p. 023810, Aug. 2003.

[131] J. Joo, W. J. Munro, and T. P. Spiller, "Quantum Metrology with Entangled Coherent States," *Physical Review Letters*, vol. 107, p. 083601, Aug. 2011.

[132] O. Hirota, K. Kato, and D. Murakami, "Effectiveness of entangled coherent state in quantum metrology," *arxiv.com*, Aug. 2011.

[133] J. Joo, K. Park, H. Jeong, W. J. Munro, K. Nemoto, and T. P. Spiller, "Quantum metrology for nonlinear phase shifts with entangled coherent states," *Physical Review A*, vol. 86, p. 043828, Oct. 2012.

[134] Y. M. Zhang, X. W. Li, W. Yang, and G. R. Jin, "Quantum Fisher information of entangled coherent states in the presence of photon loss," *Physical Review A*, vol. 88, p. 043832, Oct. 2013.

[135] H. Jeong, A. P. Lund, and T. C. Ralph, "Production of superpositions of coherent states in traveling optical fields with inefficient photon detection," *Physical Review A*, vol. 72, p. 013801, July 2005.

[136] A. Ourjoumtsev, H. Jeong, R. Tualle-Brouri, and P. Grangier, "Generation of optical 'Schrödinger cats' from photon number states," *Nature Photonics*, vol. 448, pp. 784–786, Aug. 2007.

[137] A. Ourjoumtsev, R. Tualle-Brouri, J. Laurat, and P. Grangier, "Generating optical Schrödinger kittens for quantum information processing.," *Science*, vol. 312, pp. 83–86, Apr. 2006.

[138] K. Wakui, H. Takahashi, A. Furusawa, and M. Sasaki, "Photon subtracted squeezed states generated with periodically poled $KTiOPO_4$," *Optics Express*, vol. 15, no. 6, p. 3568, 2007.

[139] Y. Takeno, M. Yukawa, H. Yonezawa, and A. Furusawa, "Observation of -9 dB quadrature squeezing with improvement of phase stability in homodyne measurement," *Optics Express*, vol. 15, no. 7, p. 4321, 2007.

[140] H. Vahlbruch, M. Mehmet, S. Chelkowski, B. Hage, A. Franzen, N. Lastzka, S. Goßler, K. Danzmann, and R. Schnabel, "Observation of Squeezed Light with 10-dB Quantum-Noise Reduction," *Physical Review Letters*, vol. 100, p. 033602, Jan. 2008.

[141] V. Händchen, T. Eberle, S. Steinlechner, A. Samblowski, T. Franz, R. F. Werner, and R. Schnabel, "Observation of one-way Einstein–Podolsky–Rosen steering," *Nature Photonics*, vol. 6, pp. 598–601, Aug. 2012.

[142] L. Huang, Q. Guo, L.-y. Jiang, G. Chen, X.-x. Xu, and W. Yuan, "M Times Photon Subtraction-Addition Coherent Superposition Operated Odd-Schrödinger-cat State: Nonclassicality and Decoherence," *International Journal of Theoretical Physics*, pp. 1–17, Jan. 2015.

[143] X.-x. Xu, H.-c. Yuan, and L. Zhou, "Nonclassicality generated by repeatedly operating photon annihilation-then-creation and creation-then-annihilation on squeezed vacuum," *Optics Communications*, vol. 335, pp. 133–139, Jan. 2015.

[144] P. Grangier, J.-M. Courty, and S. Reynaud, "Characterization of nonideal quantum non-demolition measurements," *Optics Communications*, vol. 89, pp. 99–106, Apr. 1992.

[145] S. L. Braunstein and C. M. Caves, "Statistical distance and the geometry of quantum states," *Physical Review Letters*, vol. 72, pp. 3439–3443, May 1994.

[146] S. L. Braunstein, C. M. Caves, and G. J. Milburn, "Generalized Uncertainty Relations: Theory, Examples, and Lorentz Invariance," *Annals of Physics*, vol. 247, pp. 135–173, Apr. 1996.

[147] P. T. Cochrane, G. J. Milburn, and W. J. Munro, "Macroscopically distinct quantum-superposition states as a bosonic code for amplitude damping," *Physical Review A*, vol. 59, pp. 2631–2634, Apr. 1999.

[148] P. Marek and J. Fiurášek, "Elementary gates for quantum information with superposed coherent states," *Physical Review A*, vol. 82, p. 014304, July 2010.

[149] C. R. Myers and T. C. Ralph, "Coherent state topological cluster state production," *New Journal of Physics*, vol. 13, p. 115015, Nov. 2011.

[150] J. Kim, J. Lee, S.-W. Ji, H. Nha, P. M. Anisimov, and J. P. Dowling, "Coherent-state optical qudit cluster state generation and teleportation via homodyne detection," *Optics Communications*, vol. 337, pp. 79–82, Feb. 2015.

[151] S. J. van Enk and O. Hirota, "Entangled coherent states: Teleportation and decoherence," *Physical Review A*, vol. 64, p. 022313, July 2001.

[152] H. Jeong, M. S. Kim, and J. Lee, "Quantum-information processing for a coherent superposition state via a mixedentangled coherent channel," *Physical Review A*, 2001.

[153] N. Sangouard, C. Simon, N. Gisin, J. Laurat, R. T. Brouri, and P. Grangier, "Quantum repeaters with entangled coherent states," *JOSA B*, vol. 27, pp. A137–A145, June 2010.

[154] D. S. Simon, G. Jaeger, and A. V. Sergienko, "Entangled-coherent-state quantum key distribution with entanglement witnessing," *Physical Review A*, vol. 89, p. 012315, Jan. 2014.

요약(국문초록)

양자역학적 비국소성은 처음으로 아인슈타인, 포돌스키, 로젠에 의해 양자역학의 모순을 지적하기 위해 인지되어 사용되었다. 하지만, 양자 정보처리 분야의 발전과 함께, 양자역학적 비국소성은 독립적인 키 분배, 양자 텔레포테이션, 등 여러가지 양자정보처리에 있어서 매우 중요한 리소스임이 판명되었다.

이 학위논문의 전반부에서 두개의 이차원 시스템에 대한 비국소성의 계층구조 중, 아직 알려지지 않은 양자 조정가능한 상태와, 텔레포테이션에 유용한 상태의 계층구조를 연구하고, 벨 비국소성과 양자 조정을 증명하는 효과적인 방법을 제안한다. 대략적인 제안은 다음과 같다.

벨 비국소성의 증명은 고전역학에서 가정하는 국소적 사실주의와 양자역학이 양립 할수 없는 것을 증명하는 방법으로 이를 증명하려면 국소성 허점과 측정 효율 허점을 피해야 한다. 국소성 허점은 속도가 빠른 광자를 이용하여, 측정 효율 허점은 측정이 높은 효율로 이루어지는 원자들을 이용해 피할 수 있었다. 하지만 이 두 가지 허점을 피할 수 있는 실험은 지금까지 존재하지 않는다. 우리는 이러한 노력의 하나로 양쪽의 장점을 모두 사용하기 위해 광자와 리드버그 원자의 얽힌 상태를 이용하는 실험 방법을 제안하고, 위에서 언급한 허점을 피하기 위한 현실적인 조건들을 분석한다. 특히 원자의 자발적 방출은 미세한 극저온 초전도체 가이드를 통해 막을 수 있으며, 광자를 가두는 공동의 Q인자를 향상 시킬 수 있다면 허점을 피할 수 있음을 보인다.

양자 조정이란 두개의 공간꼴 사건들 중 한쪽이 다른 쪽의 물리적 상태를 변형시킬 수 있다는 양자 상태의 비국소성을 나타낸다. 양자조정은 벨 비국소성 증명에서의 허점들로 제기되어온 측정 효율 허점과, 국소성 허점을 비교적 더 쉽게 피하면서 증명 가능한 후보이다. 본 연구에서는 얽힌 결맞음 상태에 호모다인 측정,

광자의 홀짝 측정, 광자의 유무 측정을 이용한 세 가지 경우의 양자 조정에 대해 살펴보았다. 호모다인 측정의 경우 측정효율이 낮더라도 얽힌 결맞음 상태의 진폭만 충분히만 크다면 양자 조정 값의 최대치인 1에 이를 수 이었다. 얽힌 결맞음 상태의 생성이 이상적으로 이루어진다면 실제적인 광자 유무 측정 효율을 고려했을 시 양자조정 존재의 실험적 증명이 가능하다는 것을 보일 수 있다.

이 학위 논문의 후반부는 소음없는 증폭에 대한 연구결과를 소개하고있다. 연속변수 양자상태의 상관관계를 이용하는 여러가지 양자정보처리를 증폭을 이용하면 더 효율적으로 수행할 수 있는데, 현실적으로 적용 가능한 결맞음 상태를 증폭하는 방법으로 광자를 더했다가 빼는 연산을 수행하는 증폭연산이 사용되어 왔다. 이 연구에서는 기존의 증폭연산처럼 인라인으로 구성할수 있는 광자를 두 번 더하는 연산을 증폭으로 사용했을시, 등가소음입력신호를 기준으로 큰 진폭의 결맞음 상태에 대해서 기존의 연산보다 더 소음없이 큰 진폭으로 증폭할수 있다는 결과를 보여준다. 중첩된 결맞음 상태에 대한 분석에 있어서도 동일한 결과를 보여주었는데 이는 피셔 인포메이션으로 부터 계산된 최적 위상 불확정성에 의해 유추될수 있다.

주요어 : 양자 비국소성, 소음없는 증폭, 벨 부등식, 양자조정, 텔레포테이션, 계층 구조

학번 : 2008-20433